

**PERFORMANCE OF GLUED-IN-ROD CONNECTIONS
IN CROSS-LAMINATED TIMBER**

by

Gbenga Solomon, Ayansola

B.Sc, Federal University of Agriculture, Abeokuta, 2012
MSc in Eng, Tallinn University of Technology, Estonia, 2018

THESIS SUBMITTED IN PARTIAL FULFILLMENT OF
THE REQUIREMENTS FOR THE DEGREE OF
MASTER OF SCIENCE
IN
NATURAL RESOURCES AND ENVIRONMENTAL STUDIES

UNIVERSITY OF NORTHERN BRITISH COLUMBIA

November 2020

©Gbenga Solomon Ayansola, 2020

Abstract

The widespread availability of Cross-laminated timber (CLT) provides opportunities to extend the use of wood beyond traditional low-rise residential construction. Glued-in rods (GiR) are an interesting technical solution for numerous structural applications in timber engineering. Although GiR connections have the potential to be used in combination with CLT, research on this application is scarce. In this thesis, an experimental investigation on the performance of GiR in CLT is presented. Two different 5-ply CLT panel thicknesses (139 and 175 mm), two steel rod diameters ($d = 12.7$ and 19.1 mm) and five different anchorage lengths ($l_a = 6d, 10d, 12d, 14d$ and $18d$) were considered in single and multiple rod connections. A total of 260 specimens were fabricated and subsequently tested under uni-axial quasi-static monotonic tension. The results were assessed in terms of load-carrying capacity, stiffness and failure modes and demonstrated that GiR in CLT offer an alternative high capacity timber connection.

Table of contents

Abstract.....	i
Table of contents	ii
List of tables	v
List of figures	vi
Acknowledgements	viii
1 Introduction	9
1.1 Cross-laminated timber	9
1.2 Glued-in rod connections	9
1.3 Research need	10
1.4 Objectives	11
1.5 Organisation, scope and limitations of thesis	11
2 Literature Review	13
2.1 Background information	13
2.1.1 Engineered wood products	13
2.1.2 Cross-laminated timber	13
2.1.3 Timber connections	15
2.2 Glued-in rod connections	16
2.2.1 Rod material	16
2.2.2 Adhesives used in GiR	17
2.2.3 Manufacturing of GiR	18
2.2.4 Geometric parameters	19
2.2.5 Material parameters	22
2.2.6 Loading and boundary conditions	23
2.2.7 Failure modes	24
2.2.8 Analysis methods.....	25
2.2.9 Application of GiR in CLT.....	26
2.3 Summary of literature review	28

3	Experimental investigations	30
3.1	Overview.....	30
3.2	Materials	31
3.2.1	CLT.....	31
3.2.2	Steel rod.....	31
3.2.3	Adhesive and adhesive shear strength	32
3.3	GiR Specimen configurations.....	33
3.3.1	Phase I	33
3.3.2	Phase 2.....	35
3.3.3	Phase 3.....	36
3.4	Specimen fabrication	38
3.5	Test methods.....	39
3.6	Statistical analyses	41
4	Results and discussion.....	43
4.1	Phase 1: single rod parallel to major CLT strength axis.....	43
4.1.1	Overview	43
4.1.2	Load-displacement behaviour.....	44
4.1.3	Failure modes	45
4.1.4	Statistical analysis (Phase 1)	49
4.1.5	Discussion.....	50
4.1.6	Comparison to design equations.....	53
4.2	Phase 2: Single rod perpendicular to major CLT strength axis.....	54
4.2.1	Overview	54
4.2.2	Load-displacement behaviour.....	55
4.2.3	Failure modes	56
4.2.4	Statistical analysis (Phase 2)	59
4.2.5	Discussion.....	60
4.2.6	Comparison to design equations.....	62
4.3	Phase 3: Multiple rods parallel to major strength axis of CLT.....	63
4.3.1	Overview	63

4.3.2	Load-displacement behaviour.....	64
4.3.3	Failure modes	65
4.3.4	Statistical analysis (Phase 3)	67
4.3.5	Discussion.....	68
5	Conclusions	71
5.1	Summary of results	71
5.1.1	Single rod installed parallel to the major CLT strength axis.....	71
5.1.2	Single rod installed perpendicular to the major CLT strength axis.....	72
5.1.3	Multiple rods installed parallel to the major CLT strength axis.....	73
5.2	Outlook	74
	References	75
	Appendices	85
	Appendix A: GiR test fixtures	85
	Appendix B: Load-displacement curves from Phase 1	87
	Appendix C: Load-displacement curves from Phase 2	99
	Appendix D: Load-displacement curves from Phase 3	102

List of tables

Table 3.1: Test series overview for Phase 1 35

Table 3.2: Test series overview for Phase 2 36

Table 3.3: Test series overview for multiple rods in Phase 3 37

Table 4.1: Summary of test results for Phase 1 43

Table 4.2: Summary of ANOVA for Phase 1 49

Table 4.3: Summary of Tukey test results for Phase 1 50

Table 4.4: Summary of test results for Phase 2 55

Table 4.5: Summary of ANOVA for Phase 2 59

Table 4.6: Summary of Tukey's HSD test for Phase 2 59

Table 4.7: Summary of test results for Phase 3 63

Table 4.8: Summary of ANOVA for Phase 3 67

Table 4.9: Summary of Tukey test results in Phase 3 68

List of figures

Figure 2.1: Schematic showing GiR connection parameters.....	19
Figure 2.2: Schematic showing specimen with adhesive gap	20
Figure 2.3: Different loading configurations: (a) pull-pull (b) pull-push.....	23
Figure 2.4: Typical GiR failure modes: (a) rod yielding; (b) rod pull out; (c) timber tensile failure; (d) wood plug pull out; (e) timber splitting.....	24
Figure 2.5: Failure modes for GiR in CLT: (a) complete lamination tear-out of core CLT layer; (b) edge lamination tear out of core CLT layer	26
Figure 3.1: Overview of test program	30
Figure 3.2: Steel rod tensile strength: a) test set-up; b) failed specimen.....	32
Figure 3.3: Adhesive shear strength tests: a) test set-up; b) typical failed specimen	33
Figure 3.4: Single rod schematic for (a) completely and (b) partially bonded rods.....	34
Figure 3.5: Schematic for single rods perp. to the major strength axis of CLT	36
Figure 3.6: Schematic for multiple rods par. to the major strength axis of CLT	37
Figure 3.7: Specimen manufacturing: (a) hole drilling; (b) applying adhesive; (c) rod positioning; (d) specimen storage.....	39
Figure 3.8: Test set-up for: a) Phase 1 and 2; b) Phase 3	40
Figure 4.1: Load-displacement curves of selected specimen for each series from Phase 1: a) 12.7 mm rods and b) 19.1 mm rods.....	45
Figure 4.2: Typical failure modes for 12.7 mm GiR par. to the major strength axis	47
Figure 4.3: Typical failure modes for 19.1 mm GiR par. to the major strength axis	48
Figure 4.4: Effect of anchorage length and panel thickness on F_{max} with 12.7 mm GiR	51
Figure 4.5: Effect of anchorage length and panel thickness on F_{max} with 19.1 mm GiR	52
Figure 4.6: Effect of rod diameter on F_{max} (Phase 1)	53
Figure 4.7: Comparison GIROD design precitions vs. experimental results from Phase 1	54

Figure 4.8: Load-displacement curves of selected specimen for each series from Phase 2	56
Figure 4.9: Typical failure modes for single GiR perp. to the major strength axis	58
Figure 4.10: Effect of anchorage length on F_{max} for Phase 2	60
Figure 4.11: Effect of the rod diameter on F_{max} for Phase 2	61
Figure 4.12: Comparison GIROD design equation vs. results from Phase 2	62
Figure 4.13: Load-displacement curves of selected specimen for each series from Phase 3: (a) $l_a=10d$, $s=4d$ and $6d$ (b) $l_a=18d$, $s=4d$ and $6d$	64
Figure 4.14: Typical failure modes observed in specimens with multiple rods	66
Figure 4.15: Effect of anchorage length, rod spacing and number of rods on F_{max}	69

Acknowledgements

I acknowledge the support I received from my supervisor Dr Thomas Tannert all through the duration of this research.

I also appreciate the support received from Dr Heather Bryan and Dr Pranesh Kumar for providing guidance on the statistical analysis, the lab technicians Michael Billups, Ryan Stern and the senior lab instructor Maik Gehloff for the smooth operation and use of the lab equipment and measuring devices.

1 Introduction

1.1 Cross-laminated timber

Cross-laminated Timber (CLT), an engineered wood product developed in Europe in the early '90s, has been called a game-changer in the wood construction industry [1]. CLT is produced by adhesively bonding wood lamellas together in a commonly crosswise alternating manner to form panels. CLT panels offer a good weight to strength ratio, precise off-site prefabrication, speed and ease of construction [2]. As a result, CLT has increasingly gained popularity in residential and non-residential applications, as well as in multi-story buildings [3, 4]. CLT member sizes are limited due to transportation and fabrication capabilities. Consequently, CLT walls or floor diaphragms are composed of smaller members to be jointed. For a CLT system composed of different elements, the shear strength and stiffness depend on the load-deformation characteristics of its connections [5, 6]. Connectors ensure the continuous distribution and transfer of forces from different structural members to the foundation. Connection systems for CLT range from the traditional dowel type fasteners such as nails, lag screw, bolts, rivets, etc. to the innovative connection systems such as self-tapping screw [7] or Glued-in rods (GiR).

1.2 Glued-in rod connections

GiRs are high strength connectors that are concealed inside the wood member, which is both an architecturally pleasing feature and also provides the joint with excellent fire protection when compared to conventional dowel-type timber fasteners. They have high load-carrying capacity and stiffness per cross-sectional area [8]. GiR connections are composed of multiple components, namely timber, rod (mostly steel), and adhesive. These three materials which have different properties and are expected to transfer load

and equally deform simultaneously under loading conditions [9]. Due to the different materials involved, GiRs are hybrid connections and a rather complex system [10]. The performance of GiR has been shown to depend on several parameters, mainly the anchorage or embedment length of rod (l_a), rod diameter (d), slenderness ratio (λ), which is the ratio between l_a and d , edge distance (e_d), number of rods (n), glue line thickness (t), type of adhesives, load-to-grain angle (θ), and moisture content (MC) of timber [10]. Some principal failure modes associated with GiR connections are recognized. These can be broadly categorised as yielding of the rod (if made from steel), shear along the rod, glue line failure, tensile failure or splitting of the wood member, and block shear failure in the wood member (for multiple rods). While in practice a single GiR connection is seldom used, previous research mostly focused on single rod configurations to isolate the effects of these parameters on the joint performance. In examining these parameters, previous studies focused on solid structural timber [11, 12], Glue-laminated Timber (Glulam) [13, 14], Laminated Veneer Lumber (LVL) [15], and more recently CLT [16, 17].

1.3 Research need

Although GiR connections in CLT can be used in a variety of structural applications such as for panel-to-panel joints in walls, joints between CLT walls and concrete foundation, they are not yet widely applied. Only a few studies are available on the performance of GiR connections in CLT. Azinovic et al. [16, 17] reported on different failure modes such as the edge lamination tear out, complete tear out of CLT layer, failure along non-glued timber edges and failure of timber next to adhesive, all of which deviate from the regular failure modes seen in other wood products and recommended further studies. Research gaps exist regarding the performance of single and multiple rods GiR in CLT such as the

impact of rod edge spacing, shifting of anchorage length to inner members, load-to-grain angle and spacing between multiple rods.

1.4 Objectives

Based on the aforementioned reasons, this research focused on examining the strength and stiffness of single and multiple rod GiR connections under uniaxial tension in CLT. The load-carrying capacity and stiffness of GiR connection in CLT by determining the effects of the factors: panel size, rod diameter, number of rods and anchorage length on the strength of the connection was examined. Specifically, the objectives were to:

1. Investigate the structural performance of single GiR connected parallel to the major strength axis with the rod completely and partially glued inside CLT (Phase 1).
2. Investigate the structural performance of single GiR connected perpendicular to the major strength axis with embedded rod completely glued inside CLT (Phase 2).
3. Investigate the structural performance of multiple GiR in CLT connected parallel to the major strength axis (Phase 3).

1.5 Organisation, scope and limitations of thesis

In chapter two of this thesis, the components of GiR, the manufacturing process, the mechanical behaviour of GiR, failure modes and design equations are reviewed. In chapter three, the experimental campaign is presented and in chapter four, the results are reported and discussed. The study is concluded in chapter five.

This study focused on the structural performance of single and multiple GiR in CLT under quasi-static monotonic loading in two directions; parallel and perpendicular to the major strength axis of CLT. The single steel rods were glued at both ends of timber and tested in a pull-pull test configuration in short term static loading. For every failed specimen,

the damaged rod was cut off from the timber and the second end which is undamaged was retested in similar test configuration after drilling holes into them. It was assumed that the undamaged end of the connection will have either equivalent or higher capacity than the damaged rod end of the CLT.

This study was limited to varying four main parameters: rod diameter, CLT thickness, anchorage length and the number of the rods glued-in. Threaded steel rods of grade ASTM A193 B7 with diameters 12.7 and 19.1 mm, CLT panels made from SPF species with the thickness 139 mm and 175 mm and anchorage length of $6d$, $10d$, $12d$, $14d$ and $18d$ were combined for one, two and three-rod connections. The two-component adhesive CR 821 Purbond was used. Comparisons were made between the load-carrying capacities of the experimental values and the GIROD design equations. No new analytical methods for the connection stiffness or load-carrying capacity were proposed.

The testing was limited to uniaxial quasi-static monotonic short-term tension loading in a pull-pull configuration under normal temperature and constant moisture content. Other loading conditions such as bending or shear, cyclic or long-term loading, or high temperature or fire conditions were not considered. The impact of manufacturing parameters and tolerances was beyond the scope of this research.

2 Literature Review

2.1 Background information

2.1.1 Engineered wood products

Wood is an orthotropic material; therefore, it exhibits different properties based on its three (longitudinal, radial and tangential) mutually perpendicular axes. It is hygroscopic in nature and thus, swells and shrinks when exposed to humidity variations. Engineered wood products (EWPs) are a class of products made from wood to serve as a reliable construction material for the replacement and reduction of, or in combined use with steel and concrete. The use of EWPs has provided viable building solutions that reduce the carbon footprint in construction [18, 19]. They are gaining acceptance in building applications and architectural design as evident by the many raising wooden structures across the world [20, 21, 22] and the 2-15% annual growth rate experienced by some EWPs in Europe [23]. Among the advantages of EWPs are that thinner diameter trees residues from wood processing plants and lower-quality lumber can be effectively utilized as feedstock to create products with improved dimensional stability, better durability, and enhanced performance [24, 25, 26]. Common EWPs suitable for structural applications are Glulam, LVL, and increasingly, CLT.

2.1.2 Cross-laminated timber

CLT is a prefabricated engineered structural composite which has been identified as a suitable alternative to concrete [27]. It is a plate-type product manufactured mostly with an odd number of lumber layers adhesively bonded at 90° to the adjacent layer. Usually, the same grade and species are used for all laminations in a given direction and for the adjacent layer alternative grades and lumber species may be used. The alternating grain

directions give CLT stiffness and strength in two directions. As a result of its high in-plane stiffness and out-of-plane load-bearing capacity; it is used as a shear wall or floor diaphragm [28]. It has been shown to have high thermal energy storage and high strength to weight ratio [29]. The crosswise configuration of its layers reduces swelling and shrinkage. The popularity of CLT has grown not only in Europe but also in North America, and seismic prone countries like Japan, New Zealand and China [30]. Although the mean density of CLT is similar to the base material, the variability in its properties is much lower than the base material (sawn lumber) [31].

Although CLT can be customized to meet specific width, length and thickness requirements, panels are typically produced in widths of 1.2 m, 2.4 m and 3m; lengths of up to 18 m or more and thickness of up to 500 mm [32]. In North America, CLT stress grades are achieved in two ways: one is based on the tested mechanical properties of specific panel layup whose lamination size and base material species are known to possess certain structural properties [28, 32]. The other is based on the use of alternative panel layup that can be proven to meet design requirements by the manufacturer.

For CLT design, three shear failure modes as discussed in [31, 33] are important to be checked: i) shear failure parallel to the grain in the gross cross-section of CLT occurring in unglued joints sections within the lamellae having the same shear stresses in the transverse and longitudinal layers; ii) shear failure perpendicular to the grain in the net cross-section of CLT occurring within the parts that intersect with unglued joints with the shear stresses developed in the lamella perpendicular to the joint, and iii) failure due to torsional and unidirectional shear stresses in the orthogonal lamellae. With a focus on the shear resistance of single glued nodes of CLT loaded in-plane, Brandner et al. [34] studied the influence of the layer thickness, layer width and width of gap on the shear capacity perpendicular to the grain and concluded that these parameters significantly affect the

shear strength of CLT. Specifically, the shear strength was reported to decrease with increase in the layer thickness for the three thicknesses considered, significant lower shear strength was reported in the rift grain board than the flat grain boards, shear at the edges occurred more in wider boards and in the tangential-longitudinal layer. The structural performance of CLT systems largely depends on the properties of the connectors used in the system to connect members.

2.1.3 Timber connections

Connectors in wooden structures ensure the continuous distribution and transfer of forces from different structural members to the foundation. They are essential for the performance of a structure in providing stability, strength, stiffness and ductility. Timber connectors can be broadly categorised into dowel-type mechanical fasteners such as nails, bolts, wood screws, dowels etc. It is generally a good practise to use small and multiple fasteners as it prevents the concentration of loads thereby allowing loads to spread over the connectors. However, local stresses should be checked in connections with multiple fasteners. Also, when a group of fasteners are closely spaced on timber and loaded parallel to the major strength axis, wood failure may limit the capacity of the fasteners. Second categories are carpentry joints such as grooves, holes, notches. A third category is adhesive joints which effectively transfer and distribute stresses between timber elements. The bond strengths depend on the type of adhesive, cure cycle, environmental factors, glueline thickness etc. [35, 36]. Combining the aforementioned connector categories creates a hybrid joint such as GiR that combines mechanical fasteners with adhesive bonding.

The stiffness, strength and energy dissipation of a structure depends on its connections [37]. Ductility is essential to obtain large deformation in structures, to allow stress redistribution within members, to allow for energy dissipation and to increase structural

robustness [38]. The yielding of the fastener is desirable for ductile joint failure. It has been reported [39] that ductile failure modes can be achieved when the number of connectors for a given specimen is relatively small and when the spacing and the end distances of the connectors are large enough.

When traditional connectors such as nails and screws are used to edge connect CLT members, the connection only achieves up to 30% of the panel's shear capacity [40]. Consequently, there is no balance between the load-carrying potential of CLT and the shear connection. Moreover, because the shear strength and stiffness of CLT members consisting of multiple elements are governed by the behaviour of the connection between them, to fully maximize the load-carrying potentials of CLT, it is important to use connectors with increased stiffness and load-carrying capacity. Thus, the characteristics of connectors used in structural applications are very important and must be given attention. Therefore, a potential solution is GiR which offers a suitable and effective alternative connection system to fully maximize the capacity of CLT panels.

2.2 Glued-in rod connections

2.2.1 Rod material

The most commonly used rod material for GiR connections is steel [41], either threaded or smooth. The steel rod is mostly used for a number of reasons: i) the preferred failure mode of GiR is yielding of the rod rather than adhesive or wood brittle failure [42]; ii) mild steel rod provides ductility for this connection [43]; iii) they can withstand high axial forces [41]; and iv) they can easily be connected to other steel elements [9, 10]. The threads on the steel rod ensure an effective mechanical interlock with the adhesive [10]. Although the stress is distributed along the bonded length [44], there are stress concentrations at the face and bottom of the bored hole [43]. Therefore, the positioning

of the rod is important to the performance of the joint [41]. A ductile connection can only be achieved when the rod is designed to be the weakest link. Thus, for multiple rod connections, it is important to ensure a load uniform distribution in all the rods [45, 46].

2.2.2 Adhesives used in GiR

The adhesives used in GiR connection act as an interface to transfer the forces between the rod and the timber material. The adhesive must be able to effectively bond the joint members to provide continuous adhesion [13]. Bearing in mind that shrinkage of an adhesive may occur in the initial hardening stage of the adhesive [41], it is important to avoid the adhesive from being the weakest link in the connection. Consequently, the adhesive should possess good gap filling properties. The most commonly used adhesives for GiR connections are epoxy (EPX), polyurethane (PUR) and to some extent phenol-resorcinol-formaldehyde (PRF) and melamine-urea- formaldehyde (MUF) [15]. When selecting the adhesives, properties like the viscosity, porosity, curing temperature and time, ease of application and the compatibility with the type of timber and rod should be considered [12, 47]. Since various adhesives may develop differing bonding strengths with different adherends, the pull out strength of GiR is not only related to the type of adhesive but also the wood species [41, 48]. Consideration should also be given to the timber moisture content before applying the adhesives.

The extensive GIROD research project, amongst other things, concluded that EPX and PUR adhesive joint showed the best performance. If all parameters are the same, EPX joints exhibited the highest axial capacity, followed by PUR and then PRF [49]. Other studies [44, 50] have reported that both EPX and PUR generally have good gap-filling possibilities, unlike PRF, making them appropriate for GiR applications. PUR adhesives perform well in wet conditions and for practical reasons, two-component adhesives are preferred over one component ones [15, 51]. Other recent research [52] characterised nine

different adhesives based on their stiffness, strength and rheology and also demonstrated that PUR had good bonding properties suitable for GiR joints.

2.2.3 Manufacturing of GiR

The process begins with the drilling of holes into the timber that are larger (usually between 1 and 4 mm) than the diameter of the rod to achieve a uniform glueline thickness. The hole is then cleaned using compressed air or vacuum [41] to remove excess wood shavings which may create debris and prevent the GiR components from proper adhesion. This step is followed by inserting the rod in the hole. One technique used is to fill the hole with a predetermined calculated quantity of adhesive after which the rod is twisted into the hole to remove voids. The viscosity of the adhesive determines how much twisting force is applied. The drawback to this technique is that the adhesive may not fill the whole cavity and assurance may not be given that no voids exist in the adhesive. Another way to glue the rod is to insert the rod into the hole to its full depth and then create a second hole at a lower point close to the base of the rod from which the adhesive can be injected into the drilled hole until it flows out from the top surface of the timber; however, this method is time-consuming. Another technique is to drill the rod into an undersized hole or hole of an equal diameter which is already filled with adhesive [53]. This method offers the advantage of better retention of the adhesive in the hole before curing.

Factors such as the inclination of drilled holes within the timber, time and temperature required for the adhesive to cure, uniformity of glueline, the moisture content of timber in relation to the adhesive curing requirements and the correct positioning of the rod in timber during manufacturing are critical to the optimum performance of the joint. Consequently, to achieve the optimum performance of GiR joint, quality control must be ensured when positioning the rod in timber [41] and flaws such as off-centre position, voids in the glue line, undesired slanting of the drilled hole, inclined positioning of rod

and incomplete insertion of the rod should be avoided. To avoid eccentricities, several devices such as plastic or metal rings, toothpicks [9, 13], spacers [14], a countersink hole [54] have been used. Rod contamination with dirt, oil, or rust may affect the performance of GiR connection and should also be avoided [14, 55, 56].

2.2.4 Geometric parameters

The GiR geometric parameters (c.f. Figure 2.1) that impact the load-carrying capacity include anchorage length (l_a), rod diameter (d), diameter of hole (d_h), glue-line thickness (t), edge distance (e_d), slenderness (λ), rod spacing (s), number of rods (n), and rod-to-grain angle (θ). Although in practice single GiRs are seldom used, these allow isolating geometric parameters to determine their influence on the joint performance.

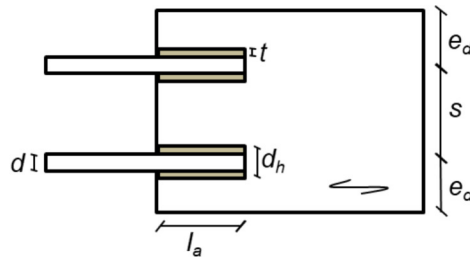


Figure 2.1: Schematic showing GiR connection parameters

The anchorage length l_a (also referred to as embedment length) refers to the length of the rod glued into the timber. Although many studies e.g. [13, 16, 43, 57] have shown that the GiR strength increase with the anchorage length, some studies have reported that this increase is not linear due to stress concentrations [43, 58, 59]. Gehri [45] suggested moving the anchorage zone of steel rod away from the surface of timber into the inner part by leaving a gap at the face of the drilled hole where no adhesive is applied along the anchorage length, thus preventing the mechanical interlock around this zone, see Figure 2.2.

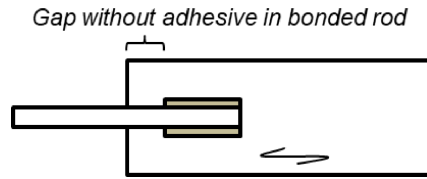


Figure 2.2: Schematic showing specimen with adhesive gap

The rod diameter (***d***) is one of the most commonly investigated GiR parameters. Most studies agree that a larger rod diameter leads to increase in strength and stiffness [12, 42, 60, 61]. Only one study reported no significant effect of rod diameter on the pull-out strength [54]. Although the influence of rod hole diameter on shear strength could not be verified in [61], it has however been reported that the diameter of steel rod had little influence on the average shear stress [60]. Reducing the rod cross-section (necking) over a given length to prevent shear force transfer and indentation at the surface facilitates the desirable plastic steel deformation inside the timber [42, 62, 63].

Rather than characterizing rod diameter as a separate factor, some studies have combined the rod diameter with embedment length [42, 64], into the term called slenderness as the ratio of anchorage length to the rod diameter: $\lambda = l_a/d$. Shear stresses in GiR joints have been shown to decrease asymptotically with slenderness ratio [8]. It was reported that the mean shear stresses in the wood/adhesive interface decrease with increasing slenderness [63] and that the strength increases with higher slenderness values [46, 59, 65]. Research has also indicated that GiR joints made with denser wood are less affected by the joint slenderness [59]. There are differences between the slenderness of rods connected parallel to grain and those connected perpendicular to the grain. For those connected parallel to the grain, the mean shear stress decreases with increasing slenderness but for the rods glued perpendicular to the grain, the shear stress is constant and also does not depend on the joint slenderness [65].

The rod distance to the edge of the timber and the spacing distance between two or more rods are other important parameters that influence the load-carrying capacities and failure modes in GiR joints. In an effort to determine the minimum edge distance and rod spacing requirement, when the edge distance and rod spacing is less than $2.5d$ and $5d$ respectively, a decrease may occur in the total load-carrying capacity [54]. Blass *et al.* [66] also reported a reduction in capacity when the edge distance used was less than $2.5d$. It was therefore recommended that the minimum edge distance should be equal or greater than $2.5d$. Likewise, Steiger *et al.* [42] found the failure load to reduce when the edge distance was less than $2.3d$. Elsewhere [57], the optimum edge distance of $3.5d$ was identified as the distance with greatly reduced splitting failure and maintained strength. The edge distances were evaluated in [67] and it was recommended that greater than $3d$ should be used to prevent splitting failure of timber.

Sufficient spacing between rods is necessary to avoid premature timber failure [57]. In previous work [13], spacings of $3d$, $4d$ and $5d$ were used and the load-carrying capacity of the connection increased with larger spacing and large spacing resulted in the yielding of the rod. Consequently, the spacing of $5d$ was recommended.

Although some studies [54, 67, 68] have pointed out that there's no proportionality between an increase in glueline thickness and higher load capacity, the glueline thickness can have a significant effect on connection failure mode [67]. The influence of the glueline is largely dependent on the adhesive properties [56]. Typically, the hole diameter on timber is drilled to an excess of between 1 and 4 mm. This guarantees a glueline thickness of between 0.5 and 2 mm [8, 41]. A larger glueline thickness increases the contact area but does not significantly increase strength [43]. A thickness of 2 mm was recommended by [48, 67].

The behaviour of GiR in timber inserted at different grain angles differs. The rod-to-grain angle is the angle between the grain direction of timber and the longitudinal axis of the rod [17]. Because timber is generally strongest in the longitudinal axis, one would assume GiR joints positioned parallel to this axis would have higher strength. While one study [69] affirmed this, several others [16, 42, 61] suggested that the specimens with GiR positioned perpendicular to the longitudinal axis exhibited higher pull-out strength.

2.2.5 Material parameters

The ability of wood as a hygroscopic material to swell and shrink depending on the prevailing environmental conditions can cause moisture-induced stresses in the glueline which can lead to cracks especially when the MC during bonding is much higher than the in-service MC [70]. Broughton and Hutchinson [71] revealed that both the strength and failure modes of GiR joints are significantly influenced by the MC of timber. Specimens were conditioned to 10%, 22% and 38% and it was reported that a MC above 25%, reduced the pull-out strength by 60-64%. Yet Otero et al. [72] reported no visual crack deformation on inspection of GiR specimens subjected to climatic cycles of relative humidity 20% to 87.5% and temperature varying from 10°C to 50°C.

A relationship has been shown to exist between the strength of a GiR joint and the density of timber. Although this relationship is not linear, according to Otero et al. [59, 73], the joint strength increases with the density of timber and the density also relates to the strength properties of the specific timber. A formula was proposed to predict the strength of GiR joint using density and slenderness. Stiffness also tends to increase with density [56]. Widmann et al. [61] stated that Norway Spruce species of GiR joints connected perpendicular to grain are less influenced by the density of their resident timber but those connected parallel to grain as reported in [42] for the same wood species are influenced

by the timber density. Higher density timber fails usually in tension but the lower density ones tend to show compressive buckling before any signal of failure in tension [74].

2.2.6 Loading and boundary conditions

To assess the pull-out capacity of GiR in timber, different loading configurations have been used. For example, the pull-pull test configuration (Figure 2.3) is a common loading set-up for connections parallel to the grain. For connections such as the moment-resisting connections where bending forces have to be accounted for, a pull-bending test set-up is appropriate [57, 75]. Variations of the pull-pull test can also be made to fit specific specimen configuration. For example, rods can be glued only on one side of the specimen as opposed to gluing the rods on both ends of the specimen. In this case, a test fixture is constructed to effectively hold down the specimen to be tested. For rods inserted perpendicular to the grain (Figure 2.3), three loading conditions can be used namely pull-compression, pull-push, and pull-pile foundation test configurations [10]. Pull-compression configuration is affected by compression stresses perpendicular to the grain, pull-push by bending stresses and tension failure can occur [76].

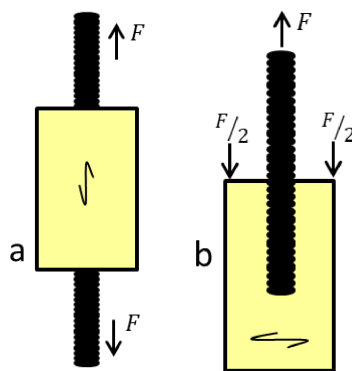


Figure 2.3: Different loading configurations: (a) pull-pull (b) pull-push

2.2.7 Failure modes

The failure mode of a GiR connection depends on the connection materials' (rod, adhesive and timber) mechanical properties and the bond between them [10]. The principal failure modes identified for GiR in timber [10, 13, 16, 41] are:

1. Rod failure
 - a. Yielding of the (steel) rod in tension. This is a desirable ductile failure mode.
 - b. Buckling of the rod if loaded in compression.
2. Rod pull-out which may be
 - a. Adhesive failure at the interface between the steel rod and adhesive
 - b. Shear failure of adhesive
 - c. Shear failure of adhesive at the interface between the adhesive and timber
 - d. Shear failure of timber close to glue line
3. Tensile failure of timber
4. Timber plug pull out
5. Splitting or cracking of timber

Additional failure modes specific to joints containing multiple GiR are group tear out and splitting of timber between rods as a result of short distances between rods.

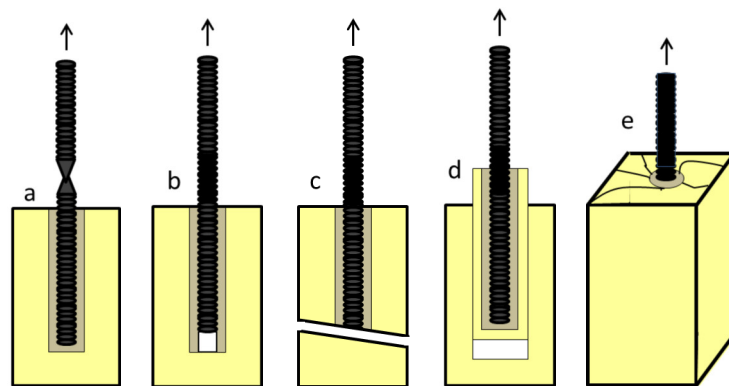


Figure 2.4: Typical GiR failure modes: (a) rod yielding; (b) rod pull out; (c) timber tensile failure; (d) wood plug pull out; (e) timber splitting

2.2.8 Analysis methods

Critical to the GiR glue-line adhesive strength analyses are the material and geometry properties of the joint such as the strength and stiffness of timber, strength of adhesive, glue-line thickness and conditions of loading [10]. Three fundamental approaches are available for analysis of the adhesive bond strength: i) Traditional strength analysis; ii) Linear Elastic Fracture Mechanics and iii) Non-linear Fracture Mechanics [77]. Based on these methods, multiple design approaches for GiR were developed.

Herein, only the approach presented in the GIROD project [49] is reported. The model allows estimating the characteristic axial capacity of a single rod GiR in Glulam:

$$\frac{P_u}{\pi dl} = \tau_f \frac{\tanh \omega}{\omega} \quad (1)$$

$$\omega = \sqrt{\frac{l_{geo}}{l_m}} \quad (2)$$

$$l_{geo} = \frac{\pi dl^2}{2} \left(\frac{1}{A_r} + \frac{E_r/E_w}{A_w} \right) \quad (3)$$

$$l_m = \frac{E_r G_f}{\tau_f^2} \quad (4)$$

l_{geo} is a geometrical length parameter

l_m is a material length parameter (a measure of the ductility of the bond line)

πdl is the area of the bond and

P_u is the characteristic axial capacity of a single rod glued-in connection

τ_f local bond line shear strength

ω Stiffness ratio of the joint

A_r The cross-sectional area of the rod (mm²)

E_r Modulus of elasticity of rod material

A_w The cross-sectional area of timber host (mm²)

E_w Modulus of elasticity of timber host

G_f Fracture energy calculated from $l_m E_r = 210,000 \text{ N/mm}^2$

2.2.9 Application of GiR in CLT

Information about the behaviour of GiR in CLT is scarce in the literature. Azinovic *et al.* [16] tested 60 GiR specimens in CLT in the pull-pull configuration. Threaded high-grade steel rods with diameters 16 and 24 mm were glued at 0° (parallel) and 90° (perpendicular) into the middle layer of the 5-ply CLT using a brittle epoxy adhesive. The anchorage lengths were varied between 80mm and 400 mm. Across all specimens, the study demonstrated that the load-carrying capacity increased with bonded length and the global connection stiffness depended more on the rod diameter rather than the bonded-length. Specifically, for the short anchorage lengths (80-240 mm), significantly different failure modes (Figure 2.5) were reported. Rod pull-out was predominant in specimens connected parallel to grain but the specimens glued perpendicular to grain were marked by the failure of the CLT panel due to edge lamination tear out of a layer. The perpendicular specimens were also reported to have more ductile response than the parallel specimens and their load-bearing capacity depended on the geometry of the panel. In contrast, the longer anchorage lengths (320 and 400 mm) specimens with larger rod diameter 24 mm failed predominantly by tear out of the CLT panel for those connected perpendicular to the grain and both pull-out of rod and CLT failure for those bonded parallel to the grain.

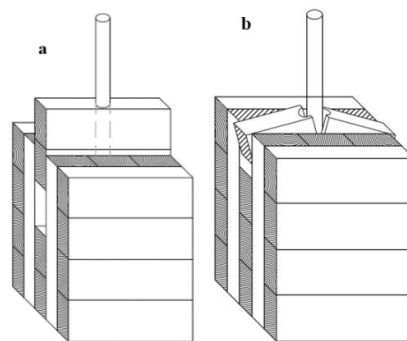


Figure 2.5: Failure modes for GiR in CLT: (a) complete lamination tear-out of core CLT layer;
(b) edge lamination tear out of core CLT layer

The experimental results were compared to six of the existing GiR design equations. The design equation tended to overestimate the maximum load of the rods embedded parallel to the grain and also underestimated the maximum load of the specimens bonded perpendicular to the grain. Although the estimated capacities with the GIROD equation was close to the experimental values, it was concluded that in most cases, these existing design equations are not suitable for GiR in CLT.

This previous study on GiR in CLT [16] had some limitations: the panels for the specimens perpendicular to the grain were relatively narrow (300 mm). As a result, it was not possible to conclude if larger panel sizes will follow a similar mode of failure. Also, the panel thickness was limited to only one size and only single rod specimens were considered. There is every tendency for the connection to display completely different behaviour when multiple rods are glued into the specimens.

Azinovic *et al.* [17] further conducted parametric finite element studies of GiR in CLT for the rod-to-grain angles 0° , 15° , 30° , 45° , 60° , 75° and 90° to examine the effects of the rod diameter, glued-in length and the rod-to grain angle on the load-carrying capacity and stiffness of the GiR connection. Generally, a good agreement was found between the experimental data and the finite element analyses. The parametric studies showed that the capacities of the rods oriented perpendicular to the grain were higher than those oriented parallel to the grain. The simulation further indicated that the maximum axial load carrying capacity and stiffness is neither at rod placed parallel (0°) nor perpendicular (90°) to the major strength axis. Rather, it is at an intermediate rod-to-grain angle of about 20° .

2.3 Summary of literature review

GiR represents an efficient and effective timber connection system because of its high load-carrying capacity and stiffness. It is often desired to be used with other structural elements due to its excellent performance, the aesthetic it offers and fire protection ability. GiR has three major components that are essential to the formation of the joint: timber, rod and adhesive. Generally, some parameters have been identified to be critical to the performance of GiR joint: anchorage or embedment length of the rod, rod diameter, slenderness ratio, rod edge distance, number of rods, spacing between rods, load-to-grain angle, type of adhesives and moisture content.

To maximize the performance of GiR joints, it is important to utilize timber which offers an equivalent load carrying potential as the joint itself. EWPs offer these possibilities. For over three decades, extensive studies have been conducted into the use of EWPs for GiR connections. These investigations have led to the identification of the failure modes occurring in GiR. They are broadly categorized as yielding of the rod (if made from steel), glueline failure, tensile failure or splitting of the wood member and block shear failure in the wood member (for multiple rods). In the numerous available studies on GiR in solid structural timber and EWP, several adhesives have been tested and consistently in these studies, EPX and PUR have been shown to possess good bonding properties suitable for GiR applications. This has informed the choice of PUR adhesive in this study.

Although GiR in CLT can be used in a variety of structural applications, the engineering community is yet to give its use the necessary attention. This largely accounts for the very few available studies on GiR connection in CLT, especially when compared with the numerous studies on glulam. CLT offers a promising alternative because of its good mechanical properties. In one of the available investigations on GiR in CLT, two distinct failure modes that have not been reported on solid structural timber and EWPs were

reported: edge lamination tear-out of core CLT layer and the complete tear out of CLT layer. In the same study, the pull-out forces from six of the available GiR design equations were compared with the experimental values. Although generally, they either overestimated or underestimated the pull-out force, the GIROD equation was reported to be the closest to the experimental values.

When dealing with GiR in CLT, additional complexities which may affect the performance of the connection are involved. For example, the thickness of CLT cross-layer may have an influence on the response of the connection since the axial stiffness and shear performance depend on the thickness of CLT layers. A different behaviour may be seen in the connection when the rod is glued in-between two-panel layers, when it is glued at the boundary between two parallel boards (edge glued or not edge glued) and a perpendicular board and when it is positioned at the intersection of two parallel boards. Also, the use of multiple GiR may trigger splitting or other failure modes when the spacing between the rods and the edge spacing is not sufficient. Information about the necessary parameters such as the optimum rod spacing and the right edge spacing to prevent splitting failure must be made available. The aforementioned reasons have necessitated the study of GiR in CLT to fulfil the three main objectives of this research.

3 Experimental investigations

3.1 Overview

The experimental investigations conducted in this work were grouped into three Phases with each Phase comprising of different test configurations in terms of the panel size and thickness, the number of rods and rod diameter as well as the anchorage length. These Phases, shown in Figure 3.1, were:

- Phase 1: Single GiR installed parallel to the major strength axis of the CLT
- Phase 2: Single GiR installed perpendicular to the major strength axis of the CLT
- Phase 3: Multiple GiR installed parallel to the major strength axis of the CLT

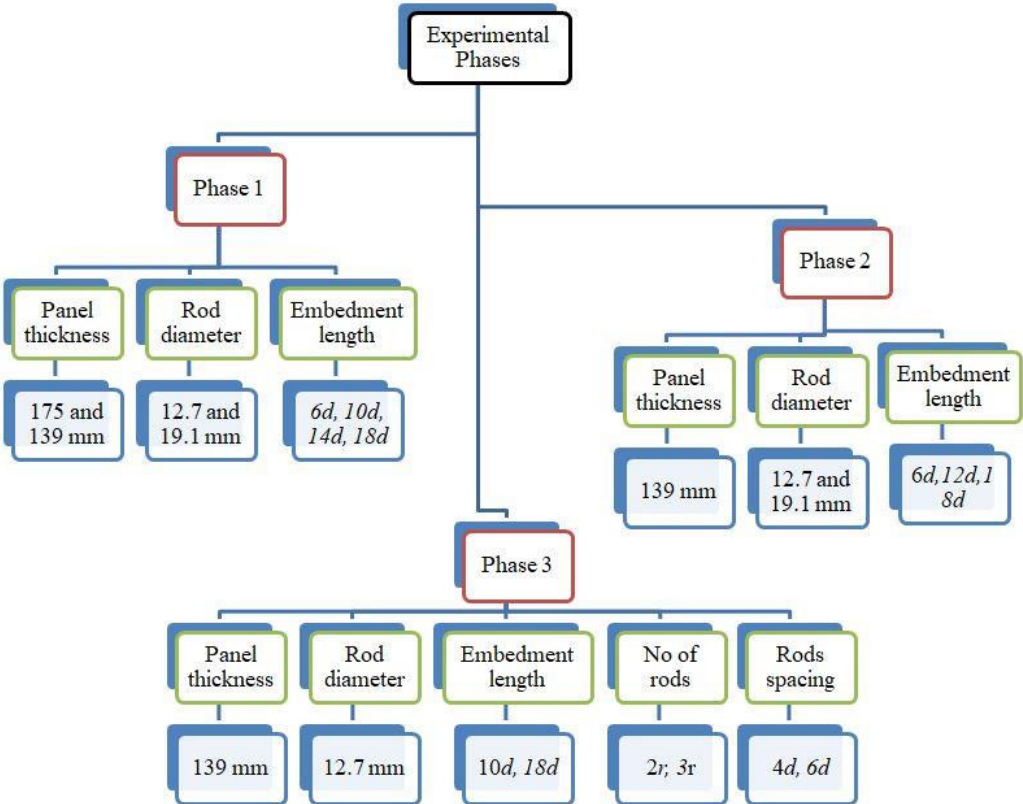


Figure 3.1: Overview of test program

3.2 Materials

3.2.1 CLT

For Phase 1, two CLT panel lay-ups were used: 1) 139 mm and 2) 175 mm thick 5-ply panels with individual layer thicknesses of 35-17-35-17-35 mm and 35-35-35-35-35 mm, respectively. The material was provided by Structurlam [78] and produced in accordance with ANSI/APA PRG320 [79]. The grade E1M4 panels were made from SPF species with an apparent density (based on the average of the weight and volume of the specimen) of 484 kg/m³ and a coefficient of variation (CoV) of 2.6% for the 139 mm CLT and 456 kg/m³ (CoV of 3.2%) for the 175 mm CLT.

The moisture content (MC) of each specimen was measured with an electronic resistance moisture meter at three different locations and then averaged for each test series. It was determined as on average 12.6% with a CoV of 2.2%. Based on the results of Phase 1, it was decided to limit CLT panel size to the 139 mm thickness for the subsequent Phases 2 and 3. In Phase 2, the 5-ply CLT panels were cut to length perpendicular to the major strength axis. The apparent density (based on the average of the weight and volume) was determined as 481 kg/m³ (CoV of 2.4%) with the average MC of 11.3% (CoV of 3.2%) and in Phase 3, the apparent density was measured as 509 kg/m³ (CoV of 2.9%) with the MC of 11.6% (CoV of 7.0).

3.2.2 Steel rod

ASTM A193 B7 [80] steel rods of diameter 1/2" (12.7 mm) and 3/4" (19.1 mm) were used for Phases 1 and 2. In Phase 3, multiple rods of only the 12.7 mm diameter were used. The yield strengths of the rods were experimentally determined following the standard test methods for tension testing of metals as outlined in ASTM E8/E8M [81]. These rods were cut to length from the supplier and no surface treatment was done. Five

samples for each rod diameter was inserted into a collet grip and tested in a 250 kN hydraulic Universal Test Machine (UTM), see Figure 3.2a. The yield strengths were determined as on average 658 MPa and 681 MPa for the 1/2" and 3/4" rods, respectively, with CoVs of 8% and 15%. Failure in all specimens occurred as necking, see Figure 3.2b.

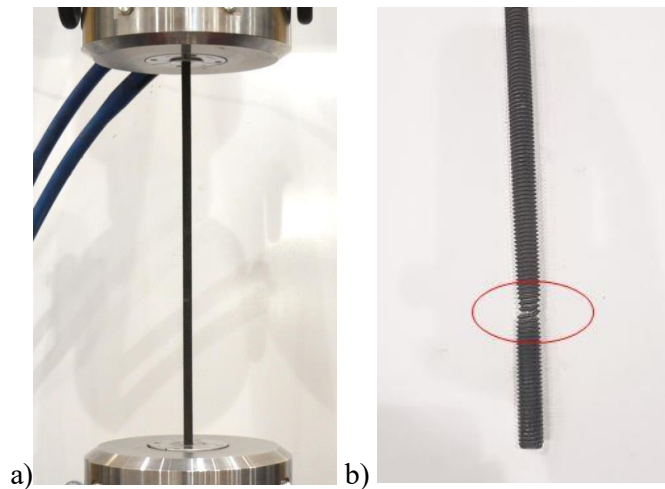


Figure 3.2: Steel rod tensile strength: a) test set-up; b) failed specimen

3.2.3 Adhesive and adhesive shear strength

Two-component polyurethane adhesive Loctite CR 821 Purbond, manufactured by Henkel, was used herein. As this adhesive was still not commercially available at the time of this study, information on the mechanical specification was not yet provided in a datasheet. The adhesive shear strength was experimentally determined following the standard test method for apparent shear strength of single-lap-joint of metal-to-metal bonded specimens by tension loading as outlined in ASTM D1002-10 [82]. Grade A36 steel plates, 102 x 25.4 mm and 6.35 mm thick, were used for the shear test. The overlap length and width of each specimen to be bonded were dimensioned to 25.4 x 25.4 mm for a gluing area of 625 mm². To avoid any potential contaminants (such as grease, oil, dirt, dust and rust particles) that may affect the results, the steel surfaces were cleaned with ethanol before applying the adhesive. The specimens were tested on a 100 kN hydraulic

UTM (see Figure 3.3a) at a displacement control rate of 1 mm/min. In total, 10 test samples were fabricated and tested. Failure in all specimens occurred at the bonding interface, see Figure 3.3b. The tensile force from the test frame was divided by the adhesive overlap shear area to obtain the shear strength of the adhesive at failure as on average 7 MPa, with a CoV of 22%.

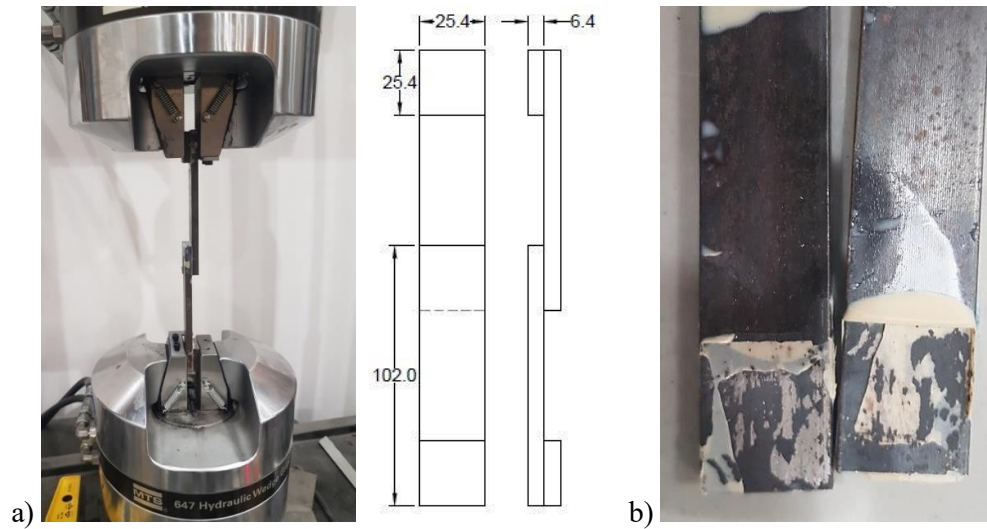


Figure 3.3: Adhesive shear strength tests: a) test set-up; b) typical failed specimen

3.3 GiR Specimen configurations

3.3.1 Phase I

Phase I consisted of 19 test series. In most series, the rods were completely glued-in all along the embedment length. In some selected test series, labelled with the # symbol, the rods were partially left un-glued ($l_u = 4d$) inside CLT. For the completely glued specimens, most CLT specimens were 200 mm wide and 600 mm long with two different thicknesses ($t = 139$ and 175 mm). Some selected test series consisted of 150 mm wide and 800 mm long panels.

Two different steel rod diameters $d = 12.7 \text{ mm}$ (1/2") and 19.1 mm (3/4") and four different anchorage lengths $l_a = 6d$, $10d$, $14d$ and $18d$ were used. Figure 3.4a illustrates all geometry parameters: l is the length of the CLT panel, l_c the clearance between the opposite rods in each specimen, l_r , the rod length, e_d the edge distance and l_u the unglued anchorage length.

To avoid wood splitting and glue line failure, the test specimens were designed with the minimum requirements for edge distance and glue line thickness as reported for solid timber and glulam [41, 57], $4d$ and 1.6 mm were used.

Each specimen combination had five replicates. In total, 18 test series for a total of 90 specimens were fabricated and subsequently tested, see Figure 3.4 and

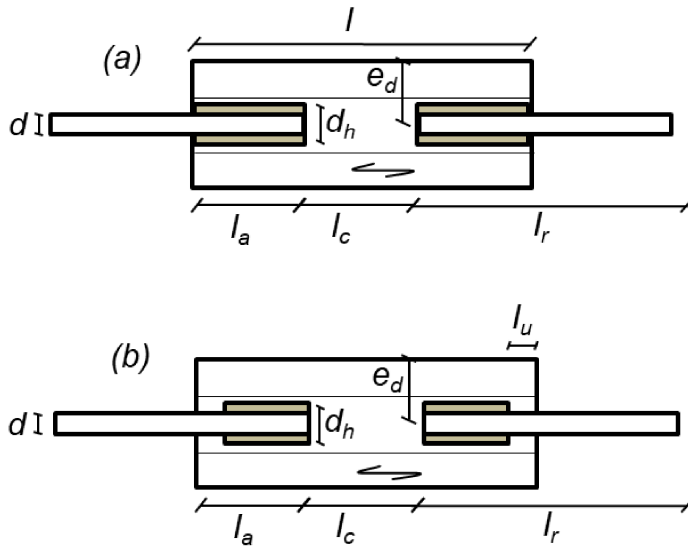


Figure 3.4: Single rod schematic for (a) completely and (b) partially bonded rods

Table 3.1. The series naming consisted of the rod diameter in inches (1/2 or 3/4), followed by anchorage length ($6L$, $10L$, $14L$ or $18L$) and the panel thickness (139 or 175). The test series with partially un-glued specimens see Figure 3.4b, included two different anchorage lengths ($l_a = 6d$ and $10d$) and were labelled as $6L\#$ and $10L\#$, respectively.

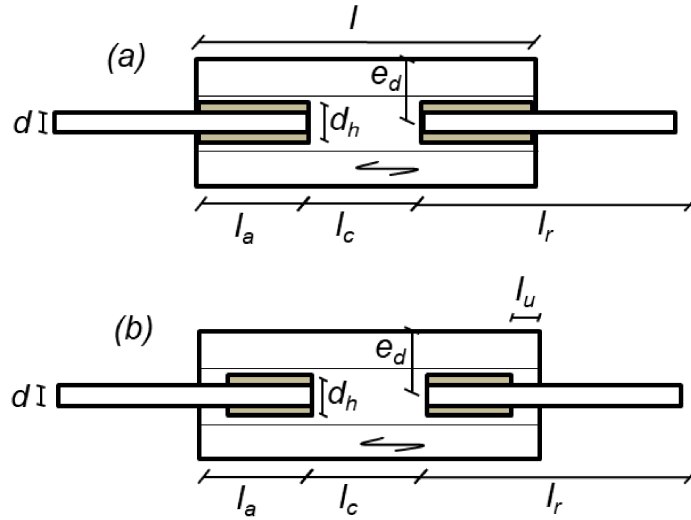


Figure 3.4: Single rod schematic for (a) completely and (b) partially bonded rods

Table 3.1: Test series overview for Phase I

Label	t (mm)	d (mm)	d_h (mm)	l (mm)	l_a (mm)	e_d (mm)	l_u (mm)	l_c (mm)	l_r (mm)
1/2-6L-175	175	12.7	15.9	600	76	100	-	448	376
1/2-10L-175	175	12.7	15.9	600	127	100	-	346	427
1/2-14L-175	175	12.7	15.9	600	178	100	-	244	478
3/4-6L-175	175	19.1	22.2	600	114	100	-	371	264
3/4-10L-175	175	19.1	22.2	600	191	100	-	219	491
3/4-14L-175	175	19.1	22.2	600	267	100	-	67	567
1/2-6L-139	139	12.7	15.9	600	76	100	-	448	376
1/2-10L-139	139	12.7	15.9	600	127	100	-	346	427
1/2-14L-139	139	12.7	15.9	600	178	100	-	244	478
1/2-18L-139	139	12.7	15.9	600	229	75	-	143	404
3/4-6L-139	139	19.1	22.2	600	114	100	-	371	414
3/4-10L-139	139	19.1	22.2	600	191	100	-	219	491
3/4-14L-139	139	19.1	22.2	600	267	100	-	67	567
3/4-18L-139	139	19.1	22.2	800	343	75	-	114	518
1/2-6L#-139	139	12.7	15.9	600	76	75	51	244	353
1/2-10L#-139	139	12.7	15.9	600	127	75	51	143	404

3/4-10L#-139	139	19.1	22.2	600	191	75	76	67	442
3/4-10L#-139	139	19.1	22.2	800	267	75	76	114	518

3.3.2 Phase 2

Most specimens in Phase 2 were composed of 200 mm wide and 500 mm long CLT strips cut out from larger panels. Series $3/4-18L-139p$ and the Lp series, comprised of 200 mm wide and 800 mm long and 400 mm wide and 500 mm long panels respectively. The panel sizes were dimensioned to ensure sufficient spacing between opposite glued rods so that no stress interactions existed between the two rods. Two-rod diameters ($d = 12.7$ and 19.1 mm) and three anchorage lengths ($l_a = 6d$, $12d$ and $18d$) were used. The geometry parameters are illustrated in Figure 3.5.

Each test series comprised of 5 fabricated replicates. A total of 8 test series (see Table 3.2) were combined in 40 specimens. The series naming consisted of the rod diameter in inches ($1/2$ or $3/4$), followed by the anchorage length ($6L$, $12L$ or $18L$), the panel thickness (139) and the letter p indicating that the series was cut perpendicular to the major strength axis. The letter L indicated that a large panel with the width 400 mm was used. For the test series $1/2-12L-139Lp$ and $3/4-12L-139Lp$, the steel rod was glued at only one end of the panel rather than both ends.

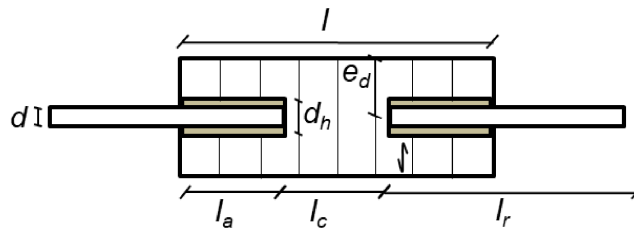


Figure 3.5: Schematic for single rods perp. to the major strength axis of CLT

Table 3.2: Test series overview for Phase 2

Label	t (mm)	d (mm)	d_h (mm)	l (mm)	l_a (mm)	e_d (mm)	l_c (mm)	l_r (mm)
1/2-6L-139p	139	12.7	15.9	500	76	100	348	251
1/2-12L-139p	139	12.7	15.9	500	152	100	195	327
1/2-18L-139p	139	12.7	15.9	500	229	100	43	404
3/4-6L-139p	139	19.1	22.2	500	114	100	271	289
3/4-12L-139p	139	19.1	22.2	500	229	100	43	404
3/4-18L-139p	139	19.1	22.2	800	343	100	114	518
1/2-12L-139Lp	139	12.7	15.9	500	152	200	-	327
3/4-12L-139Lp	139	19.1	22.2	500	152	200	-	327

3.3.3 Phase 3

The test series in Phase 3 involved the use of multiple rods on each panel, only one-rod diameter ($d = 12.7$ mm) was considered and these were glued at only one end of each specimen, see Figure 3.6. Two anchorage lengths ($l_a = 10d$ and $18d$) were considered. Two numbers of rods ($n_r = 2$ and 3) were investigated using two spacings ($s = 4d$ and $6d$). To avoid splitting failure, in accordance to the recommendations of previous work [13, 54, 67] that the minimum edge distance of at least $3d$ should be used to avoid this failure, the edge distance ($e_d \geq 4d$) was used. In Phase 3, 8 test series with 5 replicates per series for a total of 40 specimens were tested. The series naming consisted of the number of rods; $2r$ and $3r$ for two and three rods, the embedment length ($10L$ or $18L$) and the spacing between rods ($4d$ or $6d$). Specimens were made from 250 mm wide 5-ply CLT panels and either 400 or 500 mm long, see Table 3.3.

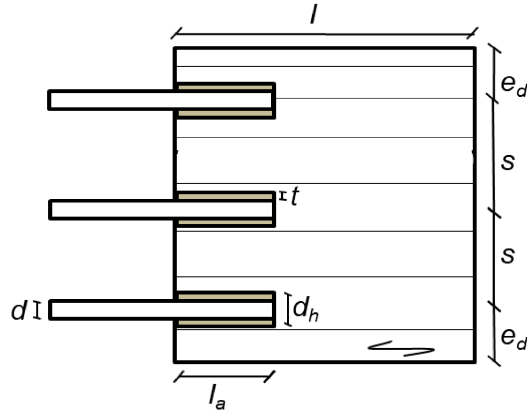


Figure 3.6: Schematic for multiple rods par. to the major strength axis of CLT

Table 3.3: Test series overview for multiple rods in Phase 3

Label	t (mm)	d (mm)	n_r	l (mm)	l_a (mm)	l_r (mm)	e_d (mm)	s (mm)
2r-10L-4d	139	12.7	2	400	127	302	99.5	51
3r-10L-4d	139	12.7	3	500	127	302	74	51
2r-10L-6d	139	12.7	2	400	229	404	87	76
2r-18L-6d	139	12.7	3	500	229	404	87	76
2r-18L-4d	139	12.7	2	400	127	302	99.5	51
3r-10L-6d	139	12.7	3	500	127	302	49	76
3r-18L-4d	139	12.7	2	400	229	404	74	51
3r-18L-6d	139	12.7	3	500	229	404	49	76

3.4 Specimen fabrication

The CLT specimens were cut from larger full-size panels and into the dimensions specified in section 3.2. Subsequently, holes were drilled into the CLT using a hand drill with custom-made jigs as a guard for proper alignment (Figure 3.7a). Holes with diameters $d_h = 15.9$ and 22.2 mm for the 12.7 and 19.1 mm diameter rods, respectively, each approx. 3 mm larger than the actual rod diameter, were drilled to allow for a 1.6 mm glue-line thickness. The holes were cleaned with compressed air to remove the residual sawdust and wood shavings. The adhesive was injected into the drilled hole using a

pneumatic glue gun to provide a reliable mix of the two-components. Calculated quantities of adhesives were injected in each hole (Figure 3.7b) and the rods were inserted in the holes by twisting them along the way to remove any trapped air. The rods were positioned straight and held in place with the use of toothpicks distributed around the circumference of the holes (Figure 3.7c). For the multiple rod test series in Phase 3, multiple holes were drilled into the CLT panels based on the required spacing between the rods. The glued specimens were left to cure and placed in a controlled climate room for at least 14 days before testing (Figure 3.7d).

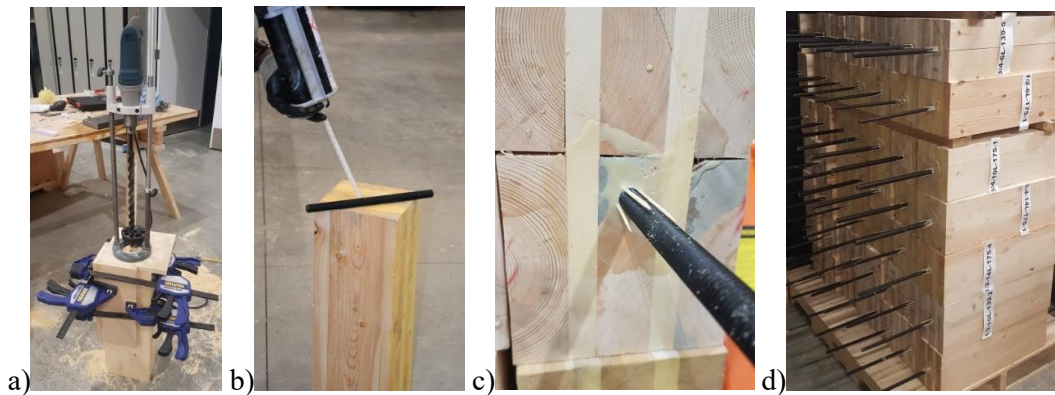


Figure 3.7: Specimen manufacturing: (a) hole drilling; (b) applying adhesive; (c) rod positioning; (d) specimen storage

3.5 Test methods

The tests were performed in a pull-pull configuration using a 500 kN hydraulic UTM in the Wood Innovation and Research Lab at the University of Northern British Columbia, Prince George, Canada. Threaded cylindrical steel sleeves were attached to the rods at both ends and inserted into the hydraulic collet grips attached to the testing machine. The collet grips held the rods firmly in position and also ensured the precise alignment during testing, see Figure 3.8a.

A steel plate (90 x 0.5 x 160 mm) was attached to each rod. Two Linear Variable Differential Transformers (LVDTs) were installed on both ends of the test specimens touching these steel plates to measure the relative displacements between the rods and CLT panel. A displacement-controlled rate of 1 mm/min was used so that each test was typically completed in approximately 5 minutes. The applied load was recorded by the test machine's calibrated load cell and subsequently plotted against the LVDT relative displacement measurement.

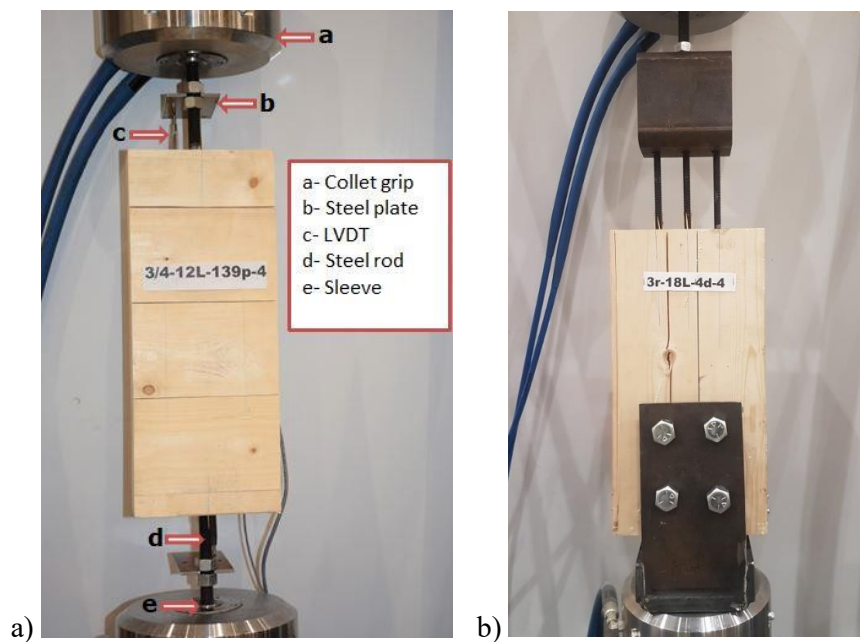


Figure 3.8: Test set-up for: a) Phase 1 and 2; b) Phase 3

In accordance to previous work [8], which showed that the first tests on two ended GiR test specimens did not significantly damage the surviving connection end, two-ended GiR test specimens were used for specimens from Phase 1. Upon failure of the connection in the first test, the rod on the failed specimen side was cut off and the unbroken second GiR was re-tested.

For the specimens with multiple rods from Phase 3, two or four holes (depending on the expected capacity of each test series) were drilled into the sides of the panels. Steel test

fixtures (see Figure 3.8b) were designed (see Appendix A: GiR test fixture) and Grade 8 steel bolts (22 mm) were used to attach the CLT panel from Phase 3 and retesting specimens from Phase 1 to the UTM. To attach the multiple rods to the testing machine, additional test fixtures were designed and fabricated. In Phase 3, no LVDTs were mounted to the individual rods; rather, the recorded actuator head movement was used as a proxy for the relative displacement between rod and CLT.

The results were assessed in terms of the load-carrying capacity (F_{\max}), the displacement at capacity ($\delta_{F,\max}$), and the initial stiffness (k). The latter was evaluated for the loading range between 10% and 40% of load-carrying capacity.

3.6 Statistical analyses

Analysis of variance (ANOVA) was performed to determine the effects of the considered individual connection parameters (anchorage length, rod diameter, number of rods and spacing between rods) and their interactions on the strength of the connection. ANOVA can be used to compare means and to determine the statistical significance of observed differences in means [83]. In an ANOVA, a p-value is computed to indicate the probability of accepting or rejecting the null hypothesis – usually stating that there is no effect of the treatments on the outcome. Thus, the p-value helps to decide whether a null hypothesis can be accepted or rejected. For all tests, this p-value was compared to a significant level (α). As typical in engineering practice, the significant level (α) of 0.05 was used [84]. In any cases where the p-value was less than or equal to α , the factor was accepted as significant and where the p-value was more than α , the factor was deemed insignificant. For those tests, where interactions between these parameters showed evidence that the means were significant, Tukey's multiple comparison test was conducted. Tukey's multiple comparison test, also called Tukey's honest significant

difference (HSD) test, is a pairwise comparison technique that can be used to determine which means amongst several means differ from the others [85].

For Phase 1, a blocked factorial design was chosen. The panel thicknesses (139 mm and 175 mm) were treated as a block. Blocking is useful in the reduction of unit variance with the expectation that similar responses may be received from units within a block [83]. The first factor; anchorage length had four levels ($6d$, $10d$, $14d$ and $18d$) and the second factor; rod diameter had two levels (12.7 and 19.1 mm). All test series consisting of the different combinations of these factors with their load-capacity were statistically analysed. For Phase 2, two-way ANOVA was performed. The first factor; anchorage length had three levels ($6d$, $12d$ and $18d$) and the second factor; rod diameter had two levels (12.7 and 19.1 mm). For Phase 3 consisting of multiple rods, a three-way ANOVA was performed. The first factor; anchorage length has two levels ($10d$ and $18d$), the second factor; number of rods had three levels (1, 2 and 3) and the third factor; spacing between rods had two levels ($4d$ and $6d$). In all three Phases, following the determination of the “main effects”, the interactions between the factors were analysed and Tukey’s HSD test was performed on the individual parameter combinations.

4 Results and discussion

4.1 Phase 1: single rod parallel to major CLT strength axis

4.1.1 Overview

Table 4.1 provides a summary of the results from the 18 series tested in Phase 1 with the average values and their respective CoVs. For $\delta_{F,\max}$ and k , the reported values are for the failed side of the test specimen.

Table 4.1: Summary of test results for Phase 1

Series	F_{\max} [kN] [CoV%]		$\delta_{F,\max}$ [mm]		k [kN/mm] [CoV%]	
	Test	Retest	Test	Retest	Test	Retest
1/2-6L-139	25.5 (41%)	35.3 (14%)	0.4	2.9	93.6 (>50%)	13.8 (>50%)
1/2-6L-175	26.0 (8%)	33.0 (11%)	1.4	2.0	29.1 (>50%)	13.5 (50%)
1/2-10L-139	49.9 (12%)	51.4 (18%)	1.1	2.9	154.2 (>50%)	23.1 (>50%)
3/4-6L-175	51.3 (17%)	52.0 (13%)	0.6	1.4	511.4(>50%)	79.6 (>50%)
1/2-10L-175	55.2 (17%)	62.6 (17%)	1.1	1.9	54 (47.5%)	61.8 (>50%)
3/4-6L-139	60.4 (13%)	61.3 (10%)	1.2	1.6	66.6 (>50%)	65.8 (>50%)
1/2-14L-139	60.6 (8%)	65.2 (12%)	2.0	2.6	246.1 (>50%)	29.5 (>50%)
1/2-14L-175	67.8 (10%)	76.2 (10%)	2.0	2.7	136.8 (>50%)	45 (42%)
1/2-18L-139	69.3 (9%)	75.2 (13%)	1.4	4.4	65.7 (37%)	445.4 (>50%)
3/4-10L-139	86.3 (13%)	99.3 (19%)	1.1	1.8	351.2 (>50%)	67.6 (>50%)
3/4-10L-175	95.9 (14%)	99.0 (11%)	1.1	1.6	141.2(>50%)	160.8 (>50%)
3/4-18L-139	103.4(25%)	146.8 (21%)	0.9	2.3	162.7 (45%)	62.4 (>50%)
3/4-14L-139	111.9 (19%)	111.5 (21%)	1.0	1.4	168.9 (>50%)	176.6 (>50%)
3/4-14L-175	115.0 (18%)	130.0 (18%)	1.2	1.7	340.3 (>50%)	511.1 (>50%)
1/2-6L#-139	38.6 (20%)	38.8 (19%)	1.0	1.7	39.7 (32%)	100.1 (>50%)
3/4-6L#-139	51.7 (23%)	71.5 (27%)	0.8	1.5	209.2 (>50%)	54.5 (>50%)
1/2-10L#-139	58.1 (13%)	66.0 (6%)	1.5	1.9	47.5 (47%)	72.7 (>50%)
3/4-10L#-139	64.7 (10%)	88.5 (11%)	0.3	1.8	333.5 (>50%)	72.9 (>50%)

The test series average load-carrying capacities as a function of the investigated geometric parameters ranged from 25 to 147 kN. Within the range of the parameters investigated, there was an increase in load-carrying capacity with increasing anchorage length up to the length of $14d$ beyond which no further increase was observed. The load-carrying capacity increased with the rod diameter between 39% and 81% for the same embedment length. The panel thickness did not have any impact on the load-carrying capacity. The displacements at maximum load ranged from 0.3 to 4.4 mm. The displacements at failure of the retested specimens were higher than those from the first tests. The test series average joint stiffness ranged from 40 to 511 kN/mm. These values, however, were characterised by high variability ($\text{CoV} > 50\%$) for most series. No consistent increase in load-carrying capacity was observed for the partially glued test series. The CoVs for those series were between 6 and 27% higher than that of the completely glued test series. The retested specimens exhibited higher capacities than the first test for all test series.

4.1.2 Load-displacement behaviour

Figure 4.1 shows the load-displacement curves of a typical specimen from each test series. All individual load-displacement curves are provided in Appendix B: Load-displacement curves from Phase 1. The responses were linear up to failure in most cases except for a few where small decreases in stiffness were observed just before reaching F_{\max} . All test specimens exhibited very small displacements at failure (between 0.5 and 3 mm) with no ductility.

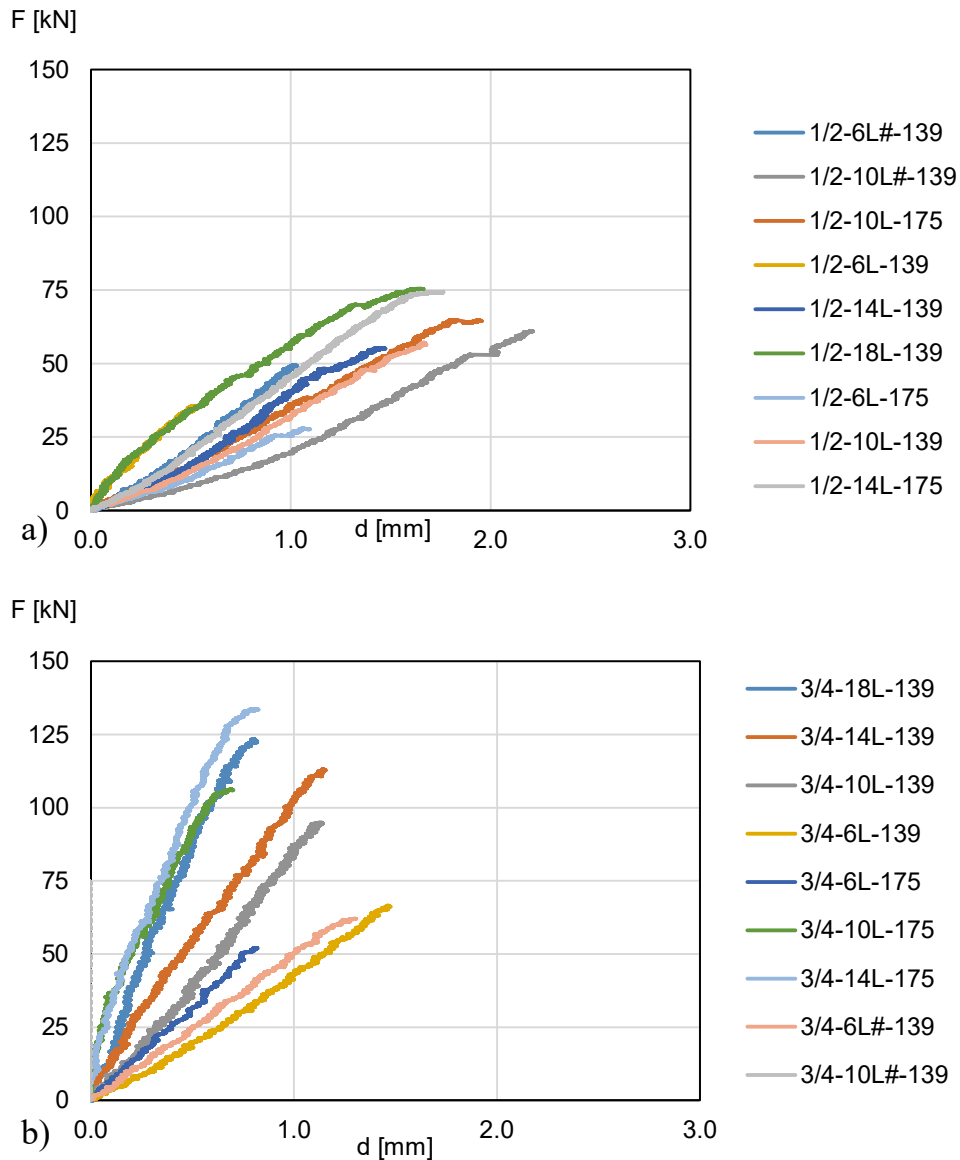


Figure 4.1: Load-displacement curves of selected specimen for each series from Phase 1: a) 12.7 mm rods and b) 19.1 mm rods

4.1.3 Failure modes

The typical failure modes, illustrated in Figure 4.2 and Figure 4.3, can be described as: 1) Rod pull-out at the interface between timber and the adhesive as a result of the loss of adhesion between the timber and adhesive (c.f. Figure 4.2a,b,d,e); and 2) Wood plug pull-out failure which is the shear failure in timber (c.f. Figure 4.3d,f-i).

The failure mode depended on the rod diameter and the anchorage length. For the specimens with 12.7 mm rods, independent of anchorage length and regardless of the panel thickness, the typical failure mode was the pull-out of the rod characterised by the failure at the interface between adhesive and wood, c.f. Figure 4.2.

However, for the specimens with 19.1 mm rods, the failure mode observed for both panel thicknesses was wood plug failure in which a large volume of the wood surrounding the rod away from the adhesive failed. In most instances, it was observed that the wood plug was larger for the longer anchorage length $10d$, $14d$ and $18d$ (Figure 4.3d,f-i) and smaller for the shorter lengths $6d$ and $10d$ (Figure 4.3a,b,e). It should be noted that some of the rods were glued in-between two non-glued edges of timber in the same CLT layer and also near the non-edge glued timber in other next layers. This could have contributed to the type of failure modes obtained.

In all test series, just as no adhesive failure was recorded, none of the specimen split. Independent of the CLT layup, the rods were glued parallel to the grain into the CLT core layer. Hence, there was no interference of the rod between two-panel laminations.

For the partially glued specimens where the anchoring zone was shifted to the inner part of the timber, the failures were internal, c.f. Figure 4.2c,g and Figure 4.3c, confirming that moving this anchoring zone worked as desired by moving the shear away from the surface. In all specimens, no visible crack or splitting failure of CLT occurred.



Figure 4.2: Typical failure modes for 12.7 mm GiR par. to the major strength axis



Figure 4.3: Typical failure modes for 19.1 mm GiR par. to the major strength axis

4.1.4 Statistical analysis (Phase 1)

Table 4.2 provides the summary of the ANOVA conducted for Phase 1. The results provide strong evidence that the parameters rod diameter and anchorage length are statistically significant for the joints load-carrying capacity. Furthermore, the results confirmed that the interaction between the rod diameter and the anchorage length is statistically significant. These factors with their interactions are explaining a significant proportion of the variance, with the R^2 value of 0.79.

Table 4.2: Summary of ANOVA for Phase 1

Factor	<i>p</i> -value
<i>d</i>	<0.0001
<i>l_a</i>	<0.0001
<i>d</i> * <i>l_a</i>	<0.0001

Additionally, knowing the influence of the levels of the significant factors on the load-carrying capacity of the connection is important; to evaluate this, Tukey's HSD test was performed. The results are summarized in Table 4.3 in which all interactions between the levels of the factors are represented. The interaction levels having the same letter are not significantly different and those with no letter in common are significantly different. Since the panel thickness has been assigned a blocked factor, the Tukey's HSD test was performed on the interaction between the variables rod diameter and anchorage length. Considering the rod diameter interaction with the anchorage lengths $18d$, $14d$, $10d$ and $6d$, while for the 19.1 mm rod, the result indicates that the capacity of the connection at the anchorage length of $18d$, is not significantly different from the anchorage length of $14d$ (they both share A) it is significantly different for the lengths $10d$ and $6d$. This implied that for this rod diameter, increase in the anchorage length from $18d$ to $14d$ did not have a significant impact, in agreement with the observations made earlier. The load-carrying capacities at the anchorage lengths of $14d$, $10d$ and $6d$ are all significantly

different. The 19.1 mm rod at the embedment length of $18d$ had the highest mean difference thereby having the greatest influence on the load capacity of the connection followed by $14d$, $10d$ and lastly $6d$. Similarly, for the smaller rod diameter of 12.7 mm, the length of $18d$ is not significantly different from the length of $14d$. This implied that for this rod diameter, increase in the anchorage length from $18d$ to $14d$ did not make any difference from the length $14d$. Although the 12.7 mm rod at the length of $6d$ (marked by D) is significantly different from the anchorage lengths of $18d$ and $14d$, there is no statistically significant difference for the 12.7 mm rod at the length of $10d$.

Table 4.3: Summary of Tukey test results for Phase 1

Category	Groups
$d-19.1*l_a-18d$	A
$d-19.1*l_a-14d$	A
$d-19.1*l_a-10d$	B
$d-12.7*l_a-18d$	B C
$d-12.7*l_a-14d$	B C
$d-19.1*l_a-6d$	C
$d-12.7*l_a-10d$	C D
$d-12.7*l_a-6d$	D

4.1.5 Discussion

From the results summarized in Table 4.1, it can be observed that F_{\max} increased with increase in l_a . This increase is attributable to the increased surface area for bonding at the rod/adhesive and timber/adhesive interface. The relations between the load-carrying capacity and embedment length across the two-panel thicknesses is illustrated in Figure 4.4 and Figure 4.5 for the 12.7 and 19.1 mm diameter rods, respectively.

Considering the specimen sides that failed first, for the 139 mm panel and the four anchorage lengths under consideration ($6d$, $10d$, $14d$ and $18d$), the greatest increase in the average capacity was seen from $6d$ to $10d$ while smaller increases were observed between

10d and 18d. A similar increasing trend was observed for the 175 mm panel. The average load-carrying capacity more than doubled from 6d to 10d and only increased by another 20% to 14d.

For the partially glued specimens, F_{max} also increased by 51% from 6d to 10d with higher l_a . Interestingly, for the 19.1 mm rod in the 139 mm panels, the load-carrying capacity in the partially glued specimens was higher than in the completely glued ones, 51% and 16% for 6d and 10d, respectively.

Comparing the retest results with the first test result, the load-carrying capacities of the retested specimen irrespective of the panel thickness were consistently higher than the first test specimens except for the 3/4-14L-139 test series which were equal (112 kN). Increases of up to 35% (3/4-18L-139) were obtained in comparison to the first test. Furthermore, the shorter embedment length specimens (specifically 6d) tend to have very similar capacities between the first test and retest.

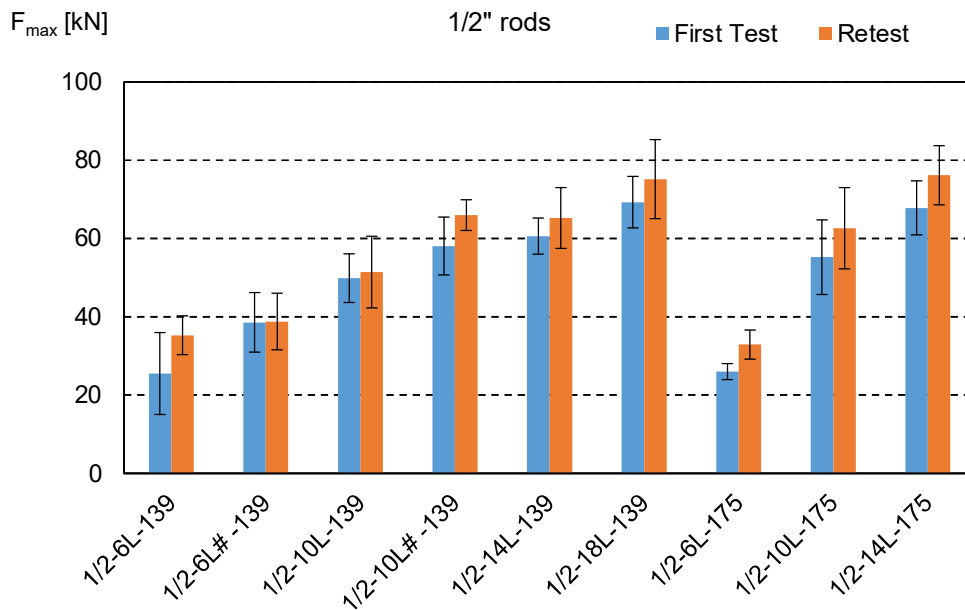


Figure 4.4: Effect of anchorage length and panel thickness on F_{max} with 12.7 mm GiR

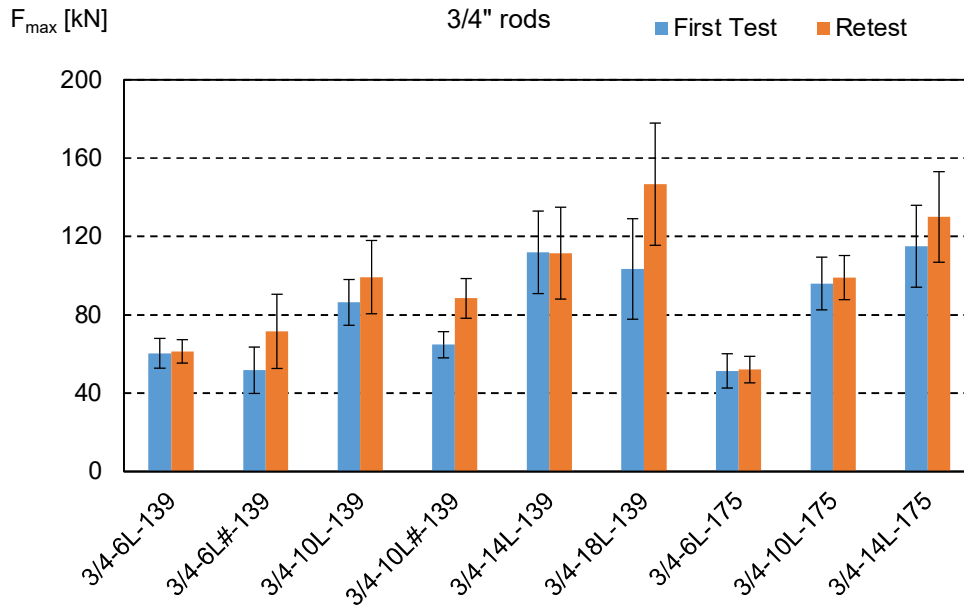


Figure 4.5: Effect of anchorage length and panel thickness on F_{max} with 19.1 mm GiR

For the 19.1 mm diameter rods, for both partially and completely embedded rods, the results obtained were similar to those reported for the 12.7 mm rods. In general, the capacity increased from lower anchorage length ($6d$) to higher length ($10d$ and $18d$) but reduced gradually with increase in anchorage length. Figure 4.5 also shows that there is no remarkable difference between the results obtained for the 139 and 175 mm panel thickness.

Figure 4.6 shows the effects of the rod diameters on the load-carrying capacity. Unlike the 12.7 mm rods, which increased for all embedment lengths considered, the increase in the 19.1 mm rods was observed until the embedment length reached $14d$ (267 mm). From the length $14d$ to $18d$ (343 mm), the load-carrying capacity of the 19.1 mm steel rod decreased by 10%. Although as stated earlier, no significant difference exists between the two-panel sizes, it was observed that the 19.1 mm steel rod had a more visible shear failure evident by the removal of a large block of timber surrounding the rod in the 175 mm panels.

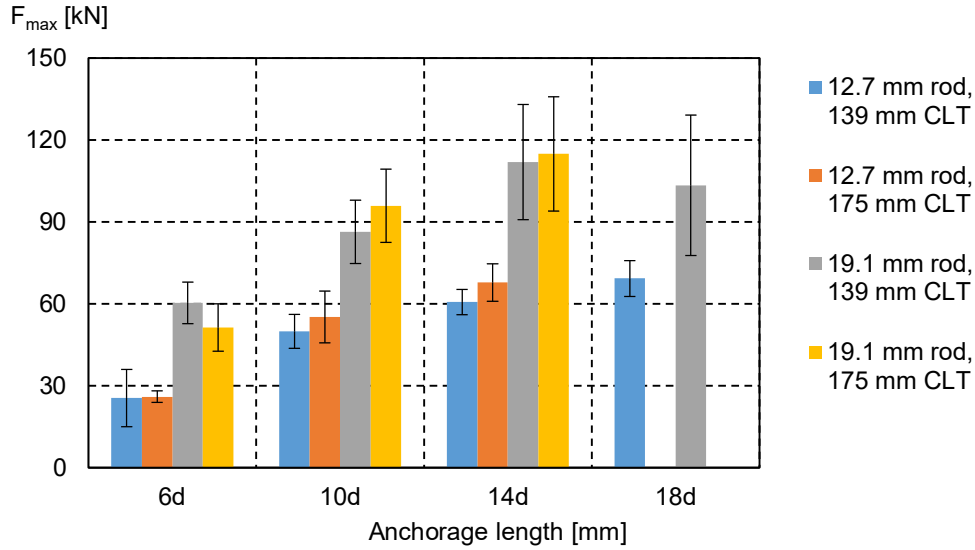


Figure 4.6: Effect of rod diameter on F_{max} (Phase 1)

4.1.6 Comparison to design equations

The experimental results of F_{max} were compared to the predictions using the GIROD design equation [49], see Figure 4.7, based on the hole diameters of 22.2 mm and 15.9 mm, and the panel thickness of 139 mm. In the calculations, the following parameter values were used: $E = 210$ GPa, $\tau_f = 7$ MPa, $E_w = 12.4$ GPa, $G_f = 1750$ Nm/m². The modulus of elasticity of the wood E was taken from the manufacturers technical design guide [78] for grade E1M4, τ_f was determined from the shear test, and the fracture parameters G_f and E_w from the literature [16].

Whereas the resulting load-carrying capacity from the GIROD design equation closely predicted the experimental data for the series with the smaller rod diameter (12.7 mm), the equation clearly overestimated the capacity of the connections for the series with the larger rod diameter (19.1 mm) at embedment lengths above 6d. Similarly, for the retest data of the 19.1 mm rod having higher load capacity, at the embedment lengths of up to 10d, the capacities of the retest series were higher than the design equation, beyond which the GIROD estimation became much higher.

It can therefore be stated that for the 19.1 mm rod, at lower embedment lengths up to 10d, the GIROD design equation closely represented the experimental data but at bonded lengths above 10d, the equation overestimated the joint capacity by up to 41%. Consequently, it is, therefore, a function of the rod diameter, anchorage length and the diameter of the hole.

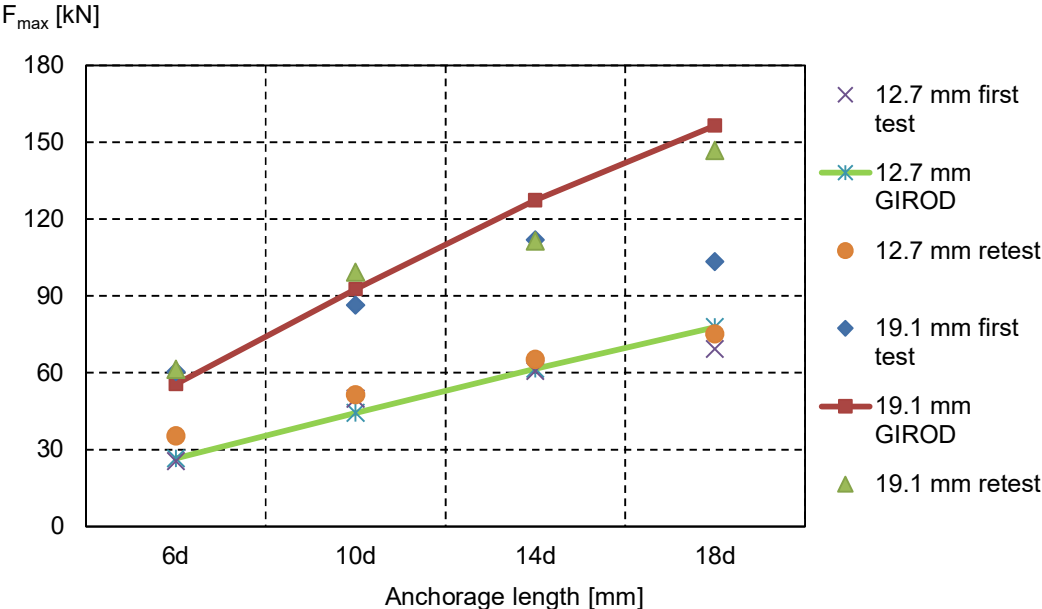


Figure 4.7: Comparison GIROD design precisions vs. experimental results from Phase 1

4.2 Phase 2: Single rod perpendicular to major CLT strength axis

4.2.1 Overview

Table 4.4 provides a summary of the test results from the 8 test series with the mean values and their respective CoV. The average load-carrying capacity of the test series ranged from 14 to 154 kN. In all test series, within the range of the parameters investigated, F_{max} increased with increasing l_a . The individual specimens exhibited a greater consistency evident by their low CoV values ranging from 3-15%. The specimens with the longest embedment length (18d) had the lowest CoV (3 and 6%) and those with

the shortest embedment length had the highest CoV (15%). The displacements at maximum load ranged from 0.9 to 6.3 mm and the test series with the larger panel width had the highest displacements. The average joint stiffness of the test series ranged from 39 to 306 kN/mm. However, some of these values were characterised by high variability (CoV > 50%).

Table 4.4: Summary of test results for Phase 2

Series	F_{\max} [kN] [CoV]	$\delta_{F,\max}$ [mm]	k [kN/mm] [CoV]
1/2-6L-139p	13.7 (15%)	0.9	305.6 (>50%)
3/4-6L-139p	41.2 (10.1%)	0.7	76.0 (9%)
1/2-12L-139p	43.5 (8.8%)	1.5	58.1 (>50%)
1/2-12L-139Lp	72.5 (10.7%)	6.3	38.9 (>50%)
1/2-18L-139p	79.6 (2.9%)	2.1	115.6 (>50%)
3/4-12L-139p	90.6 (7.9%)	1.1	117.8 (29%)
3/4-12L-139Lp	112.0 (8.3%)	2.0	107.9 (>50%)
3/4-18L-139p	154.4 (5.5%)	1.8	145.9 (26%)

4.2.2 Load-displacement behaviour

Figure 4.8 shows the load-displacement curves of a typical specimen from each test series. All individual load-displacement curves are provided in Appendix C: Load-displacement curves from Phase 2. There was a seemingly linear increase at the initial stage –in some instances– the curves flattened on reaching the maximum load. The specimens loaded perpendicular to the major strength axis exhibited the ability to continue carrying high loads after failure. The cross layering of the CLT panel may have accounted for this behaviour. Consequently, there was also less variability within each series; the load-displacement behaviour was reproducible. Despite the non-linear behaviour, none of the steel rods failed by yielding.

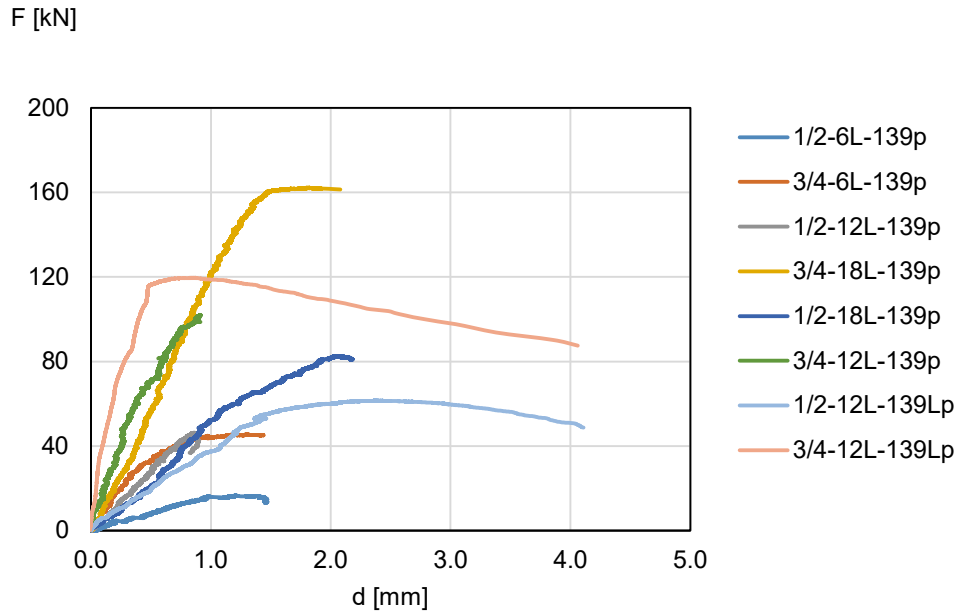


Figure 4.8: Load-displacement curves of selected specimen for each series from Phase 2

4.2.3 Failure modes

Figure 4.9 illustrates the typical failure modes observed. Unlike the failures seen in Phase 1, the failure modes observed in the specimens installed perpendicular to the major strength axis were mainly characterised by:

- 1) Partial tear-out of core CLT layer in which the first non-edge bonded panel lumber is detached from the panel (c.f. Figure 4.9a,b). This indicates the failure of the CLT adhesive.
- 2) Complete tear-out of core CLT layer. This was visible in specimens with longer anchorage length and 19.1 mm rod diameter rod (c.f. Figure 4.9c,d).
- 3) Shear failure of the CLT panel due to the edge lamination tear-out of the core CLT layer in which the rod is embedded (c.f. Figure 4.9e,f). This occurred in specimens having both rod diameters.

4) Timber failure due to rolling shear effect and panel splitting which primarily occurred in the series with the shorter panel width of 200 mm (c.f. Figure 4.9g,h).

It must be stated that in practice, the CLT panel size that will be used as a structural member will be larger than what was used in this experimental campaign. Consequently, failures like the rolling shear could be avoided if panel sizes were large enough. This assumption was confirmed with the two test series *1/2-12L-139Lp* and *3/4-12L-139Lp* with the increased panel width of 400 mm. In these two series, rolling shear and splitting of the panel did not occur but only the edge lamination tear-out and partial tear out of core CLT layer occurred. Although for all specimens in each test series, the rods were glued only in the core layer of each panel, a different failure may also have occurred if the rods were bonded between two CLT layers.

For specimens with the longer anchorage length ($12d$ and $18d$), a complete tear-out of the core CLT layer together with the rod and the edge lamination of the core layer was observed (see Figure 4.9c,d). The rod in each case was still intact and such connections may be said to not have reached their full capacity as clearly observed in Table 4.4. The only exceptions to this were the panels with the larger width sizes (*1/2-12L-139Lp* and *3/4-12L-139Lp* test series) where none of the panels had a complete tear-out of its layer nor did any split (see, Figure 4.9e,f). The panel width of 400 mm used for these two test series was sufficient to prevent splitting failure and complete tear-out of the panel core layer for both rod sizes considered.

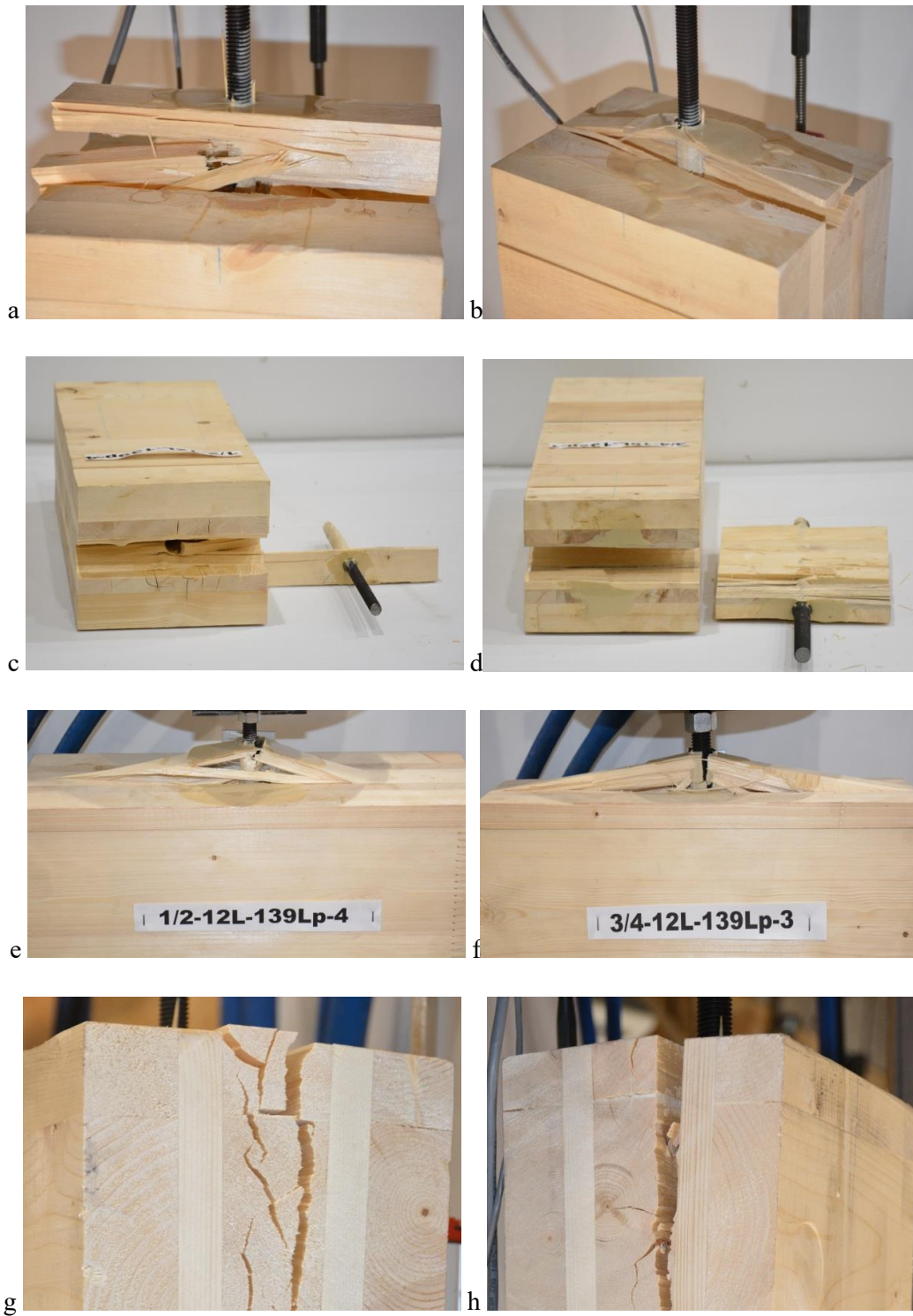


Figure 4.9: Typical failure modes for single GiR perp. to the major strength axis.

4.2.4 Statistical analysis (Phase 2)

Table 4.5 provides a summary of the ANOVA conducted for Phase 2. These results confirmed that the parameters rod diameter, anchorage length of the rods and the interaction between them are statistically significant for the joints load-carrying capacity. With a combined the R^2 value of 0.94, the rod diameter and the embedment length accounts for 32% and 62% of the variations, respectively.

Table 4.5: Summary of ANOVA for Phase 2

Factor	<i>p</i> -value
<i>d</i>	0.000
<i>l_a</i>	0.000
<i>d</i> * <i>l_a</i>	0.000

Tukey's HSD test was performed, see Table 4.6, where the factor levels having the same letter are not significantly different. For the 19.1 mm rod, the results confirmed that the three anchorage lengths ($6d$, $12d$ and $18d$) are significantly different. The difference was highest for the length $18d$, followed by $12d$ and then $6d$. Similarly, the anchorage lengths are significantly different for the 12.7 mm rod. The difference was highest at the longest length of $18d$. However, the 12.7 mm rod at the length of $12d$ is not different from the 19.1 mm rod embedded at the length of $6d$.

Table 4.6: Summary of Tukey's HSD test for Phase 2

Category	LS means	Groups
<i>d</i> -19.1* <i>l_a</i> -18 <i>d</i>	154.380	A
<i>d</i> -19.1* <i>l_a</i> -12 <i>d</i>	101.370	B
<i>d</i> -12.7* <i>l_a</i> -18 <i>d</i>	79.640	C
<i>d</i> -12.7* <i>l_a</i> -12 <i>d</i>	58.040	D
<i>d</i> -19.1* <i>l_a</i> -6 <i>d</i>	41.380	D
<i>d</i> -12.7* <i>l_a</i> -6 <i>d</i>	13.720	E

4.2.5 Discussion

As shown in Table 4.4 and Figure 4.10, F_{max} increased with increase in l_a for both rod diameters. One reason for this is the increase in the contact area for bonding at the rod/adhesive and timber/adhesive interface. The lowest capacity was recorded for the 12.7 mm rod at the embedment of $6d$. From $6d$, the capacity increased by 218% at $10d$ and at $18d$, increased by 481%. These larger increases were less for the 19.1 mm rod in which the capacities increased by 172 and 275% at $10d$ and $18d$ respectively.

Considering the test series $1/2-12L-139p$ and $1/2-12L-139Lp$ with the same anchorage length ($12d$) and rod diameter (12.7 mm) but different panel width (200 and 400 mm respectively), a considerable difference of 50% in their load-carrying capacity was achieved. Similarly, a difference of 21% was obtained for the series $3/4-12L-139p$ and $3/4-12L-139Lp$. In both cases, the wider panel (400 mm) achieved higher capacity than the 200 mm wide panels. This showed that the wider panel connections reached their full capacity before failure as against the other series that failed due to the splitting of the panels caused by insufficient panel width.

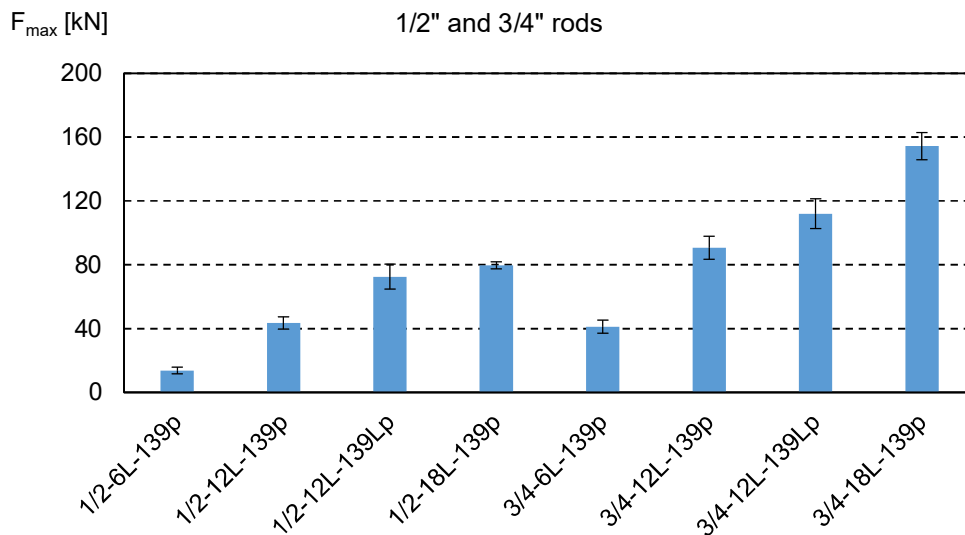


Figure 4.10: Effect of anchorage length on F_{max} for Phase 2

The lowest capacity, obtained at $6d$ (13.7 kN) is much lower than the value for the same l_a and panel configuration in Phase 1 (25.5 kN). Whereas for the other embedment lengths considered in this study and in [16] as well, the perpendicular to grain specimen consistently showed higher load carrying capacities than those connected parallel to the major strength axis, a similar lower capacity at the short embedment length of 80 mm for the perpendicularly bonded specimen was reported in [16]. It is therefore important that GiR to be bonded perpendicular to the grain should have sufficient embedment length larger than $6d$ when small-diameter steel rods are used (12.7 mm in this case).

The effects of the rod diameter on F_{max} are presented in Figure 4.11. The capacity of the connections increased with the increase in rod diameter. Across all embedment lengths, the higher diameter rod (19.1 mm) achieved a higher load-carrying capacity than the 12.7 mm steel rod. This ranged from 94% for the $18d$ length to 201% for the $6d$ anchorage length. This further support previous studies that have shown that increase in rod diameter increase the capacity of the connection [8, 16, 86].

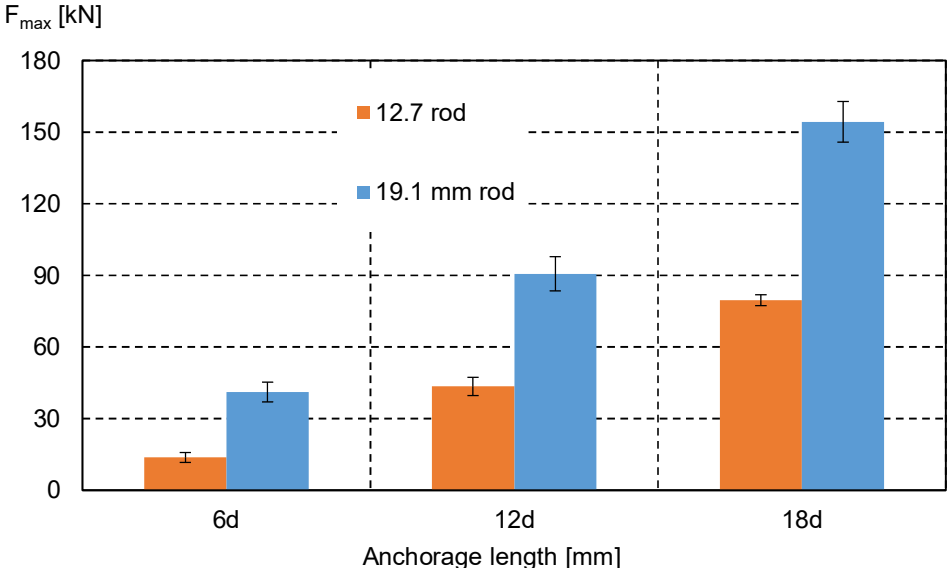


Figure 4.11: Effect of the rod diameter on F_{max} for Phase 2

4.2.6 Comparison to design equations

The results of the comparison between the load-carrying capacities of the experimental values and the GIROD design equation for the rod diameters 19.1 mm and 12.7 mm bonded perpendicular to the major strength axis of the CLT panels are shown in Figure 4.12 based on the hole diameters 22.2 mm and 15.9 mm respectively, and panel thickness 139 mm. For both rod diameters, within the range of the investigated parameters, the design equation overestimated the experimental values from the embedment $6d$ up to the highest embedment length of about $18d$. The differences were highest at the embedment length of $6d$, 64% for the 12.7 mm rod and 30% for the 19.1 mm rod. However, the design equation showed a tendency to continue to match and probably be higher than the experimental values at embedment lengths greater than $18d$. Considering the various parameters contributing to the pull-out strength of GiR bonded perpendicular in CLT and their failure modes, new design equations derived in consideration of these parameters are required.

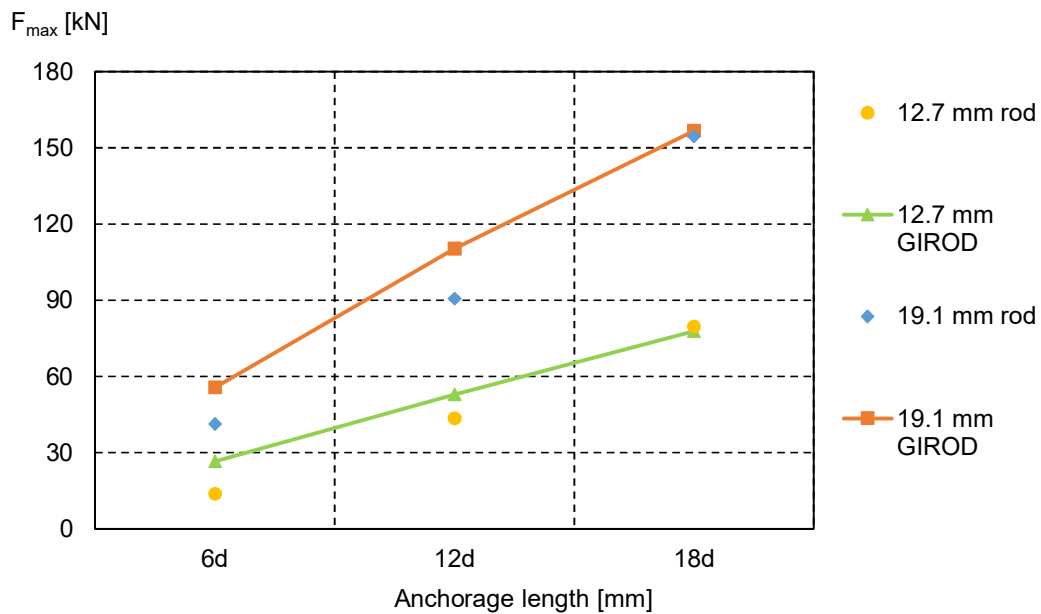


Figure 4.12: Comparison GIROD design equation vs. results from Phase 2

4.3 Phase 3: Multiple rods parallel to major strength axis of CLT

4.3.1 Overview

The summary of the results of the multiple rods test series is shown in Table 4.7. The average load-carrying capacity of the joints ranged from 50 to 167 kN. Generally, within the studied parameters in the series, the results show that with an increase in the number of rods, the distance between the rods and the embedment lengths of the rods in the panels; the capacity increased. The only exception to this is the test series *3r-10L-4d* where with 3 rods on the specimen at $4d$ rod spacing, it behaved like 2 rods spaced at $6d$ distance apart. The embedment length is seen to be of great importance to the overall capacity of the connection.

The displacements at maximum load ranged between 0.9 and 12.8 mm. The longest embedment length ($18d$) had the highest displacements. It should be noted that LVDTs were not used to record the displacements. Rather, measurements were taken directly from the test machine. Consequently, the connection's stiffness was not evaluated.

Table 4.7: Summary of test results for Phase 3

Series	F_{\max} [kN]	$\delta_{F,\max}$
1/2-10L	49.9 (12%)	0.8
1/2-18L	69.3 (9%)	1.4
2r-10L-4d	73.7 (28%)	5.3
3r-10L-4d	94.6 (13.1%)	5.9
2r-10L-6d	98.5 (12.8%)	8.6
2r-18L-6d	120.9 (3%)	12.8
2r-18L-4d	130.4 (10.9%)	10.3
3r-10L-6d	143.6 (11.3%)	9.0
3r-18L-4d	155.6 (13%)	11.4
3r-18L-6d	166.8 (11.1%)	10.4

4.3.2 Load-displacement behaviour

The load-displacement curves shown in Figure 4.13 shows the typical curves for the specimens from each test series at different anchorage lengths and rod spacing based on the numbers of rods. All individual curves from Phase 3 are provided in Appendix D. Generally, an increase in load with displacement is observed. This increase is however not linear. While the test series with embedment length of $l_a = 10d$ demonstrated increase up to failure with no plastic deformation (see Figure 4.13a), specimens with $l_a = 18d$ regardless of the rod spacing, exhibited a different behaviour. The $18d$ series (see Figure 4.13b) which was initially linear showed non-linear deformation behaviour up to failure. This was more obvious when multiple rods were used.

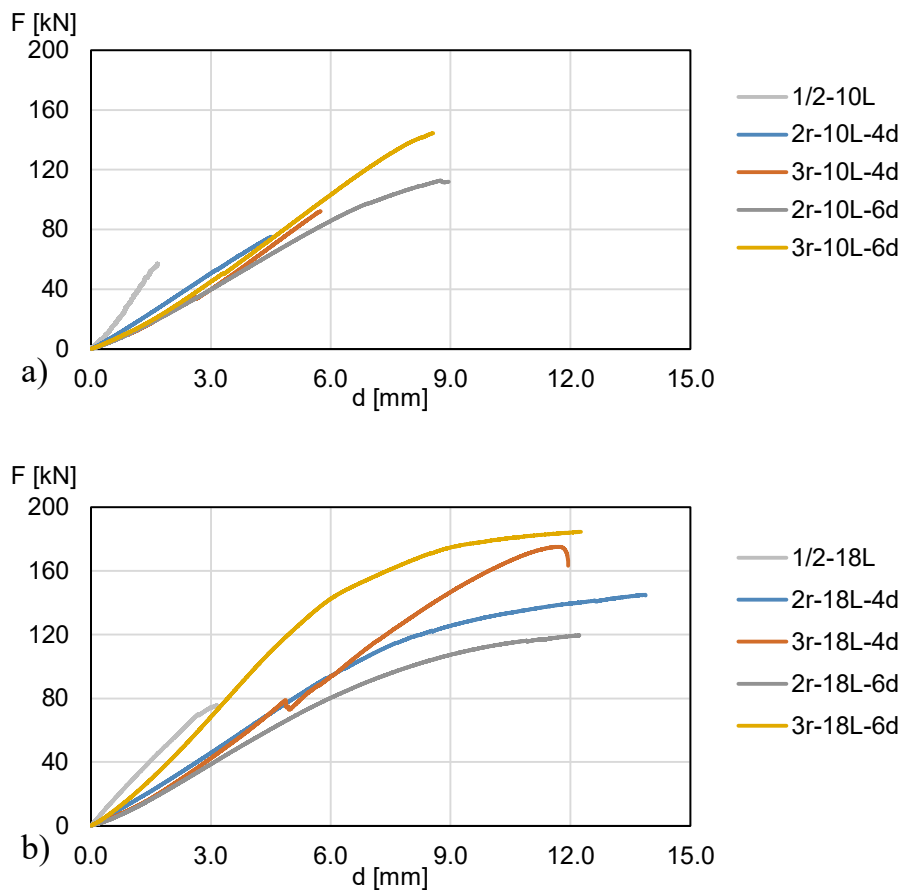


Figure 4.13: Load-displacement curves of selected specimen for each series from Phase 3: (a) $l_a = 10d$, $s = 4d$ and $6d$ (b) $l_a = 18d$, $s = 4d$ and $6d$

4.3.3 Failure modes

Figure 4.14 illustrates the typical failure modes observed in the multiple GiR test series. Similar to the failure modes obtained in Phase 1, independent of the number of rods on the specimens, two typical failure modes were observed namely: 1) Rod pull-out failure of wood at the interface between the adhesive and timber due to the loss of adhesion; and 2) Wood plug failure in which a large volume of the wood surrounding the rod away from the adhesive fails. This plug failure was caused by the shear failure of timber as evident in some of the specimens. Although with longer anchorage length and number of rods, the capacities of the connection increased, no visible difference was observed in the type of failure for the two embedment lengths. In a few specimens, a knot close to the glued rod contributed to the plug failure. These plug failures had no defined perimeter, they are sometimes large and extend to the neighbouring CLT panel lamella (Figure 4.14a), or very small (Figure 4.14b-d.)

As a result of the sufficient rod spacing ($4d$ and $6d$), there was no rod interference with other rods and no group tear out occurred. However, the failure of a rod is usually accompanied by the corresponding failure of another or more rods. It was noted in many of the specimens that failure of a rod usually triggered an accompanying failure in other rods even when the capacity of the connection was not yet reached. In some three-rods specimens (Figure 4.14e,f), one outer rod did not fail. This might have been caused by the uneven distribution of load between the rods from the crosshead due to deviations in either the orientation of the rod or the grain direction on the panel even as attempts were made to equally tighten the nuts attaching all rods to the test fixture. This led to different levels of stress on each rod end. In addition, since high-grade steel rods were used for the connections, plastic redistribution may not occur. Thus, the connection might fail before reaching the load-carrying capacity.

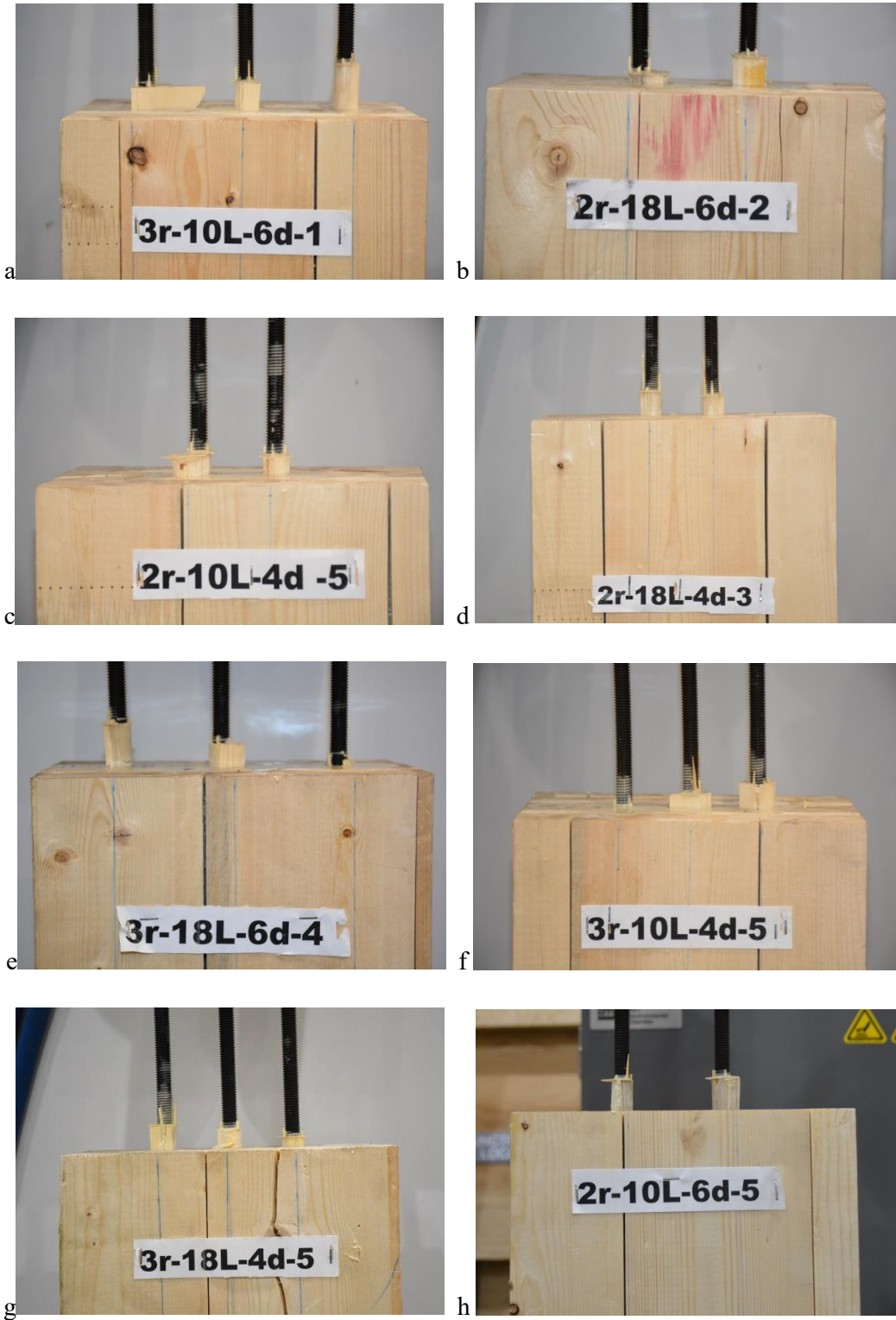


Figure 4.14: Typical failure modes observed in specimens with multiple rods.

4.3.4 Statistical analysis (Phase 3)

Table 4.8 provides a summary of the ANOVA conducted for Phase 3. These results confirmed that the number of rods, anchorage length and the spacing between rods are statistically significant for the joints load-carrying capacity. Additionally, the interactions between the number of rods and spacing between rods, as well as the anchorage length and spacing between rods are statistically significant. With the R^2 value of 0.82, these factors explain 82% of the variation.

Table 4.8: Summary of ANOVA for Phase 3

Factor	p -value
n	0.000
l_a	0.000
s	0.001
$n*l_a$	0.782
$n*s$	0.018
l_a*s	0.000
$n*l_a*s$	0.847

To identify the differences between the treatment levels of the significant factors, Tukey's HSD test was performed. The results, summarized in Table 4.9, show that there is a significant difference between the numbers of rods and the spacing between rods. The load-carrying capacities of the joints are significantly different between $n=3$, $n=2$ and $n=1$ as well as between $s=4d$ and $s=6d$. The capacities of the test series with $n=3$ and spaced at $6d$ significantly differ from those spaced at $4d$. The highest difference was at the spacing of $6d$. Similarly, the series with $n=2$ and spaced at $s=6d$ and those spaced at $4d$ significantly differ. Interestingly, there is no significant difference in the load-carrying capacity of the joint between the series with 3 rods spaced at $4d$ and those with 2 rods spaced at $6d$. Additionally, for the anchorage length of $18d$, there is no significant difference between the two spacings $4d$ and $6d$ (both share E). This result has confirmed that at sufficiently deeper embedment length-in this case $18d$, changing the rod spacing

from $4d$ to $6d$ did not have significant impact and thus, is not significantly different from the larger spacing of $6d$. However, for the embedment length of $10d$, the two spacing are significantly different.

Table 4.9: Summary of Tukey test results in Phase 3

Category	LS means	Groups
$n-3*s-76$	155.190	A
$n-3*s-51$	125.150	B
$n-2*s-76$	109.730	B C
$n-2*s-51$	102.070	C
$n-1*s--$	59.660	D
$l_a-18d*s-76$	143.820	E
$l_a-18d*s-51$	143.030	E
$l_a-10d*s-76$	121.100	F
$l_a-10d*s-51$	84.190	G

4.3.5 Discussion

Figure 4.15 shows the capacities of the single and multiple rod test series at the different embedment lengths under consideration. The figure summarizes the effects of the anchorage lengths, the rod spacing and the number of rods on each specimen in determining the load-carrying capacities of multiple GiR. From Figure 4.15, it can be seen that for every specimen with multiple rods, there was a consistent increase in capacity with increasing embedment depth. This increase varied from 50 kN for a single rod to 167 kN for multiple rods depending on the number of rods and the spacing between the rods.

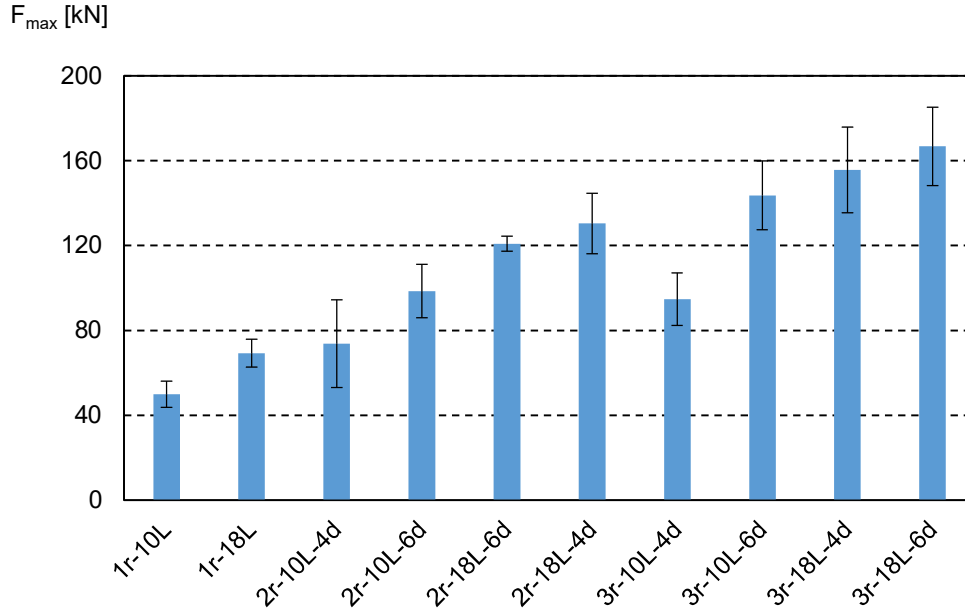


Figure 4.15: Effect of anchorage length, rod spacing and number of rods on F_{max}

Comparing the single rod specimens with those of two rods, it can be seen that for $l_a = 10d$, F_{max} increased by 48% at spacing of $4d$ and when the distance was increased to $6d$, there was a 97% increase in F_{max} . A similar result was obtained when the anchorage length was increased to $18d$. The capacity increased by 75% and 88% for double rods at the spacing of $6d$ and $4d$ respectively. With the percentage difference of 7.6% between the capacities at these two spacing ($6d$ and $4d$), it may, therefore, be deduced that at deeper embedment of rods, in this case, $18d$, no pronounced difference is seen in the joint capacity with an increase in rod spacing.

Comparing the single rod specimens with those of three rods, at $l_a = 10d$, there was 90% increase in the joint capacity at spacing of $4d$ and 188% at the spacing of $6d$. While the former represents about two times the capacity of the single rod, the latter represent about three times the capacity of a single rod. Thus, a threefold increase in the number of rods increased the capacity by approximately a factor of three. Similarly, at the anchorage

length of $18d$, the connection capacity increased by 125% and 141% at the spacing of $4d$ and $6d$ respectively.

Generally, the load-carrying capacity increased with increase in the rod spacing except for the $2r-18L$ test series where a slight decrease of 7.3% occurred in the joint capacity. The results showed that the capacity of multiple GiR joints can be increased by just changing the rod spacing. This change for the $4d$ spacing represents a little over two times the capacity for the single rod and about two and half times the capacity for the $6d$ spacing. It can also be observed that the capacity between the $4d$ and $6d$ spacing has a difference of 7% which is the same as the value (7%) obtained for the double rod embedment of $10L$. Again at the anchorage length of $18L$, the difference (here, 11 kN) between the capacities at the two considered spacing ($4d$ and $6d$) is not pronounced. Therefore, it can be said that at sufficiently deeper embedment length (in this case $18d$), changing the rod spacing does not make a significant difference in the joints capacity.

5 Conclusions

5.1 Summary of results

In the research presented herein, the performance of single and multiple GiR in CLT oriented parallel and perpendicular to the major strength directions were investigated under quasi-static monotonic tension loading. The single rods were partially and completely glued in the timber and the multiple rods were completely glued-in with either two or three rods embedded in the timber. Based on the 260 tests, the results allow for the following conclusions to be drawn

5.1.1 Single rod installed parallel to the major CLT strength axis

- 1) Within the range of the parameters investigated, there was an increase in load-carrying capacity with increasing anchorage length up to the length of 14d beyond which no further increase was observed.
- 2) The load-carrying capacity increased with the rod diameter. The higher diameter rods (19.1 mm) attained higher load-carrying capacity than the lower diameter (12.7 mm) rods (between 39% and 81%).
- 3) The panel thickness (herein 139 and 175 mm) did not impact the load-carrying capacity of the connections.
- 4) The GiR connections were very stiff but there was very large variability between and within tests series.
- 5) The displacements at failure for all test series were very small ranging from 1.4 to 4.4 mm for the retested specimen and from 0.3 and 2.0 for the first tests.
- 6) The predominant failure modes were rod pull-out at the interface between timber and the adhesive and wood plug pull out failure which is the shear failure in timber. These failure modes depended on the rod diameter and the anchorage length.

- 7) The impact of partially moving the anchoring zone towards the centre of the CLT panels on the load-carrying capacity was not consistent across test series.
- 8) For all test series (except one), the retested specimens achieved a higher load-carrying capacity than the first test (up to 35%). The second test showed that the connection was not damaged by the first test performed.
- 9) The GIROD design equation closely predicted the experimental data for the test series with the smaller rod diameter (12.7 mm), but the equation overestimated the capacity of the connections for the series with the higher rod diameter (19.1 mm) at embedment lengths above $8d$.

5.1.2 Single rod installed perpendicular to the major CLT strength axis

- 1) Within the range of the investigated parameters, there was an increase in the load-carrying capacity with increasing anchorage length which is much higher than those of the parallel to the major strength direction in Phase 1.
- 2) The load-carrying capacity increased with the rod diameter. The higher diameter rods of 19.1 mm attained higher load-carrying capacity than the lower diameter rods (12.7 mm). This increase ranged between 54% and 200%.
- 3) The capacity of the panel also played a vital role in determining the load-carrying capacity of the connection at failure because of its cross-layer arrangement. Having insufficient panel width reduced the capacity of the connection by up to 50%.
- 4) The GiR connections were very stiff and there was high consistency within the test series. However, there was large variability (CoV) in some of the test series.
- 5) The displacements of the test series at failure were small ranging from 0.9 to 6.3 mm.
- 6) The predominant failure modes were panel splitting and rolling shear failure for test series with the short width of 200 mm, shear failure of CLT due to the edge lamination

of the core layer of CLT, and the partial and complete tear-out of the core CLT layer which indicates the CLT adhesive glueline failure.

- 7) The GIROD design equation overestimated the experimental values from the embedment $6d$ up to the highest embedment length of about $18d$. The differences were highest at the embedment length of $6d$, 64% for the 12.7 mm rod and 30% for the 19.1 mm rod.

5.1.3 Multiple rods installed parallel to the major CLT strength axis

- 1) Within the range of the studies parameters, the load-carrying capacity increased with the number of rods and with the rod spacing for all the test series.
- 2) The load-carrying capacity increased between 48% and 188% with an increase in the number of rods (from 1 to 2 and 3) and rod spacing (from $4d$ to $6d$). The increase was up to 97% for the two-rod specimen and 188% for the three-rod specimen at the highest spacing of $6d$.
- 3) The minimum rod spacing of $4d$ as used herein was sufficient to avoid failure as a result of multiple rod interference.
- 4) At sufficiently deeper embedment length (in this case $18d$), changing the rod spacing from $4d$ to $6d$ did not make a significant difference in the joint's capacity.
- 5) The displacements at failure for all test series ranged from 0.8 to 12.8 mm.
- 6) The predominant failure modes were rod pull-out of wood at the interface between the adhesive and timber, and wood plug failure caused by the shear failure of timber. Although with longer anchorage length and the number of rods, the load-carrying capacities increased, no visible difference was observed in the type of failure for the two anchorage lengths (herein $10d$ and $18d$).

5.2 Outlook

This thesis presented the experimental tests on single and multiple GiR connections in CLT. To transition into the use of GiR in CLT for construction applications, the following areas for further studies can be identified:

- 1) It is anticipated that the performance of GiR in CLT will be different based on the location of the rod in the panel. In this thesis, the rods were located in the core layer of the panels but for example, the rod may be located between two layers of the panel, between two edge glued or non-edge glued panel lamella in one or two layers, etc. Similarly, multiple rods may be located likewise in these positions other than the core layer of the panel. Further studies are required.
- 2) Numerical analysis for GiR in CLT design equation which incorporates and account for the various configurations unique to CLT such as the alternating layer of the panel, number of panel ply, etc. and the failure modes that have been reported are required for the accurate prediction of the pull-out force of GiR in CLT.
- 3) The load-carrying capacity of GiR is influenced by environmental conditions. As GiR in CLT will potentially be used for indoor and outdoor applications, studies on the impact of environmental factors; especially the exposure to varying (high and low) temperature and humidity are needed to provide guidance for the eventual formulation of a regulatory framework for GiR in CLT. The performance of GiR under fire long-term should also be studied.
- 4) The load-carrying capacity of GiR is influenced by the loading conditions. Studies on the long-term and fatigue performance of GiR joints are recommended for further development of this research.

References

- [1] S. Gagnon, E. M. Bilek, L. Podesto and P. Crespell, Introduction to cross-laminated timber, FPInnovation, 2013.
- [2] S. Lehmann, “Developing a Prefabricated Low-Carbon Construction System Using Cross-Laminated Timber (CLT) Panels for Multistorey Inner-City Infill Housing In Australia,” *Journal of Green Building.*, vol. 7, no. 3, pp. 131--150, 2012.
- [3] M. C. D. M. Pereira and C. Calil, “Strength and Stiffness of Cross Laminated Timber (CLT) panels produced with Pinus and Eucalyptus: experimental and analytical comparisons,” *Matéria (Rio de Janeiro)*, vol. 24, no. 4, 2019.
- [4] A. Ringhofer and G. Schickhofer, “Timber- in- Town - current examples for residential buildings in CLT and tasks for the future,” in *Focus Solid Timber Solutions- European Conference on Cross Laminated Timber (CLT)*,, Bath:University of Bath, 2013.
- [5] T. Schmidt and H. J. Blab, “Contact joints in engineered wood products,” in *Proceeding of World Conference on Timber Engineering*, Vienna, 2016.
- [6] M. Mohammad, B. Douglas, D. Rammer and S. E. Pryor, CLT Handbook- Connection in cross-laminated timber buildings, FPInnovation, 2013.
- [7] A. Hossain, I. Danzig and T. Tannert, “Cross-laminated timber connections with double-angled self-tapping screw assemblies,” *Journal of Structural Engineering*, vol. 142, no. 11, 2016.
- [8] H. Zhu, P. Faghani and T. Tannert, “Experimental investigations on timber joints with single glued-in FRP,” *Construction and Building Materials*, vol. 140, pp. 167-172, 2017.
- [9] E. Gonzales, T. Tannert and T. Vallee, “The impact of defects on the capacity of timber joints with glued-in rods,” *International Journal of Adhesion and Adhesives*, vol. 65, pp. 33-40, 2016.

- [10] G. Tlustochowicz, E. Serrano and R. Steige, “State-of-the art review on timber connections with glued-in steel rods,” *Materials and Structures*, vol. 44, pp. 997-1020, 2011.
- [11] D. Yeboah, S. Taylor, D. McPolin, R. Gilfillan and S. Gilbert, “Behaviour of joints with bonded-in steel bars loaded parallel to the grain of timber elements,” *2011*, vol. 25, pp. 2312-2317, *Constr Build Mater*.
- [12] D. Otero, J. Estevez-Cimadevila , E. Martin-Gutierrez and P. Vazquez-Rodriguez, ““Failure modes in double-sided pull-out test of threaded steel rods glued in hardwood,” in *Proceeding of the World Conference on Timber Engineering (WCTE 2010)*, Riva del Garda, 2010.
- [13] E. Gonzales, C. Avez and T. Tannert, “Timber joints with multiple glued-in steel rods,” *The Journal of Adhesion*, vol. 92, pp. 635-651, 2016.
- [14] N. Ratsch, S. Böhma, M. Voß and M. Kaufmann, “Influence of imperfections on the load capacity and stiffness of glued-in rod connections.,” *Construction and Building Materials*, vol. 226, pp. 200-211, 2019.
- [15] C. Grunwald, T. Vallée, S. Fecht, B.-M. Oliver, F. Diehl, L. Bathon, S. Myslicki, R. Scholz and F. Walther, “Rods glued in engineered hardwood products part I: Experimental results under quasi-static loading. In,” *International Journal of Adhesion and Adhesives*, vol. 90, pp. 163-181, 2019.
- [16] B. Azinovic, E. Serrano, M. Kramar and T. Pazlar, “Experimental investigation of the axial strength of glued-in rods in cross laminated timber,” *Materials and Structures*, vol. 51, p. 143, 2018.
- [17] B. Azinovic , H. Danielsson, E. Serrano and M. Kramar, “Glued-in rods in cross laminated timber-numerical simulations and parametric studies.,” *Construction and Building Materials*, vol. 212, pp. 431-441, 2019.
- [18] M. K. Kuzman, S. Klaric , A. P. Barcic, R. P. Vlosky, M. M. Janakieska and P. Groselj, “Architect perceptions of engineered wood products: An exploratory study of selected countries in Central and Southeast Europe,” *Construction and Building Materials*, vol. 179, pp. 360-370, 2018.

- [19] N. Winchester and J. M. Reily, “The economic and emissions benefits of engineered wood products in a low-carbon future,” *Energy Economics*, vol. 85, no. 104596, 2020.
- [20] I. Lukacs, A. Björnfort and R. Tomasi, “Strength and stiffness of cross-laminated timber (CLT) shear walls: state-of-the-art of analytical approaches,” *Engineering Structures*, vol. 178, no. 1, pp. 136-147, 2019.
- [21] K. Jones, J. Stegermann, J. Sykes and P. Winslow, “Adoption of unconventional approaches in construction: the case of cross-laminated timber,” *Construction and Building Material*, vol. 125, pp. 690-702, 2016.
- [22] A. Sotayo, D. Bradley, M. Bather, P. Sarah , M. Oudjene, I. El-Houjeyri, A. M. Harte, S. Mehra, C. O’Ceallaigh, P. Haller, S. Namari, A. Makradi, S. Belouettar, L. Bouhala, F. Deneufbourg and Z. Gaun, “Review of state of the art of dowel laminated timber members and densified wood materials as sustainable engineered wood products for construction and building applications,” *Developments in the Built Environment*, vol. 1, no. 100004, 2020.
- [23] J. Hildebrandt, N. Hagemann and D. Thrän, “The contribution of wood-based construction materials for leveraging a low carbon building sector in Europe,” *Sustainable Cities and Society*, vol. 34, pp. 405-418, 2017.
- [24] D. Sandberg, “Additives in Wood Products—Today and Future Development, Environmental Impacts of Traditional and Innovative Forest-based Bioproducts,” in *Environmental Impacts of Traditional and Innovative Forest-based Bioproducts*, Springer, 2016, pp. 105-172.
- [25] M. H. Ramage, H. Burrige, M. Busse-Wicher, G. Fereday, T. Reynolds, D. U. Shah, G. Wu, L. Yu, P. Fleming, D. Densley-Tingley, J. Allwood, P. Dupree, P. F. Linden and O. Scherman, “The wood from the trees: the use of timber in construction,” *Renewable and Sustainable Energy Reviews*, vol. 68, no. 1, pp. 333-359, 2017.
- [26] N. Mohd Yusof, P. Md Tahir, S. H. Lee, M. A. Khan and M. S. J. Redzuan , “Mechanical and physical properties of Cross-Laminated Timber made from Acacia

- mangium wood as function of adhesive types,” *Journal of Wood Science*, vol. 65, no. 20, 2019.
- [27] R. Cherry, A. Manalo, W. Karunasena and G. Stringer, “Out-of-grade sawn pine: A state-of-the-art review on challenges and new opportunities in cross laminated timber (CLT),” *Construction and Building Materials*, vol. 211, pp. 858-868, 2019.
- [28] M. Jeleč, D. Varevac and V. Rajčić, “Cross-laminated timber (CLT) – a state of the art report,” *GRAĐEVINAR*, vol. 70, no. 2, pp. 75-95, 2018.
- [29] H. Ferik, “Some building science aspects for building with CLT, Focus solid timber solutions,” in *European Conference on cross laminated timber (CLT)*, BATH, 2013.
- [30] R. Brandner, “Production and technology of cross laminated timber (CLT): State-of-the-art-report, Focus solid timber solutions,” in *European conference on cross laminated timber (CLT)*, Bath, 2013.
- [31] G. Schickhofer, R. Brandner and H. Bauer, “Introduction to CLT, Product Properties, Strength Classes,” in *Joint Conference of COST Actions FP1402 and FP1404*, KTH Stockholm, Sweden, 2016.
- [32] L. Evans, “Cross Laminated Timber: taking wood buildings to the next level,” reThink Wood, American Wood Council, and FPInnovations, 2013.
- [33] M. Flaig and H. J. Blaß, “Shear strength and shear stiffness of CLTbeams,” in *Proceedings of 46th CIB-W18 Meeting*, Vancouver, Canada, 2013.
- [34] r. Brandner, T. Bogensperger and G. Schickhofer, “In plane Shear Strength of Cross Laminated Timber (CLT): Test Configuration, Quantification and influencing Parameters,” in *International Council for Research and Innovation in Building and Construction, Working Commission W18 - Timber Structures*, Vancouver, Canada, 2013.
- [35] Z. Ahmed, M. P. Ansell and D. Smedley, “Bonding Strength Properties of Adhesively-Timber Joint with Thixotropic and Room Temperature Cured Epoxy Based Adhesive Reinforced with Nano- and Micro-particles,” *Materials Science and Engineering*, vol. 17, no. 012007, 2011.

- [36] G. Davies, “The performance of adhesive systems for structural timbers,” *International Journal of Adhesion and Adhesives*, vol. 17, pp. 247-255, 1997.
- [37] M. Shahnewaz , S. M. Alam and T. Tannert , “In-Plane Strength and Stiffness of Cross-Laminated Timber Shear Walls,” *Buildings*, vol. 8, no. 8, p. 100, 2018.
- [38] A. J. Jorissen and M. Fragiacomio, “General notes on ductility in timber structures,” *Engineering Structures*, vol. 33, no. 11, pp. 2987-2997, 2011.
- [39] R. Crocetti, p. J. Gustafsson, U. A. GiRhammar, L. Costa and A. Asimakidis, “Nailed Steel Plate Connections: Strength and Ductile Failure Modes,” *Structures*, vol. 8, pp. 44-52, 2016.
- [40] T. Schmidt and H. J. Blaß, “Recent development in CLT connections part I: In-plane shear connection for CLT bracing elements under static loads,” *Wood and Fiber Science*, vol. 50, pp. 48-57, 2018.
- [41] R. Steiger, E. Serrano, M. Stepinac, V. Rajcic, C. O’Neill, D. McPolin and R. Widmann, “Strengthening of timber structures with glued-in rods,” *Construction and Building Materials*, vol. 97, pp. 90-105, 2015.
- [42] R. Steiger, E. Gehri and R. Widmann, “Pull-out strenght of axially loaded steel rods bonded in glulam parallel to the grain,” *Materials and Structures*, vol. 40, pp. 69-78, 2006.
- [43] E. Martín, J. Estévez and D. Otero, “Influence of geometric and mechanical parameters on stress states caused by threaded rods glued in wood,” *European journal of wood and wood product*, vol. 71, pp. 259-266, 2013.
- [44] V. Di Maria and A. Ianakiev, “Adhesive Connections in Timber: A Comparison between Rough and Smooth Wood Bonding Surfaces,” *International Journal of Structural and Construction Engineering*, vol. 9, no. 3, pp. 395-401, 2015.
- [45] E. Gehri, “Ductile behaviour and group effect of glued-in steel rods,” in *Proceedings of International RILEM Symposium on Joints in Timber Structures*, Stuttgart, Germany, 2001.
- [46] E. Gehri, “High performing jointing techniques using glued-in rods,” in *11th World Conference on Timber Engineering WCTE*, Riva del Garda, Italy, 2010.

- [47] K. Harvey and M. P. Ansell, “Improved timber connections using bonded-in GFRP,” in *Proceedings of the 6th World Conference on Timber Engineering*, Whistler, Canada, 2000.
- [48] K. Harvey and M. P. Ansell, “Improved timber connections using bonded-in GFRP rods,” in *Proceedings of the 6th World Conference on Timber Engineering*, Whistler, Canada, 2000.
- [49] C. Bengtsson and C.-J. Johansson, “GIROD: Glued in rods for timber structures. SP report 2002:26,” Swedish national testing and research Institute, Boras, Sweden, 2002.
- [50] J. Fueyo, J. A. Cabezas, M. P. Rubio and M. Domínguez , “Reduction of perpendicular-to-grain stresses in the apex zone of curved beams using glued-in rods,” *Materials and Structures*, vol. 43, pp. 463-474, 2010.
- [51] C. R. Frihart, “Adhesive Groups and How They Relate to the Durability of Bonded Wood,” *Journal of Adhesion Science and Technology*, vol. 23, pp. 601-617, 2009.
- [52] C. Grunwald, T. Vallée, S. Fecht, O. Bletz-Mühldorfer, F. Diehl, L. Bathon, W. Frank, R. Scholz and S. Myslicki, “Rods glued in engineered hardwood products part II: Numerical modelling and capacity prediction,” *International Journal of Adhesion and Adhesives*, vol. 90, pp. 182-198, 2019.
- [53] R. Bainbridge, C. Mettem, K. Harvey and M. Ansell, “Bonded-in rod connections for timber structures—development of design methods and test observations,” *International Journal of Adhesion and Adhesives*, vol. 22, no. 1, pp. 47-59, 2002.
- [54] J. G. Broughton and A. R. Hutchinson, “Pull-out behaviour of steel rods bonded into timber,” *Materials and Structures*, vol. 34, no. 2, pp. 100-109, 2001.
- [55] D. Kohl, N. Ratsch, S. Böhm, M. Voß, M. Kaufmann and T. Vallée , “Influence of manufacturing methods and imperfections on the load capacity of glued-in rods,” *Journal of Adhesion*, vol. 96, no. 8, pp. 738-759, 2020.
- [56] B.-H. Xu, J.-H. Guo and A. Bouchaïr, “Effects of glue-line thickness and manufacturing defects on the pull-out behavior of glued-in rods,” *International Journal of Adhesion and Adhesives*, vol. 98, p. 102517, 2020.

- [57] C. O'Neill, D. McPolin, S. E. Taylor, T. Martin and A. M. Harte, "Glued-in basalt FRP rods under combined axial force and bending moment: An experimental study," *Composite Structures*, vol. 186, pp. 267-273, 2018.
- [58] D. Otero, J. Estevez, E. Martin and J. A. Vazquez, "Failure modes in double-side pull-out test of threaded steel rods glued in hardwood," in *Proceeding of the World Conference on Timber Engineering*, Riva del Garda, Italy, 2010.
- [59] C. D. Otero, C. J. Estevez and G. E. Martin, "Withdrawal strength of threaded steel rods glued with epoxy in wood," *International Journal of Adhesion and Adhesives*, vol. 44, pp. 115-121, 2013.
- [60] D. Yeboah, S. Taylor, D. McPolin, R. Gilfillan and S. Gilbert, "Behaviour of joints with bonded-in steel bars loaded parallel to the grain of timber elements," *Construction and Building Materials*, vol. 25, pp. 2312-2317, 2011.
- [61] R. Widmann, R. Steiger and E. Gheri, "Pull-out strength of axially loaded steel rods bonded in glulam perpendicular to the grain," *Materials and Structures*, vol. 40, pp. 827-838, 2007.
- [62] J. X. Deng, "Strength of epoxy bonded steel connections in glued-laminated timber," Civil Engineering Research Report 97/4, University of Canterbury, Christchurch, New Zealand, 1997.
- [63] M. B. U. Pedersen, C. O. Clorius, L. Damkilde and P. Hoffmeyer, "Residual Strength of Glued-in Bolts After 9 Years In Situ Loading," in *Proceedings of the 1996 International Conference on Wood Mechanics*, Stuttgart, Germany, 1996.
- [64] T. Y. Li, B. Shan, Y. Xiao, Y. R. Guo and M. P. Zhang, "Axially loaded single threaded rod glued in glulam joint," *Construction and Building Materials*, vol. 224, p. 118302, 2020.
- [65] A. Rossignon and B. Espion, "Experimental assessment of the pull-out strength of single rods bonded in glulam parallel to the grain," *European Journal of Wood and wood Product*, vol. 66, pp. 419-432, 2008.

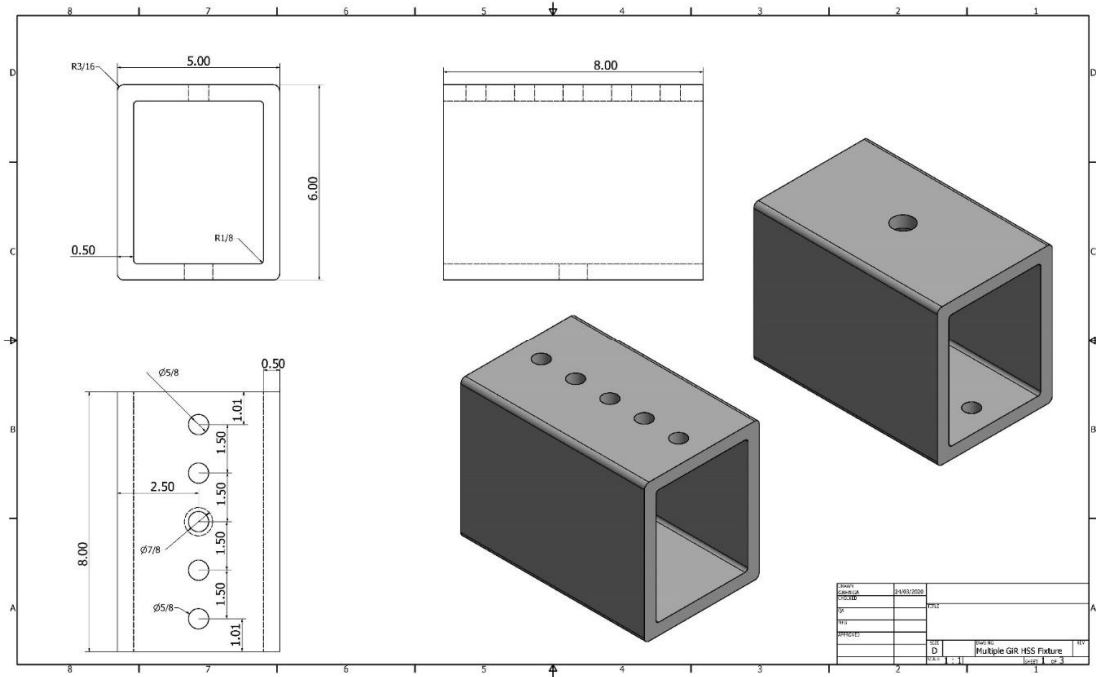
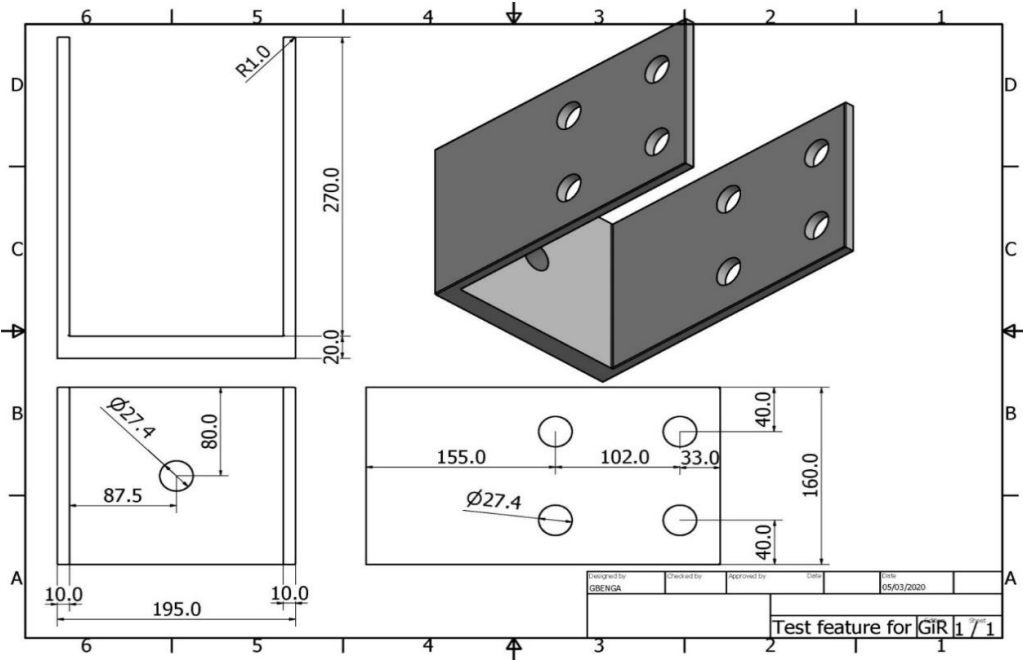
- [66] H. J. Blass and B. Laskewitz, "Effect of spacing and edge distance on the axial strength of glued-in rods," in *Proceedings of 32nd Conference of CIB-W18*, Graz, Austria, 1999.
- [67] X. Zhang, Z. Jiang, B. Fei, C. Fang and H. Liu, "Experimental performance of threaded steel glued into laminated bamboo," *Construction and Building Materials*, vol. 249, p. 118780, 2020.
- [68] M. Madhoushi and M. P. Ansell, "Effect of glue-line thickness on pull-out behavior of glued-in GFRP rods in LVL: Finite element analysis," *Polymer Testing*, vol. 62, pp. 196-202, 2017.
- [69] P. J. Gustafson and E. Serrano, "Glued-in rods for timberstructures-development of a calculation model. Report TVSM-3056," Lund University, Lund, 2001.
- [70] A. Ranta-Maunus and J. Kangas, "Glued-in steel rods in V-shape.," in *Pacific Timber Engineering Conference*, Gold Coast, Australia, 1994.
- [71] J. G. Broughton and A. R. Hutchinson, "Effect of timber moisture content on bonded-in rods," *Construction and Building Materials*, vol. 15, no. 1, pp. 17-25, 2001.
- [72] D. Otero-Chans, J. Estévez-Cimadevila and E. Martín-Gutiérrez, "Joints with bars glued-in softwood laminated timber subjected to climatic cycles," *International Journal of Adhesion and Adshesives*, vol. 82, pp. 27-35, 2018.
- [73] M. D. Otero-Chans, J. Estevez- Cimadevila, G. E. Martin and J. A. Vázquez-Rodríguez, "Influence of timber density on the axial strength of joints made with glued-insteel rods: An experimental approach," *International Journal of Adhesion & Adhesives*, vol. 30, pp. 380-385, 2010.
- [74] P. Alam, M. P. Ansell and D. Smedley, "Mechanical repair of timber beams fractured in flexureusing bonded-in reinforcements," *Composites: Part B*, vol. 40, pp. 95-106, 2009.
- [75] R. TC, "RC 5 Bond test for reinforcement steel. 1. Beam test, 1982," in *RILEM Recommendations for the Testing and Use of Constructions Materials*, E & F SPON, 1994, pp. 213-217.

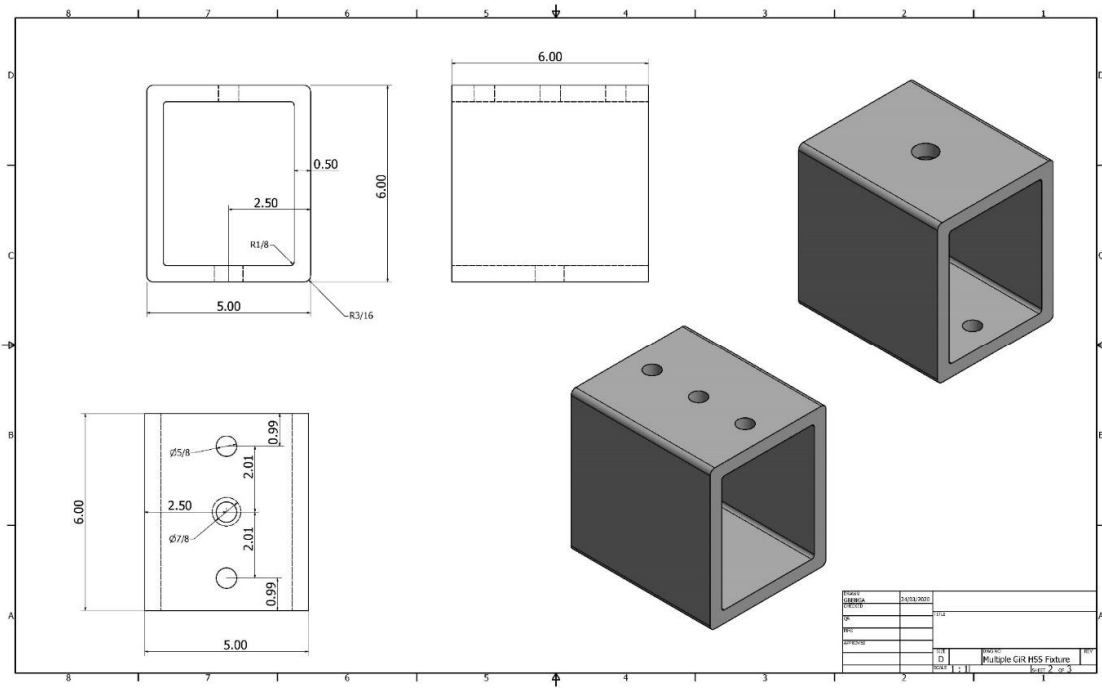
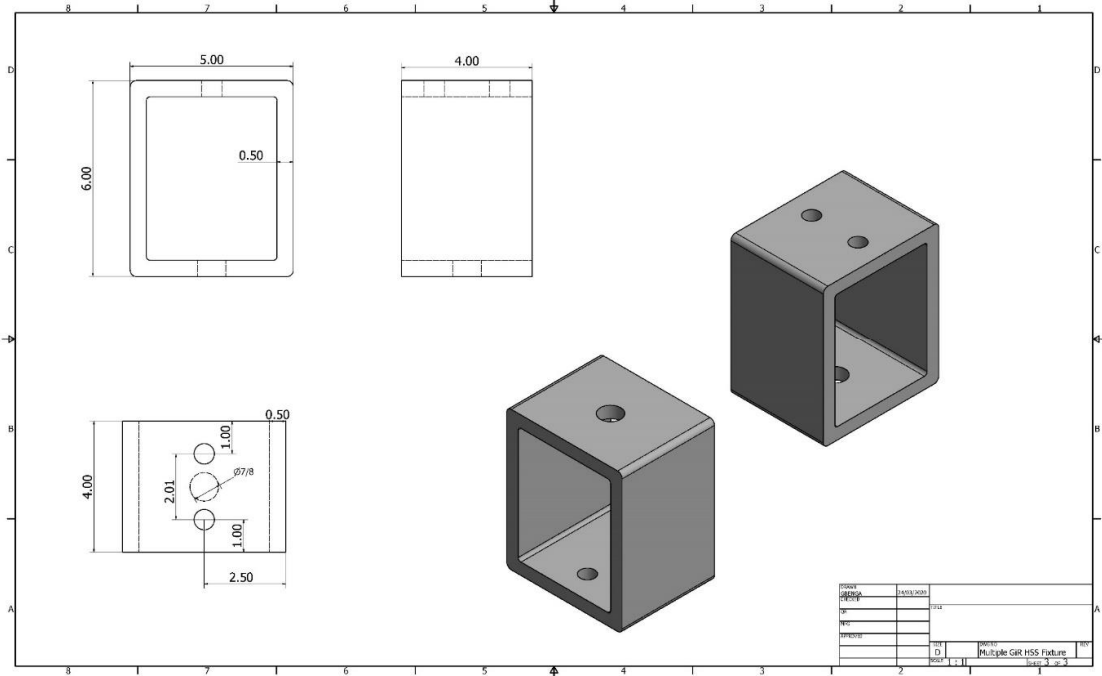
- [76] H. J. Blass and B. Laskewitz, “Load carrying capacity of axially loaded rods glued in perpendicular to the grain,” in *Proceedings of the international RILEM symposium on joints in timber structures*, Stuttgart, Germany, 2001.
- [77] P. Hvizdoš, P. Tatarko, A. Duszova and J. Dusza, “Ceramic Nanocomposites,” in *Failure mechanisms of ceramic nanocomposites*, Woodhead Publishing, 2013, pp. 117-152.
- [78] S. M. T. Corporation, “Crosslam CLT Technical Design Guide v4.0,” Structurlam, Canada, 2018.
- [79] A. P. 320-2019, “Standard for performance-rated Cross-Laminated Timber. The Engineered wood Association,” American National Standards Institute (ANSI) and Engineered Wood Association (APA), New York, 2019.
- [80] A. International, “A191/A193M-20 Standard Specification for Alloy-Steel and Stainless Steel Bolting for High Temperature or High Pressure Service and Other Special Purpose Applications,” ASTM International, West Conshohocken, PA, 2020.
- [81] A. International, “E8/E8M-16ae1 Standard Test Methods for Tension Testing of Metallic Materials.,” ASTM International, West Conshohocken, PA, 2016.
- [82] ASTM, “D1002 - 10. Standard Test Method for Apparaent Shear Strength of Single-Lap-Joint Adhesively Bonded Metal Specimens by Tension Loading (Metal-to-Metal). West Conshohocken, PA,” *ASTM International*, 2019.
- [83] G. W. Oehlert, *A first course in design and analysis of experiemnts*, New York: W.H. Freeman and Company, 2010.
- [84] T. Tannert, T. Vallee and S. Hehl, “Experimental and numerical investigations on adhesively bonded hardwood joints,” *International Journal of Adhesion and Adhesives*, vol. 37, pp. 65-69, 2012.
- [85] S. Lee and D. K. Lee, “What is the proper way to apply the multiple comparison test?,” *Korean Journal of Anesthesiology*, vol. 71, no. 5, pp. 353-360, 2018.

- [86] P. Gabriela, H. Johnsson and M. Fragiaco, "Provisions for ductile behaviour of timber-to-steel connections with multiple glued-in rods," *Journal of Structural Engineering*, vol. 139, no. 9, pp. 1468-1477, 2013.

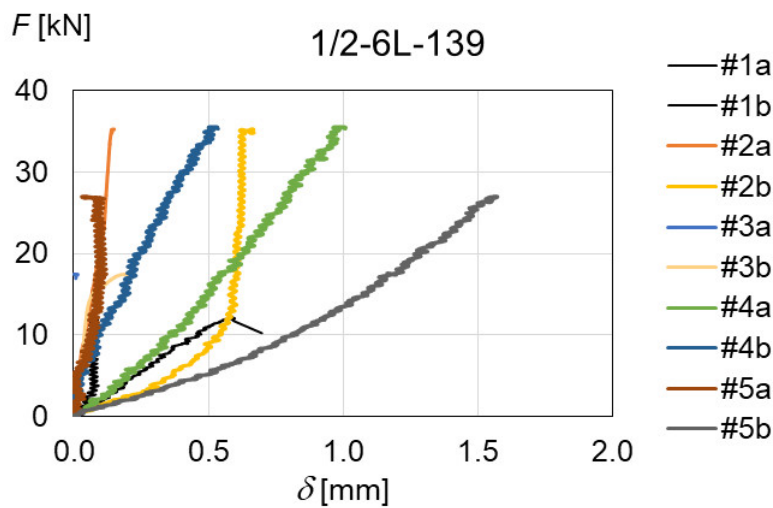
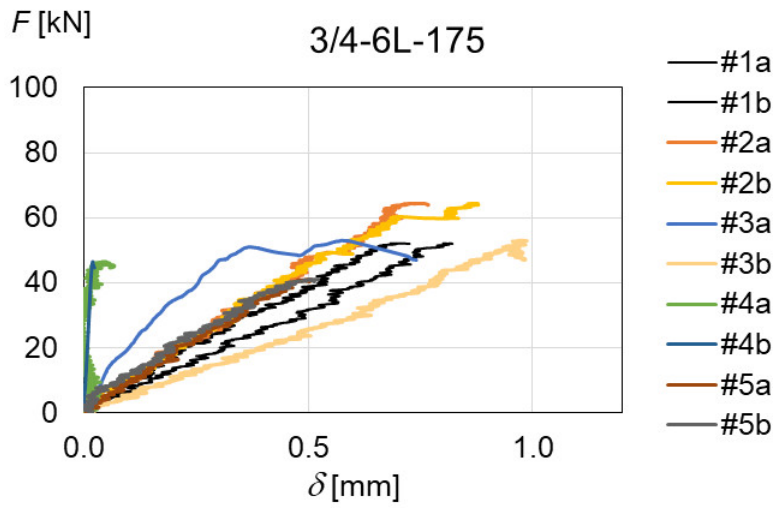
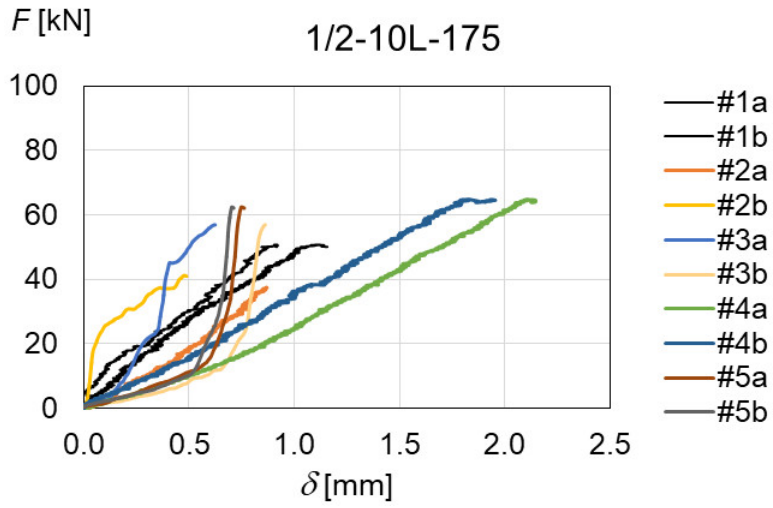
Appendices

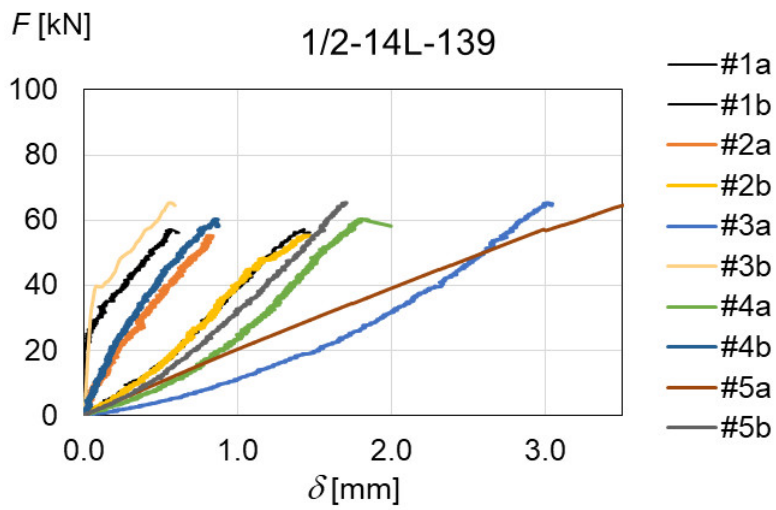
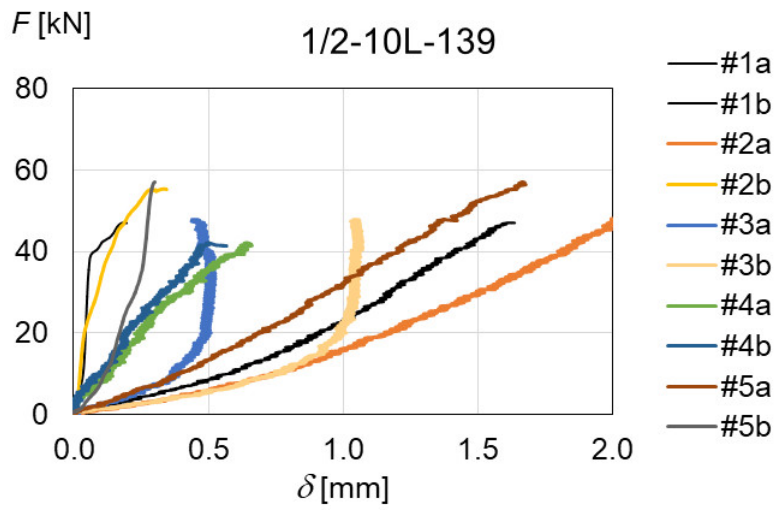
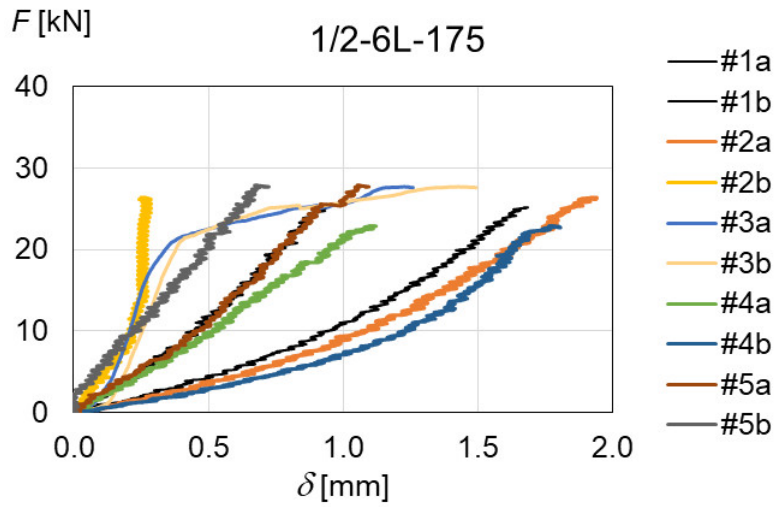
Appendix A: GiR test fixtures

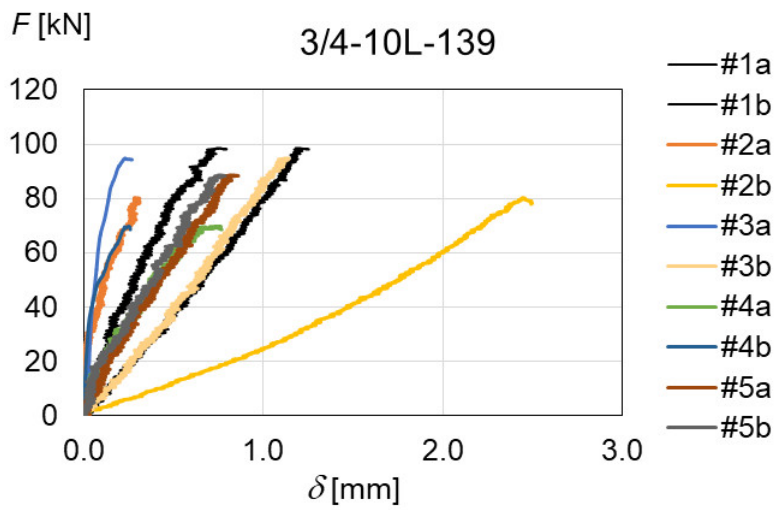
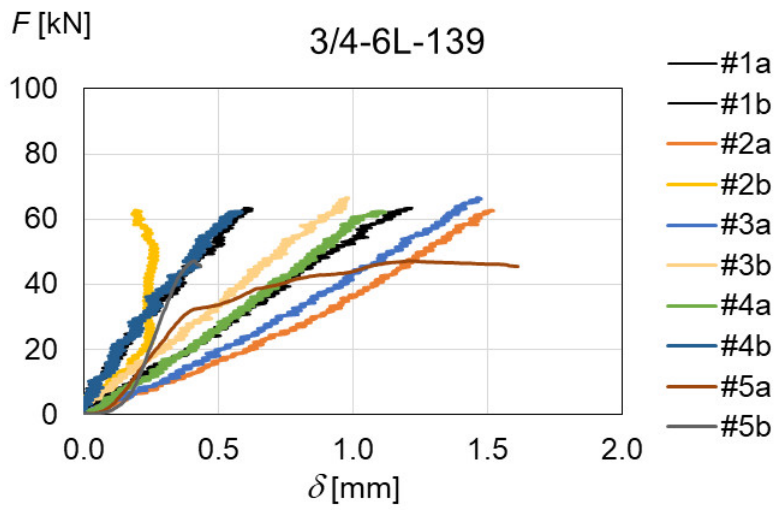
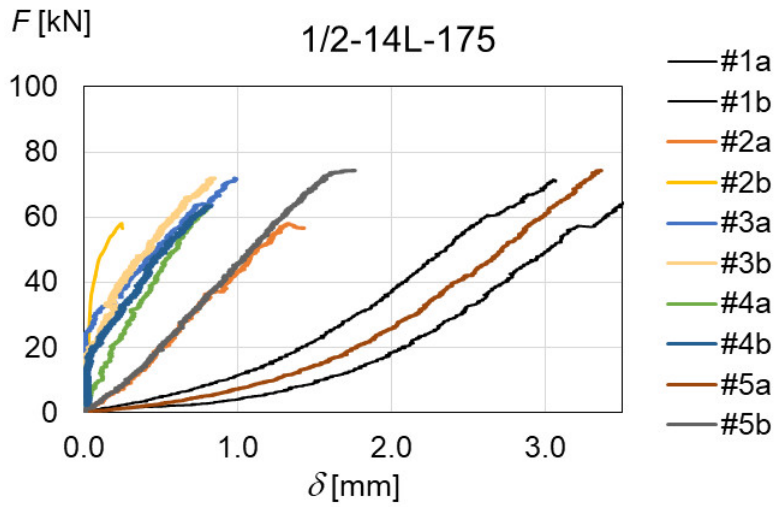


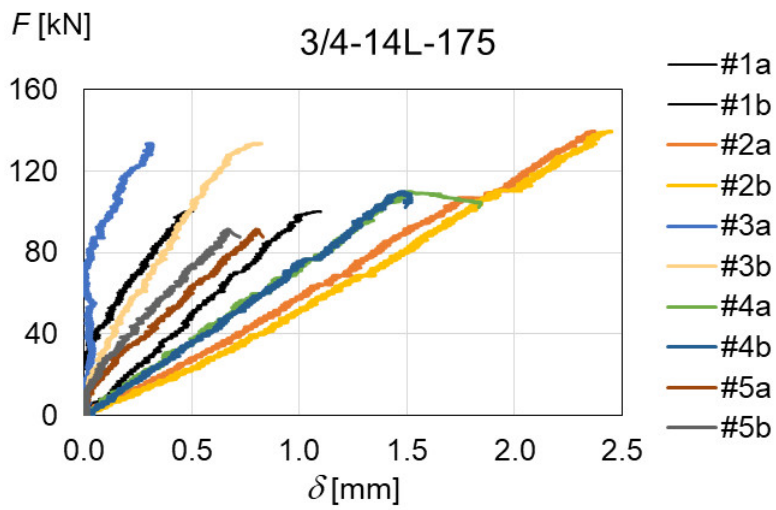
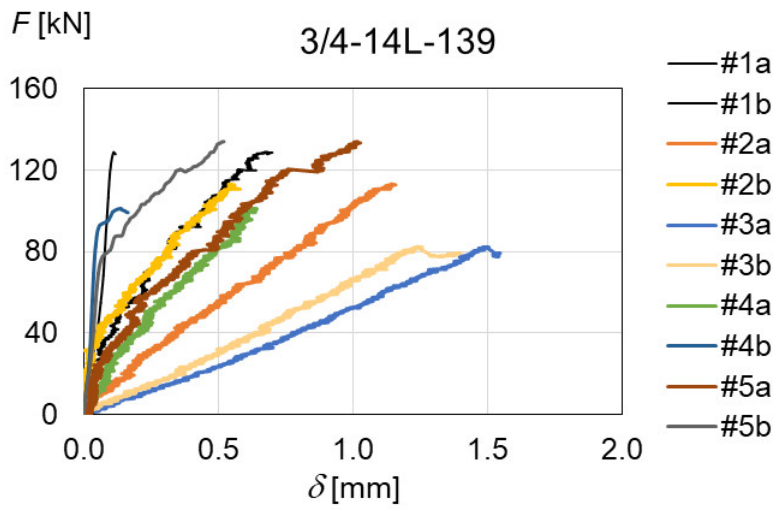
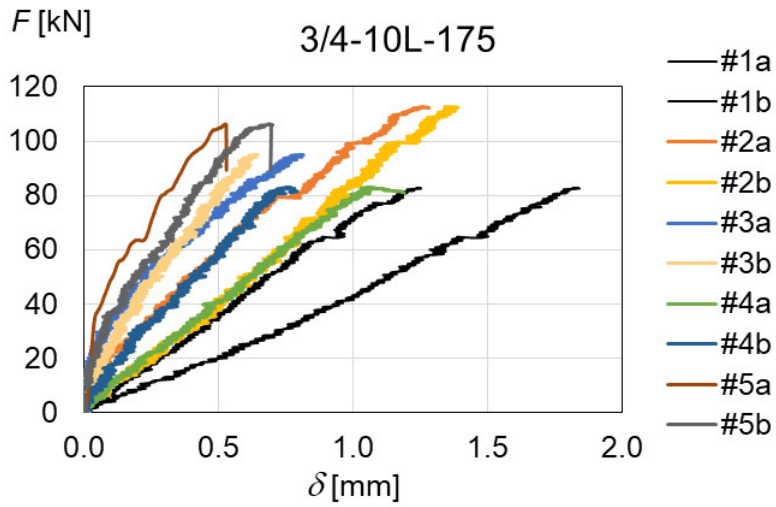


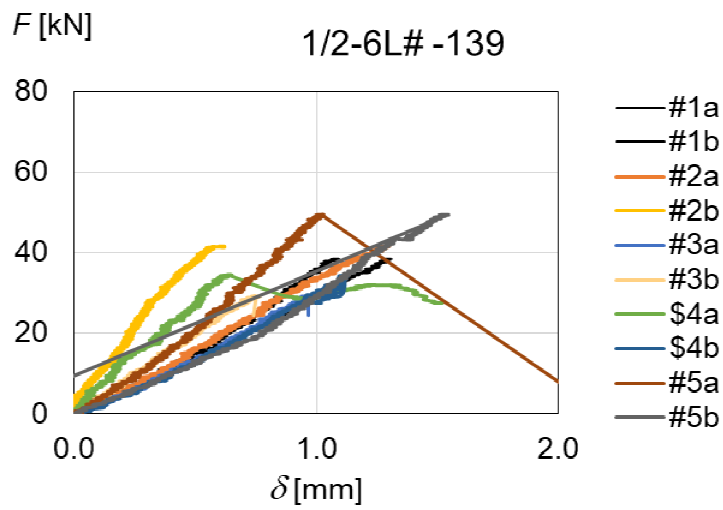
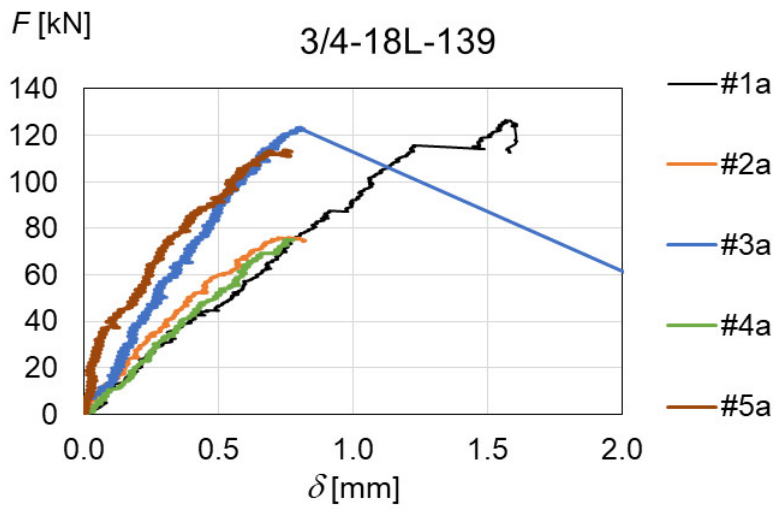
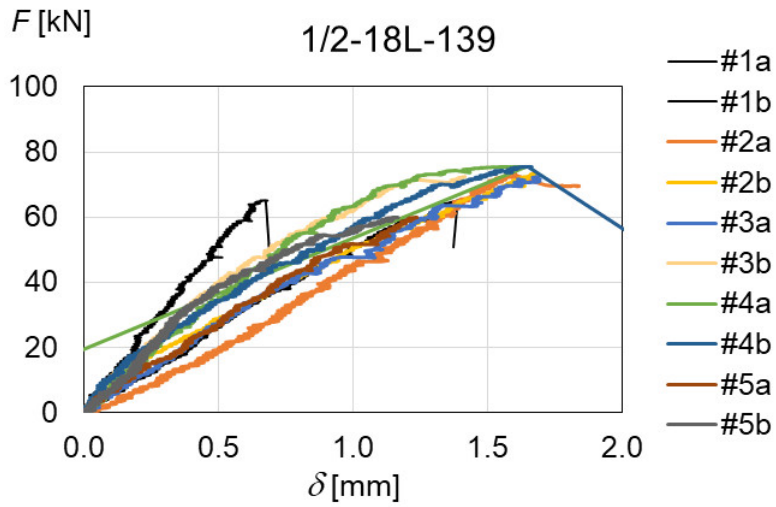
Appendix B: Load-displacement curves from Phase 1

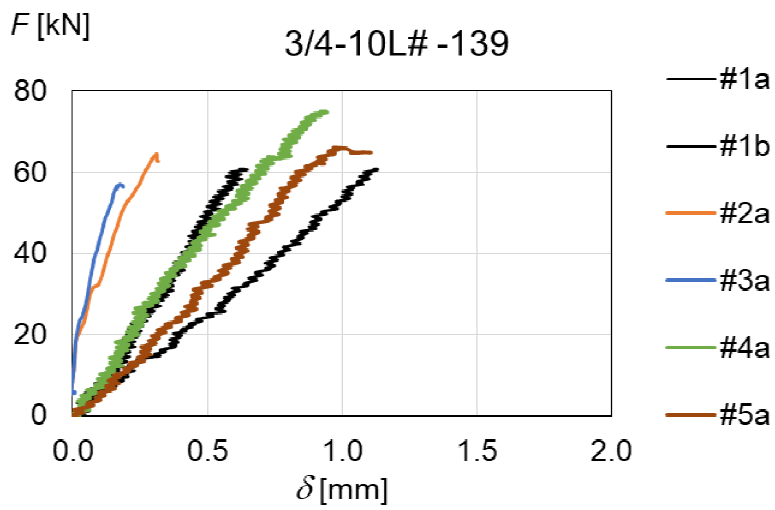
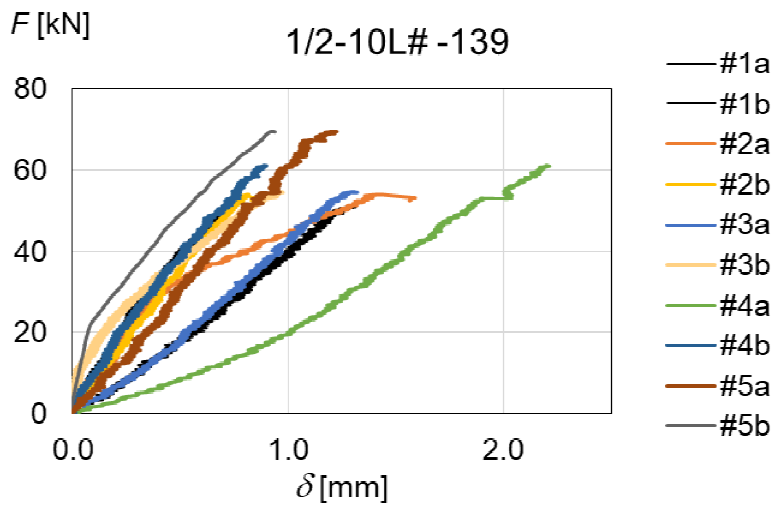
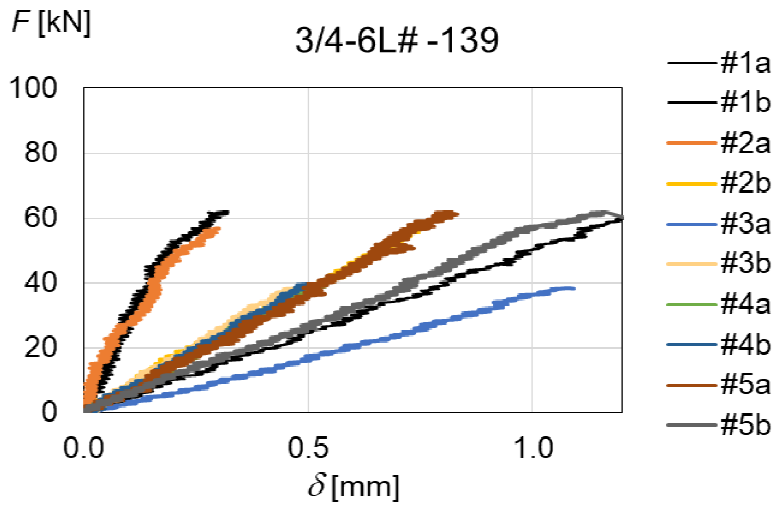


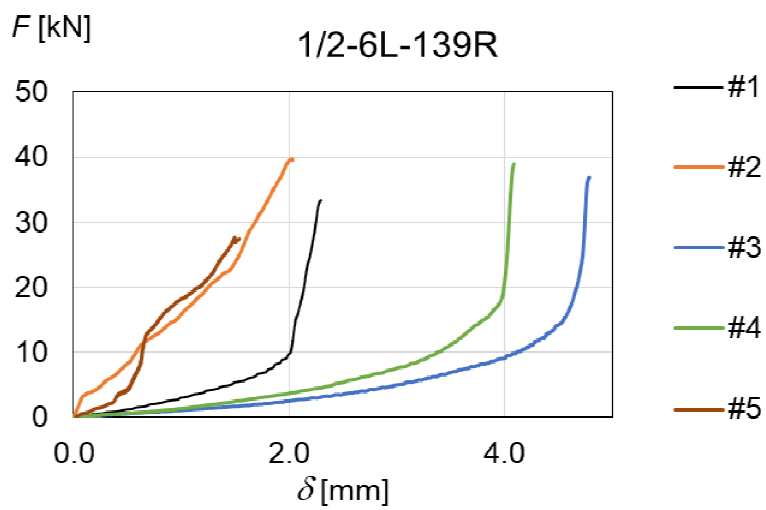
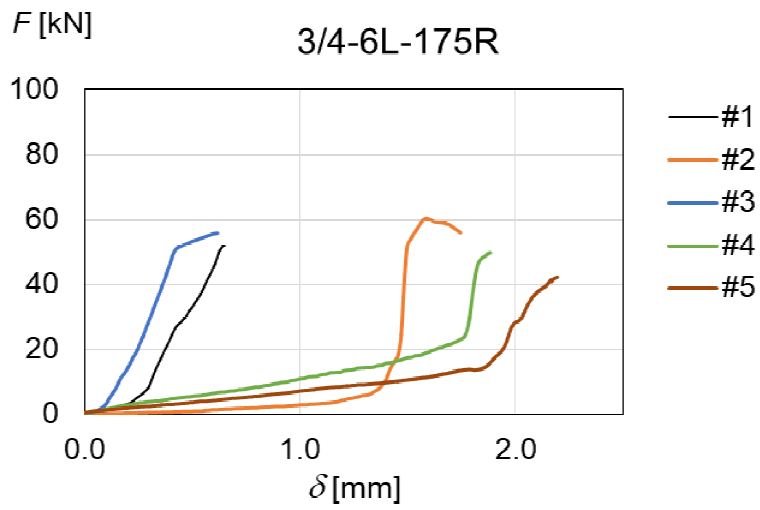
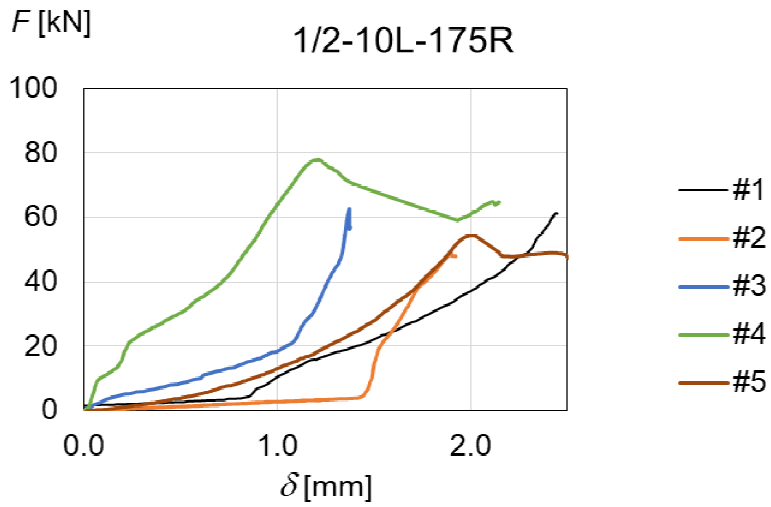


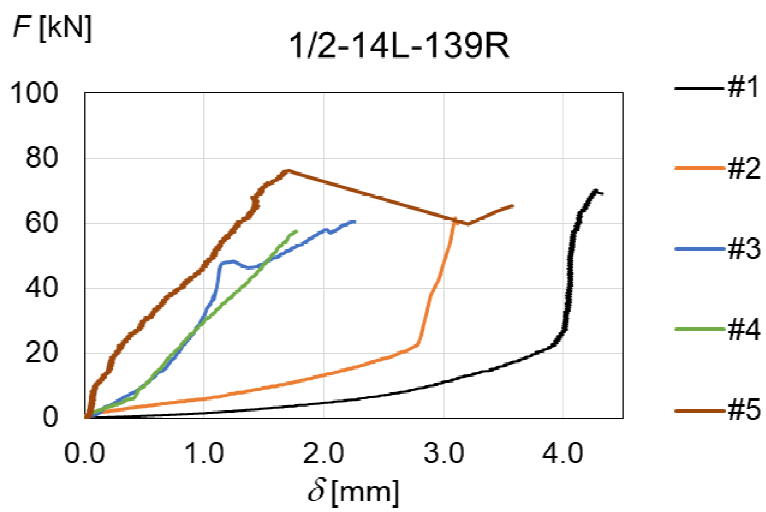
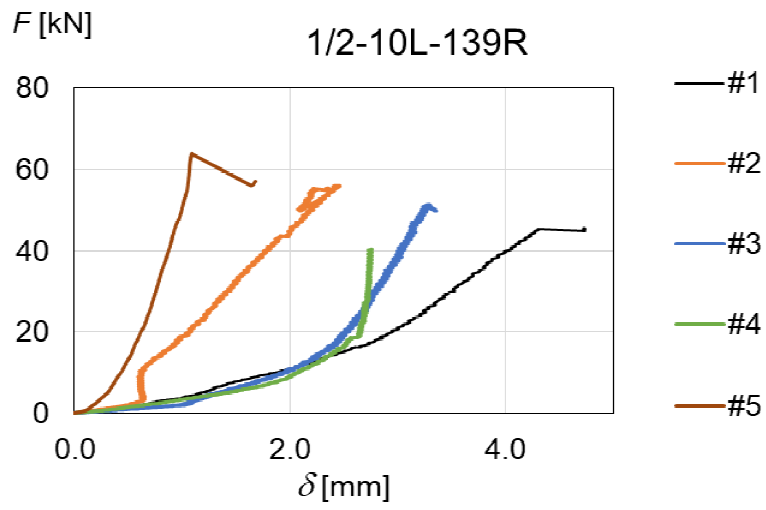
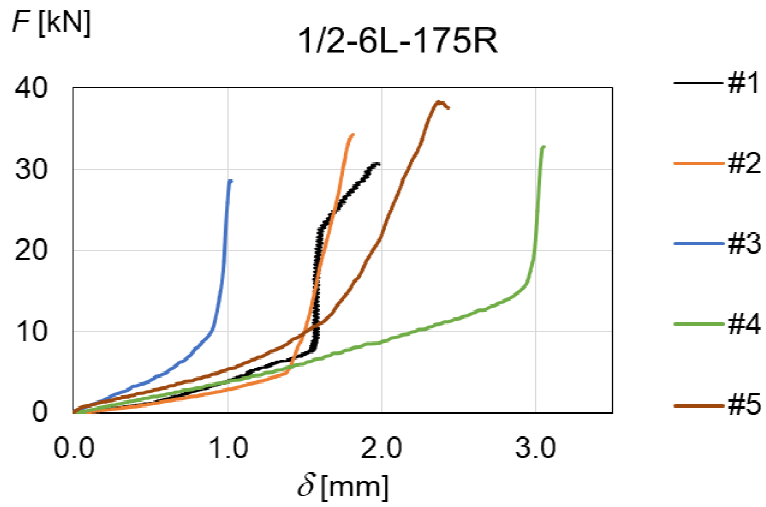


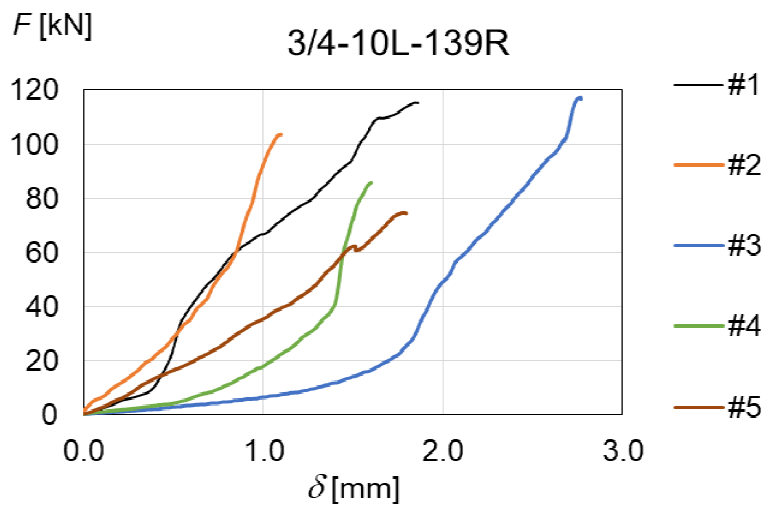
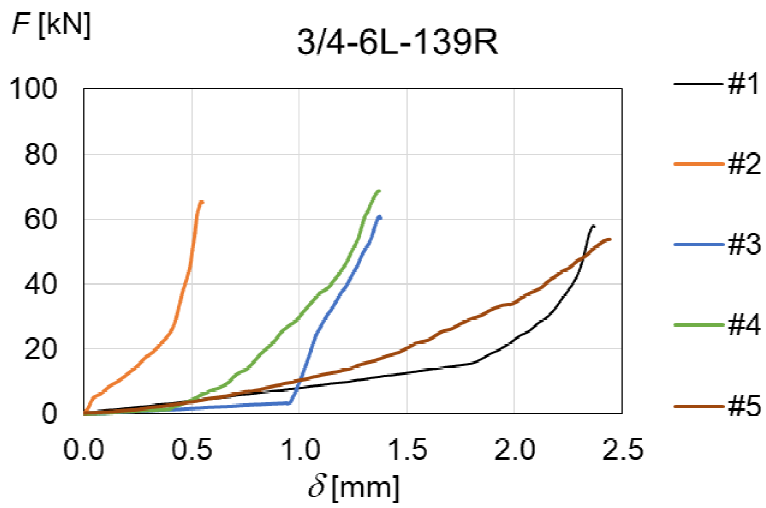
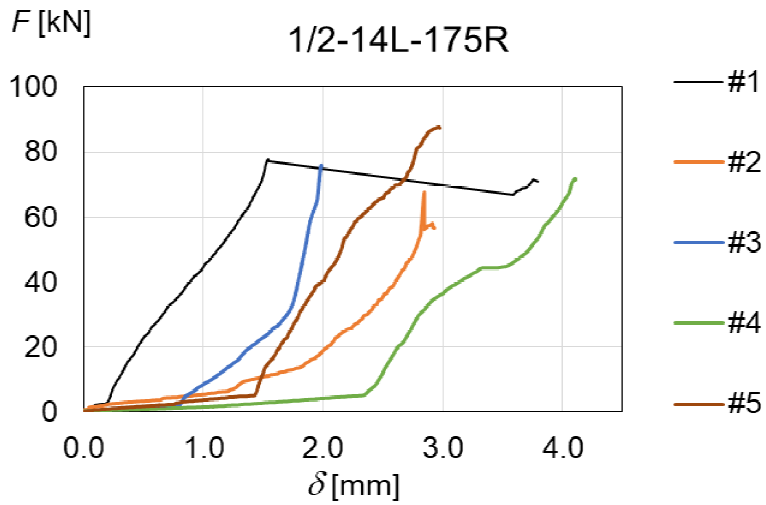


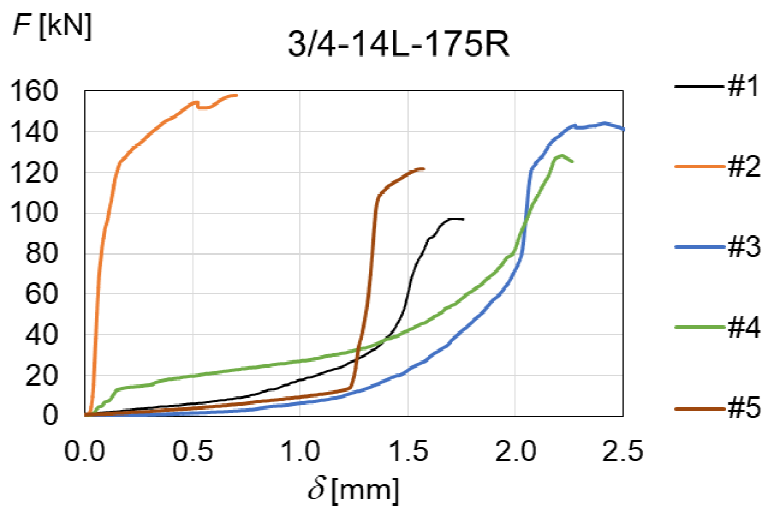
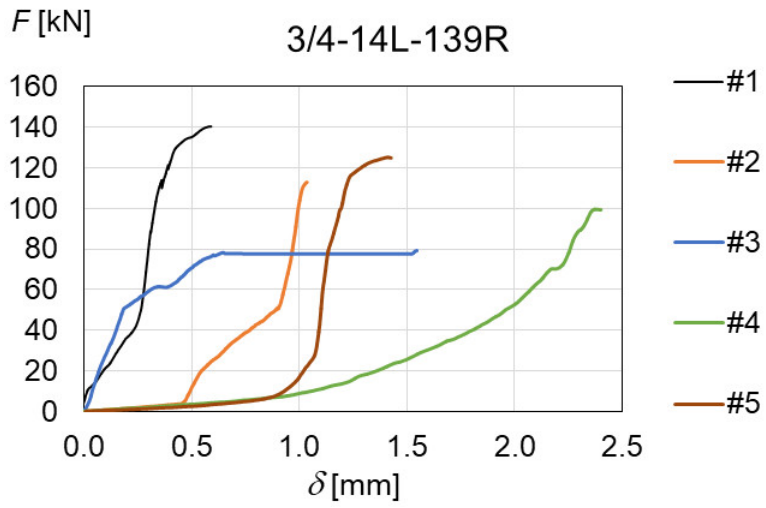
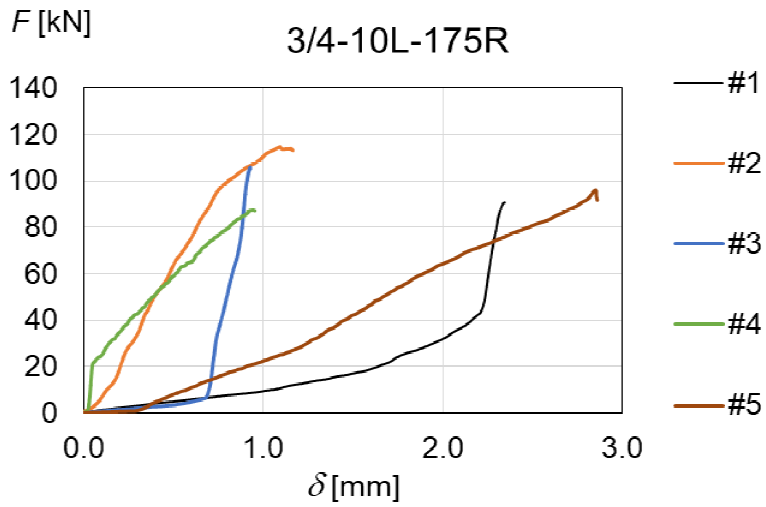


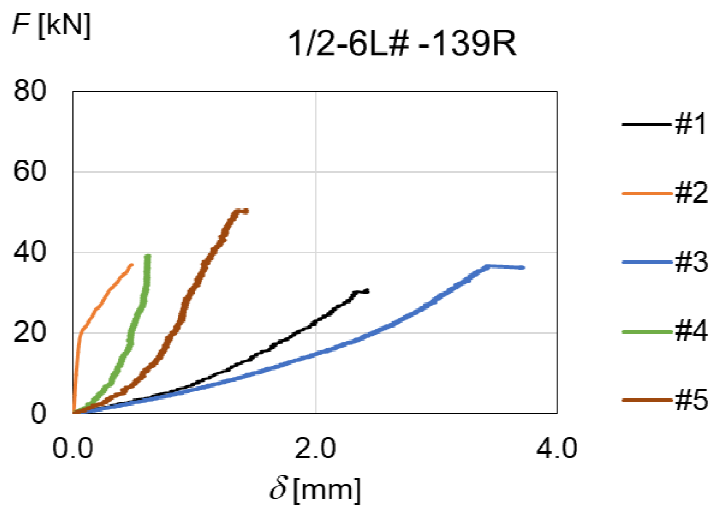
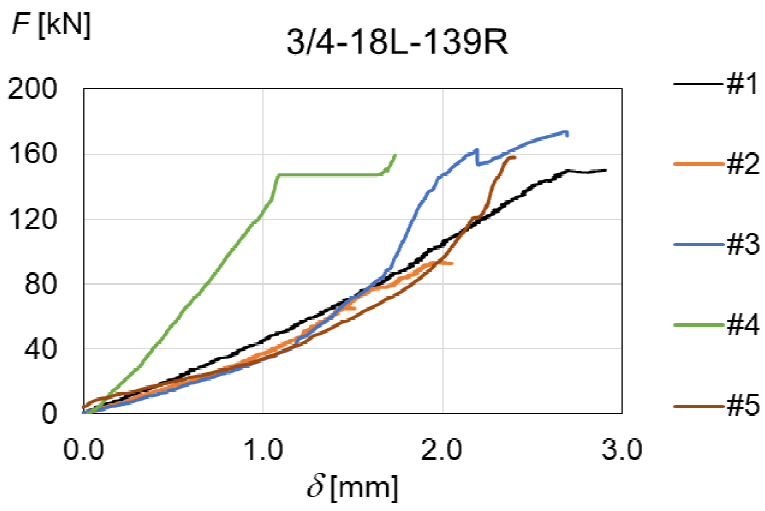
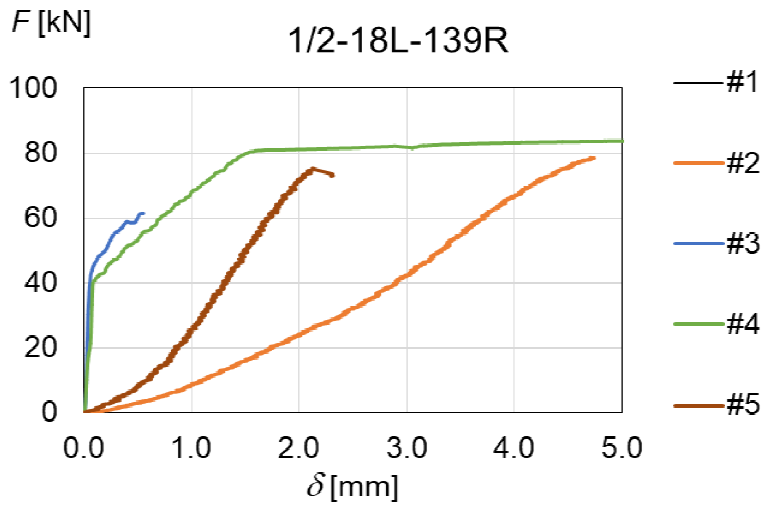


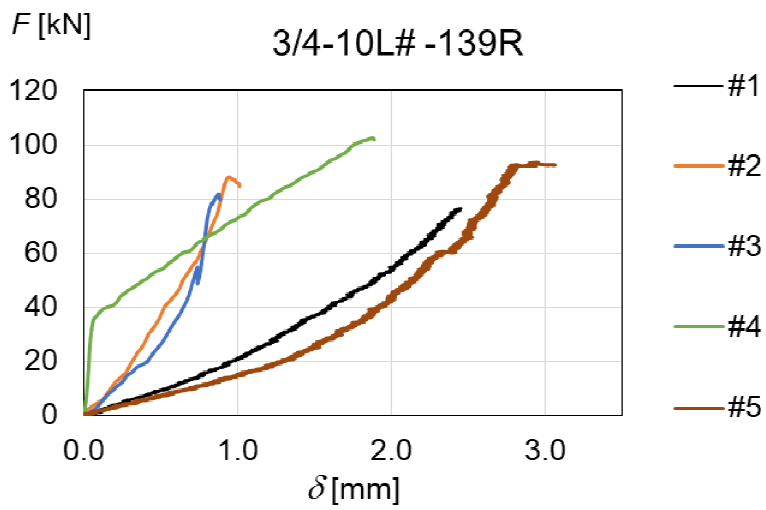
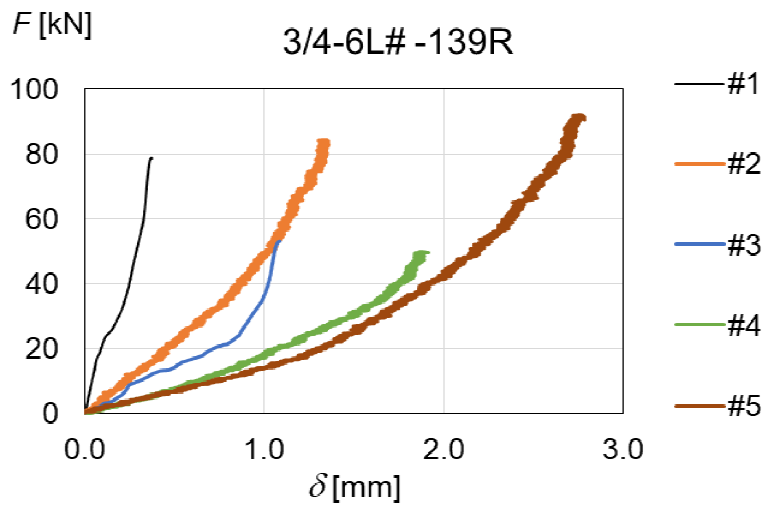
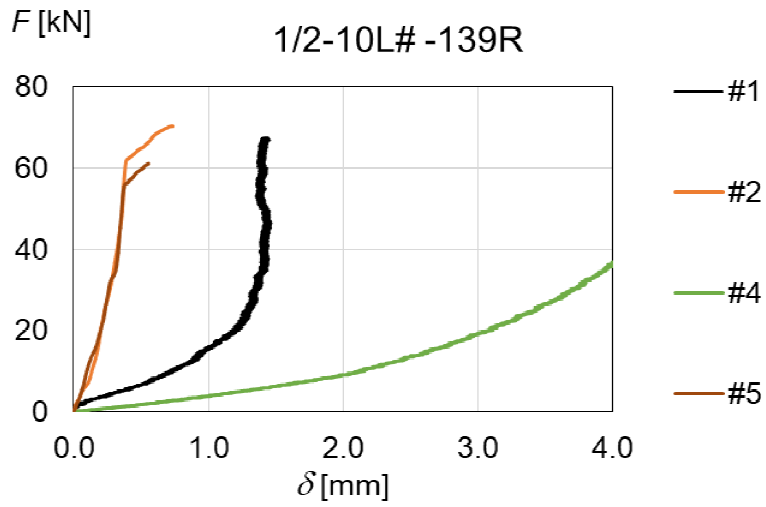




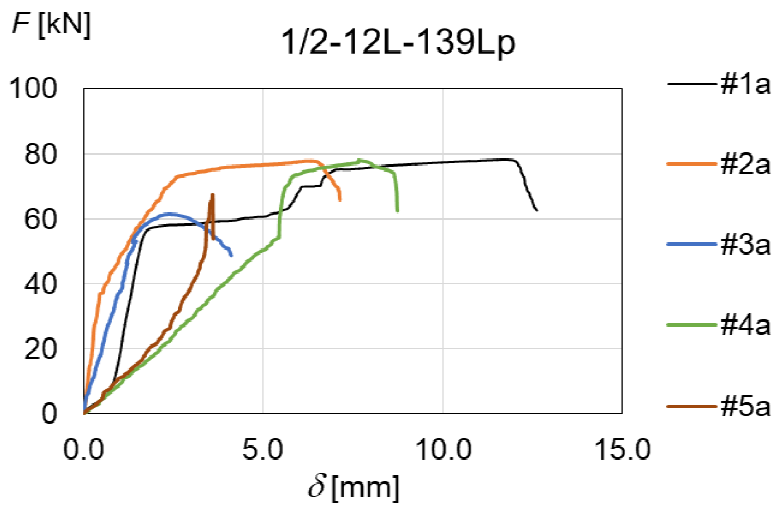
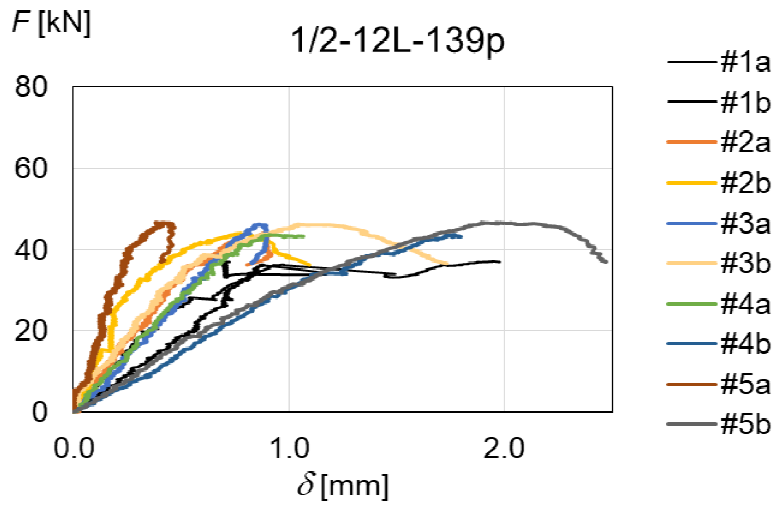
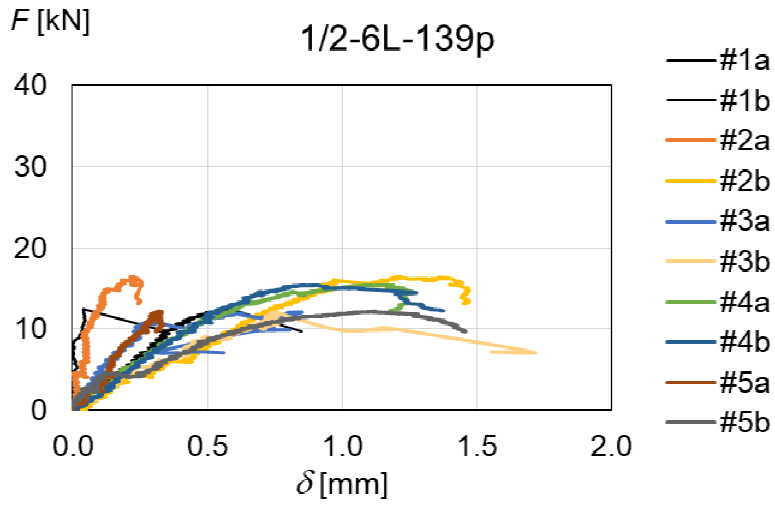


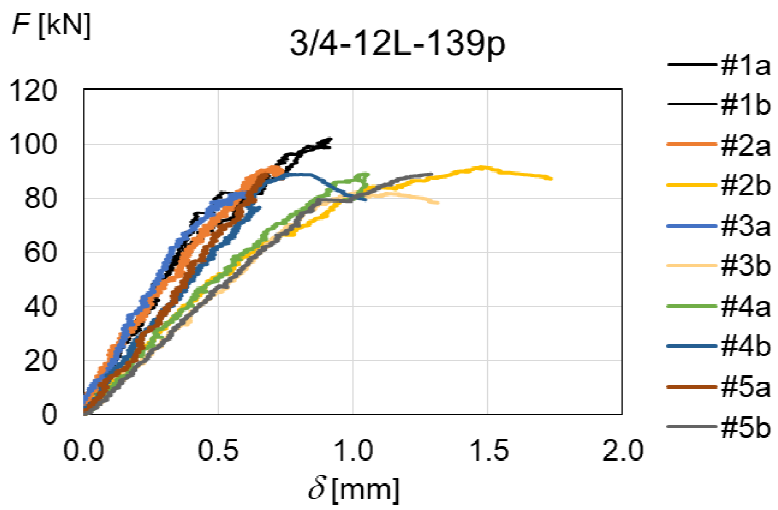
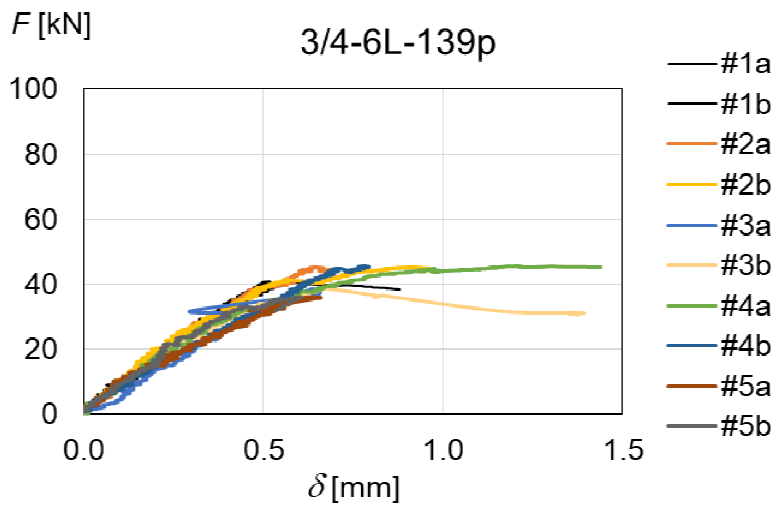
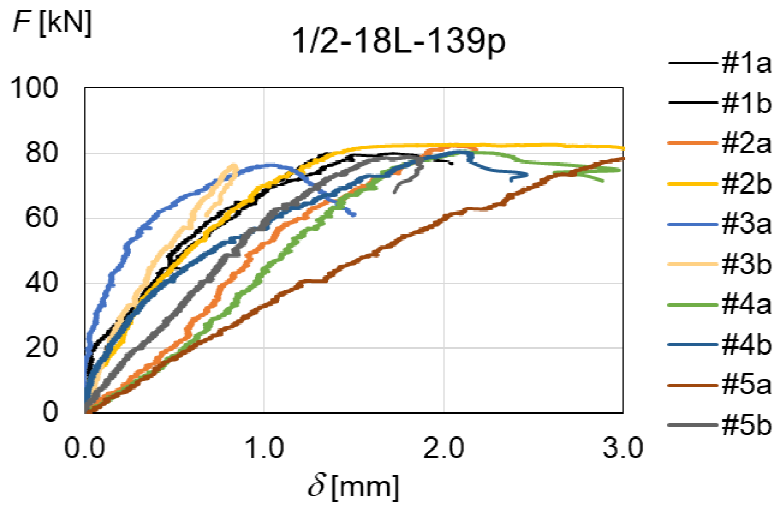


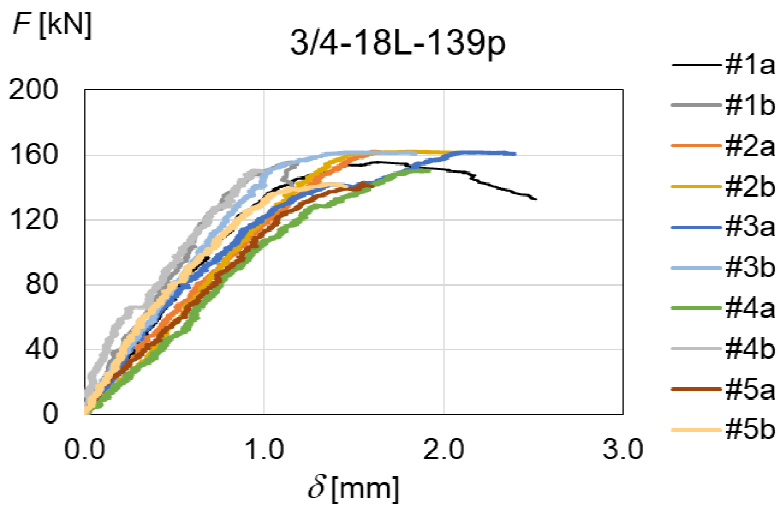
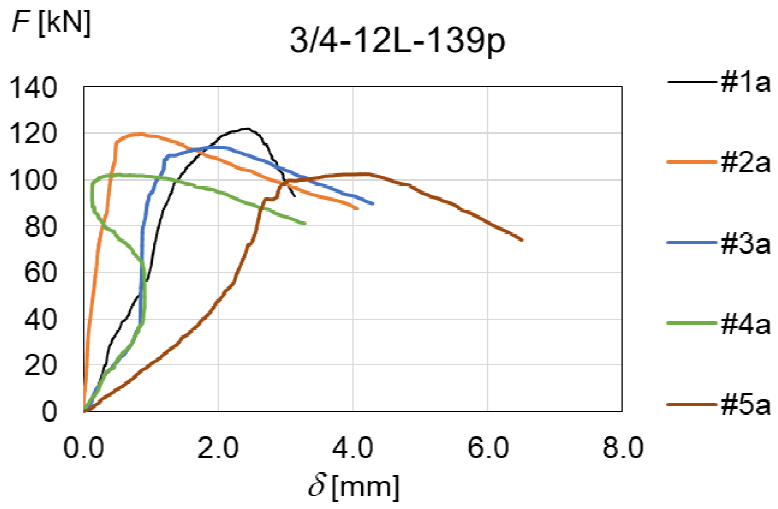




Appendix C: Load-displacement curves from Phase 2







Appendix D: Load-displacement curves from Phase 3

